

# Master of Science Thesis

Investigation on vertical motions of cargo and HTV during offshore discharge and loading

Xuelel Feng

Technische Universiteit Delft





# MASTER OF SCIENCE THESIS

## INVESTIGATION ON VERTICAL MOTIONS OF CARGO AND HTV DURING OFFSHORE DISCHARGE AND LOADING

by

**Xuelel Feng**

in partial fulfillment of the requirements for the degree of

**Master of Science**  
in Offshore and Dredging Engineering

at the Delft University of Technology,  
to be defended publicly on Tuesday June 30, 2016 at 02:00 PM.

Supervisor:	Ir. O. A. J. Peters,	Dockwise
	Prof. dr. ir. R. H. M. Huijsmans,	TU Delft
Thesis committee:	Prof. dr. ir. R. H. M. Huijsmans,	TU Delft
	Dr. ir. S. A. Miedema,	TU Delft
	Ir. O. A. J. Peters,	Dockwise
	Dr. ir. M. Godjevac,	TU Delft

*This thesis is confidential and cannot be made public until 30 June, 2021*

An electronic version of this thesis is available at <http://repository.tudelft.nl/>.



# ABSTRACT

Heavy transport vessels (HTVs) are widely used in long-distanced dry-tow transport. Currently, two end operations, loading and discharge, are executed in harbours or protected waters where waves are virtually non-existent. There is potentially a huge market demand to execute these operations at offshore sites.

To expand such operations to the offshore open seas, a systematic investigation of vertical motions between HTV and cargo is needed. The main challenge brought by these offshore discharge and loading operations is the small gap between HTV and cargo, both subject to environment conditions (waves, current, wind etc). Non-linearity due to gap flow is found from previous forced oscillation tests and CFD calculations. This thesis seeks to tackle this non-linearity in the time-domain framework.

The thesis report starts with the literature study based on Molin where the external forced due to forced-oscillation is described for a deeply-submerged circular disc extremely close to seabed. It has been found that inertial and cushioning forces are dominant for the small gap problem. Essentially, both forces can be expressed by added mass. The evaluations cases in the thesis are circular cylinders with certain drafts, for which the free surface effect must also be addressed by employing separation of frequency technique. The problem is divided into two parts for time domain equations in convolution form: gap part and free surface part. Gap part is frequency independent whereas free surface part is frequency dependent due to radiated waves generated by oscillating cargo. For the latter, it has been concluded that free surface part is largely independent of gap part, thus keeping radiation force by convolution integration untouched.

After separation of frequency, the main task is to find the proper formulations to quantify the gap part force. Two important variables have been identified: gap height and inclination angle. The quantification starts with verification for two numerical tools: AQWA and New method. Both tools are sufficiently accurate to quantify the influence from gap height and inclination angle on added mass of vertical motions. Thus, the external force is obtained and validated against measurements from forced oscillation tests and analytical results from Molin. With constructed formulations for added mass, the DLL for external force can be implemented into time domain solver. The implementation can be done via two approaches: interpolation of database approach and direct formulation approach. Moreover, a systematic scheme has been proposed to implement time domain simulations for the small gap problem.

Preliminary time domain simulations of regular waves at natural frequency show that the conventional linear results over-predict the heave response compared to non-linear results. This systematic methodology to implement time domain simulations will throw light on further analysis for workability.



# PREFACE

It is a tremendous two-year for me. Imagine this: my first ever plane-taking flight started with a long-distanced travelling from Beijing to Amsterdam on 16 August, 2014. Now, this part of 'study life' in the Netherlands would end with a master thesis, daily supervised by Onno Peters, who has always been patient with my stupidities and naiveties. As a hydrodynamic specialist, he refuses to go into 'murky' approach without comprehension. I learn a lot from this aspect and I am definitely a big fan of him, especially his extensive knowledge as well as his warm-heart and humour. Without his guidance, I could not possibly have completed this thesis so early, also thanks to the sponsor Boskalis.

I would also like to thank my TU supervisor Prof. Huijsmans for his valuable and witty feedback during progress meetings. I will always remember his grasp for physical essence and disregard for triviality. For me, he is an inspiring figure.

I have quite enjoyed my life at Delft, thanks to a group of Dutch friends, with whom I spent much unforgettable time. Life becomes easier instead of 'de laatste loodjes wegen het zwaarst.' Also gratitude to my family, who provided me tuition fee and unconditional love.

Lastly, I am indebted to my girl friend, Yuxi Zhang, for her support and companion since we met.

*Xuelei Feng*  
*Delft, June 14, 2016*



# CONTENTS

<b>Abstract</b>	<b>iii</b>
<b>Preface</b>	<b>v</b>
<b>1 Introduction</b>	<b>1</b>
1.1 Industrial Background . . . . .	1
1.2 HTV and Cargo Overview. . . . .	2
1.3 Offshore Discharge and Loading. . . . .	3
<b>2 Problem Overview</b>	<b>5</b>
2.1 Physical Model . . . . .	5
2.2 Problem Statement . . . . .	6
2.3 Objective. . . . .	7
<b>3 Hydrodynamic Description</b>	<b>9</b>
3.1 Thin Disc Theory . . . . .	9
3.2 Truncated Cylinder Theory. . . . .	15
3.3 Time Domain Theory. . . . .	20
3.4 Non-linear Model for Gap Problem . . . . .	21
3.4.1 Assumptions . . . . .	21
3.4.2 Model Interpretation. . . . .	22
<b>4 Separation of Frequency</b>	<b>25</b>
4.1 Applicability of New Method. . . . .	25
4.1.1 Evaluation Definition . . . . .	26
4.1.2 Heave Mode . . . . .	26
4.1.3 Pitch Mode . . . . .	27
4.2 Separation Methods . . . . .	28
4.2.1 Use of New Method . . . . .	28
4.2.2 Evaluation of free surface effect. . . . .	28
4.2.3 Separation at Infinite Frequency . . . . .	30
4.3 Conclusions . . . . .	33
<b>5 Quantification For Gap Flow Part</b>	<b>35</b>
5.1 Influence of Gap Height . . . . .	35
5.2 Influence of Asymmetry . . . . .	37
5.3 Influence of Shape . . . . .	39
5.4 Summary . . . . .	40
5.4.1 Formulations for External Force. . . . .	41
5.4.2 Conclusions. . . . .	42
<b>6 Time Domain Simulation</b>	<b>43</b>
6.1 Evaluation Scheme . . . . .	43
6.2 Verification for Forced Oscillation Traces . . . . .	44
6.3 Time domain Calculations . . . . .	46
6.3.1 Regular Wave Case . . . . .	46

---

6.3.2 Irregular Wave Case . . . . .	48
6.4 Conclusions . . . . .	49
<b>7 Conclusions and Recommendations</b>	<b>51</b>
<b>Bibliography</b>	<b>53</b>
<b>Appendices</b>	<b>55</b>
<b>A Asymmetric Calculation Cases</b>	<b>57</b>
<b>B Analytical Results</b>	<b>61</b>
<b>C Shape factors</b>	<b>67</b>
<b>D Verification with Measurement</b>	<b>69</b>
<b>E 3D Potential Theory</b>	<b>71</b>

# 1

## INTRODUCTION

### 1.1. INDUSTRIAL BACKGROUND

The past two decades, despite recent evaporation of oil price as of writing, have witnessed a remarkable progress in offshore oil and gas industry, with gigantic platforms deployed further in the deeper ocean and in harsher conditions.

The continuously fast growing demand of energy, especially from golden BRICS (Brazil, Russia, India, China and South Africa), has prompted significant technical advancements and, simultaneously, challenges unsolved associated with construction, installation, commissioning, production, maintenance, decommissioning etc.

For marine transport, the destinations of many platforms often are hub reservoir regions including North Sea, North Sea, Gulf of Mexico, West Africa, Brazil, Northwest Australia etc. On the other hand, the fabrication yards for these mega structures are located in East Asia, which created opportunities for long-distanced transporting.

To accommodate this long-distanced transporting challenge, two methods have been used: wet tow and dry tow. Wet tow uses tug boat to tow a self-floating platform with its own buoyancy to the designated site. Dry tow first loads the platform onto a barge or heavy transport vessel (HTV), then transporting the platform as the cargo on the deck. Two advantages of dry tow over wet tow are time saving and integrated fabrication. With dry tow, the transit time will be significantly reduced, thus leading to an earlier production time with good financing. The way of transport can also influence the basic construction philosophy as dry tow enables the transport of the fully integrated platform, which can be well fabricated at onshore shipyards. Consequently, offshore installation work such as topsides mating will be minimized even cancelled, thus saving time of deployment and decreasing risks of installation.

Apart from offshore transport, a potential market for offshore dry-docking [1] of FPSOs is beneficial to inspection, maintenance and repair (IMR) of FPSO without disconnecting from the mooring system, thus allowing for production even during IMR work. When the offshore dry-docking is not permissible due to severe seastates, an alternative called quay-side dry-docking may undertake IMR work by using local content, instead of using onshore dry-docks far away.

What is in common for both dry tow and dry-docking on a HTV is to make the cargo float on/off the HTV. This is normally realized in sheltered harbour or protected sea, with very limited wind speed and virtually no waves. The float on/off operation is thus executed on a static basis, nullifying the need of dynamic analysis. However, in some occasions, be it adverse sea conditions or outright

offshore site, the assessment of motions and forces is essential, due to high risks involved within the operation. The outcome of the assessment and downtime analysis may aid the vessel Master to make a better decision of execution or not. Sometimes when the platform's production site is remotely offshore, even though it's possible to do float-on in harbour, the float-off operation will still be a challenge with open seas. For the sake of unity, float-on and -off will be named as loading and discharge respectively.

Here we introduce the definition of offshore loading and discharge from Peters [2]:

***Loading and Discharge operations in non-sheltered location, while exposed to wave conditions, with acceptable workability.***

From the design point of view, the fundamental forces and motions during offshore discharge and loading must be understood thoroughly in order to determine the criteria for the designed components, i.e. mooring lines, winches, cribbing wood, guiding post etc. With detailed and reliable knowledge on these float-on/off operations, new components can even be designed to extend the workability to a larger range.

These backgrounds highly motivate the the research here on hydrodynamic behaviour during offshore loading and discharge operations.

## 1.2. HTV AND CARGO OVERVIEW

Two research objects for this thesis are heavy transport vessel and its cargo. Both geometric particulars and mass properties will be used as input data for subsequent hydrodynamic analysis.

For dry transport operations, heavy transport vessels are used to transport marine cargoes. Currently, HTVs can be categorized into four types:

- type 0: open stern and bow with accommodation casing placed on one side and other movable casings. The deck is open aft and fore.
- type 1: open stern with bow accommodation unit and other casings mostly at the stern free to move. The deck is open to the stern.
- type 2: closed stern with lower mid-section part.
- type 3: dock-type with walls on each side of the deck and the ramp at the stern.

Here a brief review of some HTVs from Dockwise is made to summarize the geometric characteristics for these vessels.

Vessel name –	Deadweight [MT]	Deck space (L*B) [m × m]	Water-depth above main deck [m]
Dockwise Vanguard	117,000	275.00 × 70.00	16.00 <i>FPP/APP</i>
Blue Marlin	76,061	178.20 × 63.00	11.42/15.10 <i>FPP/APP</i>
White Marlin	72,146	177.60 × 63.00	13.00 <i>FPP/APP</i>
Black Marlin	57,021	165.60 × 42.00	10.00 <i>FPP/APP</i>
Mighty Servant	45,407	150.00 × 50.00	10.00/14.00 <i>FPP/APP</i>
Triumph	53,818	130.00 × 44.50	9.00 <i>FPP/APP</i>
Talisman	53,000	130.00 × 44.50	9.00 <i>FPP/APP</i>

Table 1.1: Particulars for some Dockwise HTVs

With large deck space and deadweight of HTVs as listed in Table 1.1, various huge floating cargoes can be dry transported:

- Ship-shaped FPSO, navy ship, barge
- Semisubmersible, TLP
- Jack-up, liftboat
- Cylinder FPSO
- SPAR
- Others

### 1.3. OFFSHORE DISCHARGE AND LOADING

Compared to dry transport, two end operations — loading and discharge — are vital to the execution for the future offshore project. It must also be mentioned here that the real offshore discharge and loading operations for mega platforms have never been carried out due to lack of experience and analysis. As a reference for offshore operations, the sequence of loading and discharge in sheltered locations is outlined.

First begins the preparation stage with the HTV and cargo. Cribbing beams and guideposts are installed on the pre-defined locations for HTV. Cribbing beams are used to support the cargo and evenly distribute its load to the HTV hull. Guideposts are used to guide the cargo to its designated position without actual restrictions for cargo movement. Then the HTV is ballasted to the loading draft, thus its deck submerged in water awaiting cargo to come onto.

Second, weather window arriving, with the aid of tugs and work-boats, the floating cargo is brought and positioned over the HTV. This loading stage requires accurate positioning and orientating the cargo over the HTV.

Third, HTV will be de-ballasted to the transport draft. Now two things happen during the de-ballasting process: the water gap between HTV and cargo reduced gradually until cargo sitting on top of HTV cribbing; HTV and cargo together de-ballasted until HTV reaches transport draft.

The next stage is to disconnect tugs and work-boats, double check cargo position and make sea-going preparations.

When HTV and cargo reach the destination site, the discharge of cargo will be carried out, following very similar procedures as the loading ones, but in a reversed order. Attention should still paid on clearance between cargo and HTV during ballasting and offloading.

Summarizing the above-mentioned sequence for discharge and loading, the key issue is the gap between cargo and HTV, which requires our further comprehension.



# 2

## PROBLEM OVERVIEW

### 2.1. PHYSICAL MODEL

The scope of this work is mainly focusing on vertical motions (namely heave, roll and pitch) of the large cargo relative to the HTV during offshore discharge and loading [3]. To evaluate hydrodynamic properties for the vertical motions of an arbitrary flat-bottom-shaped body, radiation problems must be accommodated. One important hydrodynamic feature of the cargo is its proximity to HTV. Besides, the size of the cargo is much larger than the gap height between the cargo and HTV. Considering different types and dimensions of the cargoes and HTVs, a systematic methodology to address this challenge is needed.

The first step to build the physical model requires a simplification of the HTV-cargo model. Before simplifying the problem, at least several features of the two-body system should be identified:

- For the cargo alone during discharge and loading operations, it is submerged in a local shallow water depth ranging from 9 [m] to 16 [m], see table 1.1.
- The casings on the HTVs have very small water plane areas during operations, compared to the large hull water plane area at normal transit draft.
- The water gap between HTV and cargo is relatively small and the bottom area of the cargo is large.

Though most offshore discharge and loading operations will be implemented in rather deep water, for the cargo itself, the local water depth provided by the HTV submerged deck is very shallow. This is a starting analysis point for the cargo, regardless of the actual in-site bathymetry.

Intuitively, given the fact that the gap flow due to relative vertical motions is dominant, the physical model here considers the HTV deck as the artificial seabed, thus simplifying the problem into cargo-alone model in shallow water.

Here we define the simplified hydrodynamic model:

***A vertically oscillating single body system with close proximity to seabed in extremely shallow water depth.***

## 2.2. PROBLEM STATEMENT

The most important dynamic feature is the water gap between HTV and cargo. Phenomenologically, the gap problem is analogous to the pipe flow problem with sudden contraction due to upward movement and sudden expansion due to downward movement, see Peters [2]:

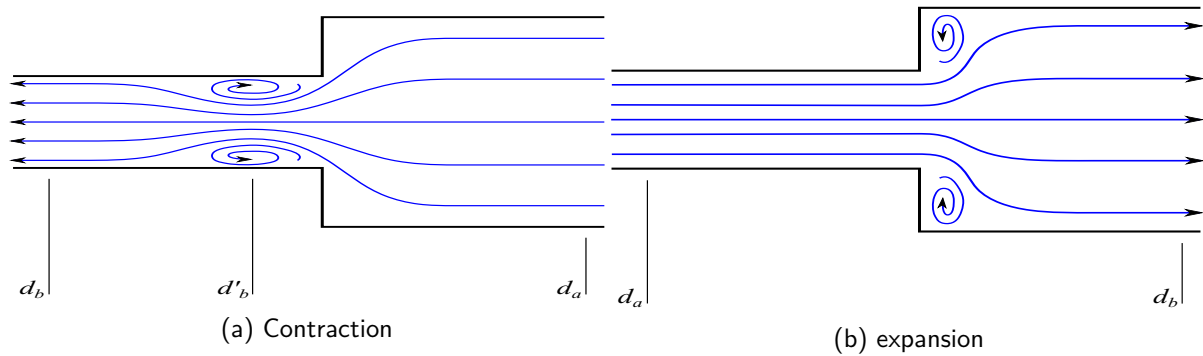


Figure 2.1: gap flow problem [2]

Corresponding to the contraction during upward movement when water is sucked into the gap, the cargo will experience a sticking effect. When the cargo moves downward, the water is being squeezed out of the gap with a cushioning effect to the cargo. The source of non-linearity mainly comes from this gap part[2]. This non-linearity is found by forced oscillation tests where linear result is compared to measurements[2], as shown in 2.2. Clearly, the linear result has substantially underestimate the force due to forced heave motion. Also results from CFD calculation have confirmed the existence of non-linearity due to gap part[2].

***The main problem to be investigated in this thesis is non-linearity due to gap flow between cargo and HTV.***

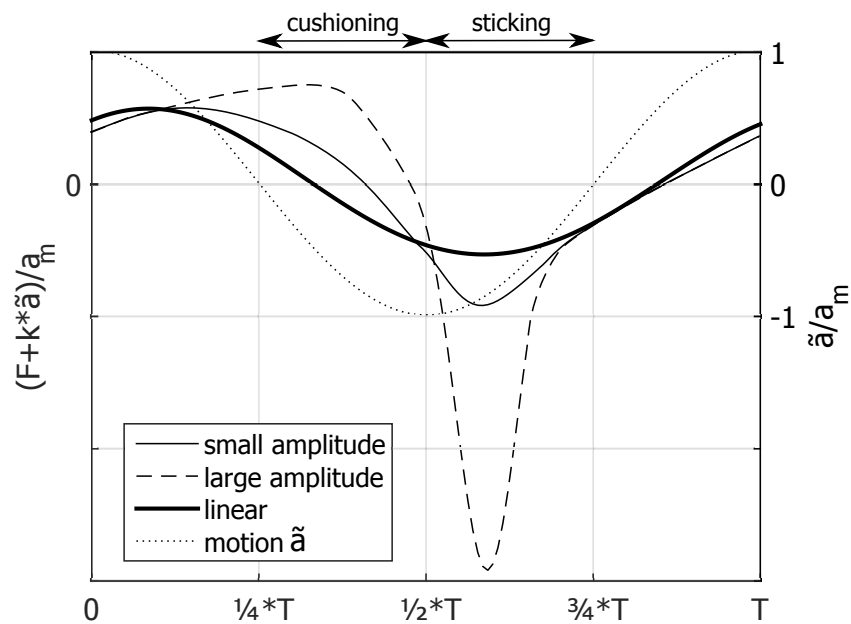


Figure 2.2: Non-linearity due to squeeze flow [2]

### 2.3. OBJECTIVE

The focus of this thesis research is the hydrodynamic behaviour during offshore discharge and loading in support of a PhD program. Motion-wise, this problem can be subdivided into two perspectives: horizontal and vertical motions. The horizontal motions, i.e surge, sway and yaw, will be dealt with elsewhere by another student, along with a new designed cargo handling system to restrict horizontal motions. Naturally, the topic for this thesis will duly be on relative vertical motions between HTV and its cargo during offshore discharge and loading.

Statement of industrial background and challenges lead to this thesis main objective:

- **Find a systematic methodology to predict non-linear behaviour associated with gap flow in time domain.**

Above all, the ultimate purpose, the author wishes, is to provide some basis for potential offshore discharge and loading activities in future.



# 3

## HYDRODYNAMIC DESCRIPTION

The conventional method to predict motion behaviour of floating structures in waves is 3D diffraction theory (see Appendix E). Employing the linearized potential flow theory, hydrodynamic characteristics are determined based on this theory, which is then used in frequency-domain or time domain solvers.

As standard linearized theory is not available to capture the non-linear loads involved in the gap flow problem, other theories have been explored. A summary of important methods is given below. Also, some background is given about time-domain solver, which is the basis for predicting non-linear behaviour.

### 3.1. THIN DISC THEORY

The aim of introducing the thin disc oscillating close to seabed is to find mathematical description for non-linear hydrodynamic loading for the physical model 2.1. The common characteristic between the physical model and thin disc case is that both are subject to small gap problem, which is the main source of non-linearity. The solution of thin disc oscillating close to seabed will be illuminating to the problem concerned in this thesis. Starting from simplest geometry, related papers on submerged circular heaving plates close to seabed give closed-form expressions for added mass and radiation damping. Molin (1999) *et al.* [4] derived hydrodynamic properties of the heaving disc, a physical model for the jack-up footings approximating the seabed under induced vertical motions by waves. Partly consistent with the assumptions in 3.4.1, several assumptions implicitly used in his paper are outlined as:

- The water depth is sufficiently deep that the influence from the heaving disc is negligible at the infinite boundary, namely free surface.
- The gap between heaving disc and seabed is sufficiently small compared to the radius of the disc that the flow is locally 2-dimensional near the disc boundary
- The disc model has flat bottom but no thickness, oscillating vertically above a flat seabed.

Within potential theory framework, assuming fluid inviscid and irrotational, Molin gave the expression of hydrodynamic force starting from kinematic energy  $E_c$  in the fluid domain  $V$  confined by the control surface  $\Sigma$ :

$$E_c = \frac{1}{2}\rho \iiint_V (\nabla\Phi)^2 dV \quad (3.1a)$$

Also, the kinematic energy in terms of added mass:

$$E_c = \frac{1}{2} M_{33} U^2 \quad (3.1b)$$

Now, the time derivative of Eqs. 3.1a :

$$\frac{dE_c}{dt} = -\vec{F} \cdot \vec{U} + \rho \iint_{\Sigma} \Phi_t \nabla \Phi \cdot \vec{n} dS \quad (3.2a)$$

with control surface  $\Sigma$  extending to infinity, the second term of the above equation on the RHS vanishes.

Similarly, the time derivative of Eqs. 3.1b :

$$\frac{dE_c}{dt} = \frac{1}{2} U^2 \frac{dM_{33}}{dt} + M_{33} \frac{dU}{dt} \quad (3.2b)$$

Thus, with Eqs. 3.2a and Eqs. 3.2b, the hydrodynamic force related to forced heave motions is described as:

$$F = -M_{33} \frac{dU}{dt} - \frac{1}{2} U \frac{dM_{33}}{dt} \quad (3.3)$$

The subsequent work falls on determining added mass within potential framework, in which Molin utilized a method of matched asymptotic expansion, pioneered by Van Dyke (1964) [5], later Tuck (1971, 1975) [6][7] to investigate the water wave transmission problem for small-apertured structure. Mei (1989) [8] applied this technique for breakwater gap problem. The key assumption with this technique is that the local geometries (aperture, gap, clearance etc.) are very small compared to the complete structure dimension. This assumption is consistent with Molin 3.1, thus providing the important basis for the disc problem.

Here we give a brief introduction on matched asymptotic expansion formally described by Linton and McIver (2001) [9]:

The problem is defined in two domains, namely inner domain and outer domain. The parameter  $\varepsilon$  indicates the comparably small geometric feature  $a$ , on which solutions for both inner and outer domains are dependent. Hence, we have limite  $\varepsilon \rightarrow 0$ .

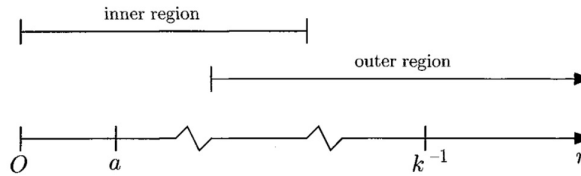


Figure 3.1: Sketch of inner and outer region[9]

For inner domain, the solution is described in dimensionless coordinate  $\rho$  and parameter  $\varepsilon$ :

$$\psi_0(\rho) + \varepsilon \psi_1(\rho) + \varepsilon^2 \psi_2(\rho) + \dots + \varepsilon^n \psi_n(\rho) \equiv \psi^{(n)}(\rho; \varepsilon) \quad (3.4)$$

For outer domain, the solution is described in dimensionless coordinate  $R$ , where  $R = \varepsilon \rho$ :

$$\chi_0(R) + \varepsilon \chi_1(R) + \varepsilon^2 \chi_2(R) + \dots + \varepsilon^m \chi_m(R) \equiv \chi^{(m)}(R; \varepsilon) \quad (3.5)$$

The outer solution must match the outer expansion of the inner solution, and, similarly, the inner solution must match the expansion of the outer solution. The formal matching principle works as:

$$\chi^{(m,n)} \equiv \psi^{(n,m)} \quad (3.6)$$

Using matching equation above, the unknowns for the solution are solved, truncating the series  $\varepsilon$  to obtain desirable accuracy. What should be noted here is that the Eqs. 3.6 is expressed within the same set of coordinate system, be it inner or outer coordinate.

Molin used the matched asymptotic method as stated above to solve unknowns in potential formulations for a three dimensional case of a circular disc of radius  $a$  and clearance of  $d$  to seabed. First, he gave the boundary value problem for the potential flow:

$$\begin{aligned} \nabla\Phi &\rightarrow 0 && \text{Infinity condition} \\ \Delta\Phi &= 0 && \text{Fluid domain } V \\ \Phi_z &= 0 && \text{On seabed } F \\ \Phi_z &= U(t) = \dot{d} && \text{On disc } P \end{aligned} \quad (3.7)$$

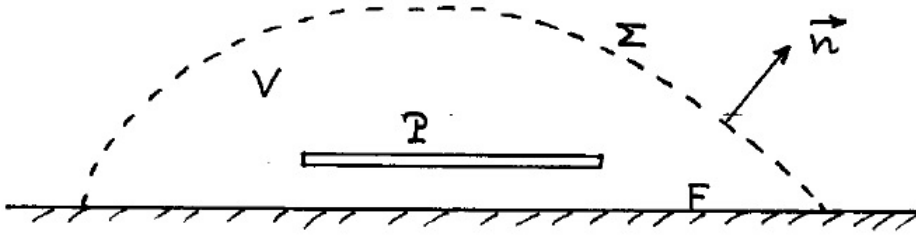


Figure 3.2: Fluid domain around the disc.[4]

The fluid domain is then divided into three parts:

- Domain 1: Under the disc
- Domain 2: Gap outlet area
- Domain 3: Outer domain

By constructing potential formulations for each of these three domains, the matching procedures then will be done. Here we give a summary of potential expressions due to heave motion for three domains without explanation: Under the circular disc, the potential in cylindrical coordinates is expressed as:

$$\Phi_1(R, z, t) = \frac{U(t)}{2d(t)} \left( z^2 - \frac{R^2}{2} \right) + A_1(t) \quad (3.8)$$

At the gap outlet area, using conformal mapping in complex plane  $\zeta = x + iy$ , where  $x = \frac{R-a}{d}$ ,  $y = \frac{z}{d}$ , the complex potential is:

$$f_2(\zeta, t) = -\frac{U(t)a}{2\pi} \ln(\zeta) + A_2(t) \quad (3.9)$$

For the outer domain, it consists of source distributed over the surface of the disc and along the boundary of the disc:

$$\begin{aligned} \Phi_3(R, z, t) &= -\frac{U(t)}{2\pi} \int_0^{2\pi} d\theta \int_0^a \frac{r dr}{\sqrt{z^2 + R^2 + r^2 - 2Rr \cos(\theta)}} \\ &+ \frac{U(t)a^2}{4\pi} \int_0^{2\pi} \frac{1}{\sqrt{z^2 + R^2 + a^2 - 2Ra \cos(\theta)}} d\theta \end{aligned} \quad (3.10)$$

After obtaining potentials for three domains, we start the matching procedures based on Eqs.3.6. First  $A_2$  from Eqs.3.9 is known from connecting domain 2 and domain 3. Then by connecting domain 1 and 2,  $A_1$  from Eqs.3.8 is obtained. With all the unknowns for potentials from three domains solved, heave added mass is derived as:

$$M_{33} = \rho \iint_S (\Phi_1 - \Phi_3) dS \quad (3.11)$$

Thus the heave added mass for a heaving disc is obtained:

$$M_{33} = \rho \pi a^3 \left[ \frac{a}{8d} + \frac{1}{2\pi} \ln \left( \frac{8\pi a}{d} \right) - \frac{4}{3\pi} + \frac{d}{2a} \right] \quad (3.12)$$

Vinje [10] derived a similar formulation for heave added mass of a circular disc near seabed using matched asymptotic technique:

$$M_{33} = \rho \pi a^3 \left[ \frac{a}{8d} + \frac{1}{2\pi} \ln \left( \frac{8\pi a}{d} \right) - \frac{5}{6\pi} \right] \quad (3.13)$$

Since disk radius is assumed much larger than the gap height, Molin and Vinje equations are almost identical with the first two terms  $\rho \pi a^3 \left[ \frac{a}{8d} + \frac{1}{2\pi} \ln \left( \frac{8\pi a}{d} \right) \right]$  dominant for large radius-to-gap ratio, consistent with assumptions 3.4.1. As to the negligible difference between Molin and Vinje<sup>1</sup>, it is out of the scope for this thesis.

Brennan (1982) [11] derived the total force experienced by the body in close proximity to a solid boundary. He found that the inertial force is substantially increased due to “*fluid being accelerated in the region between the fluid and the boundary.*” Starting from 2D plate close to a solid boundary, the gap height is a function of time with its first derivative  $\frac{dh}{dt}$  and second derivative  $\frac{d^2h}{dt^2}$  corresponding to velocity and acceleration respectively. The assumption here is that  $h$  is much smaller compared to the width of 2D plate.

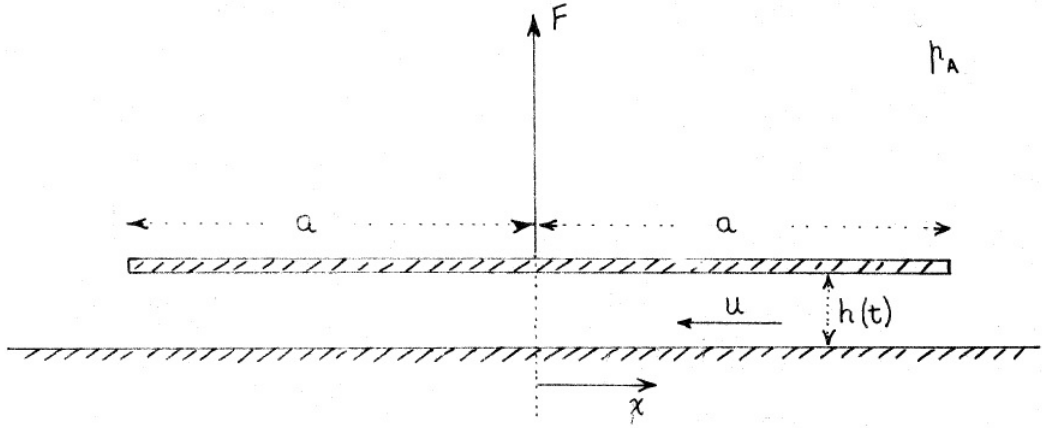


Figure 3.3: Two dimensional problem with plat width  $2a$  and gap height  $h(t)$

Given an initial upward velocity, the plate, according to mass conservation law, will generate rather large horizontal velocity  $u$ . In the gap, we have the mass conservation relation:

$$h \cdot u = -\frac{dh}{dt} x \quad (3.14)$$

<sup>1</sup>Indeed in principle the two added masses from Molin and Vinje should be equal, but since the cargo bottom size is much larger than the gap height, the added mass from third terms onward is considerably smaller than the first two terms.

Neglecting the viscous force, the momentum conservation law leads to:

$$\frac{1}{\rho} \frac{\partial p}{\partial x} + 2u \frac{\partial u}{\partial x} + \frac{1}{h} \frac{\partial}{\partial t} (hu) = 0 \quad (3.15)$$

where  $p(x, t)$  is the pressure.

After substitution and integration, the pressure distribution inside the gap is obtained as:

$$p = p_E + \frac{\rho h}{2} (a^2 - x^2) \frac{\partial^2}{\partial t^2} \left( \frac{1}{h} \right) \quad (3.16)$$

where  $p_E$  is the edge pressure. Brennen assumes the continuity for pressure, thus edge pressure  $p_E$  equal to ambient pressure  $p_A$ .

Further integrating pressure 3.16 over the area of the plate, the total inviscid force caused by heave motion is:

$$F = \frac{2}{3} \frac{\rho a^3}{h} \ddot{h} - \frac{4}{3} \frac{\rho a^3}{h^2} (\dot{h})^2 \quad (3.17)$$

Similar to Eqs. 3.3, the first term of Eqs. 3.17 is inertial force expressed with added mass:

$$M_a = \frac{2}{3} \frac{\rho a^3}{h} \quad (3.18)$$

Following the same spirit as Brennen, for the 3D circular disk case with a radius of  $a$ , we have horizontal velocity due to vertically heaving disc:

$$\begin{aligned} u_r \cdot (2\pi r h) dt &= -\pi r^2 dh \\ u_r &= -\frac{r}{2h} \dot{h} \end{aligned} \quad (3.19)$$

With Bernoulli equation:

$$\frac{1}{\rho} \frac{\partial P}{\partial r} + \frac{\partial u_r}{\partial t} + u_r \frac{\partial u_r}{\partial r} = 0 \quad (3.20)$$

after substitution and integration,

$$P = P_e + \frac{\rho}{4h} (a^2 - r^2) \ddot{h} \quad (3.21)$$

Integrating the pressure over the bottom of the disc leads to the inertial force:

$$F = \int_0^a P (2\pi r) dr = \rho \pi a^3 \left[ \frac{a}{8h} \right] \ddot{h} \quad (3.22)$$

Consequently, added mass for the circular disc is given as:

$$M_{33} = \rho \pi a^3 \left[ \frac{a}{8h} \right] \quad (3.23)$$

Now, with analytical formations of heave added mass for the circular disc from Molin 3.12, Vinje 3.13 and Brennen 3.23, a brief summary is listed here:

As shown from Tab. 3.1, the leading term of all three formulations is the same:  $\rho \pi a^3 \left[ \frac{a}{8h} \right]$ . This asserts the fact that added mass is inversely proportional to gap height if only the first term is considered.

	Analytical expressions
Brennen	$\rho\pi a^3 \left[ \frac{a}{8d} \right]$
Vinje	$\rho\pi a^3 \left[ \frac{a}{8d} + \frac{1}{2\pi} \ln\left(\frac{8\pi a}{d}\right) - \frac{5}{6\pi} \right]$
Molin	$\rho\pi a^3 \left[ \frac{a}{8d} + \frac{1}{2\pi} \ln\left(\frac{8\pi a}{d}\right) - \frac{4}{3\pi} + \frac{d}{2a} \right]$

Table 3.1: Comparison of analytical heave added mass for a circular disc

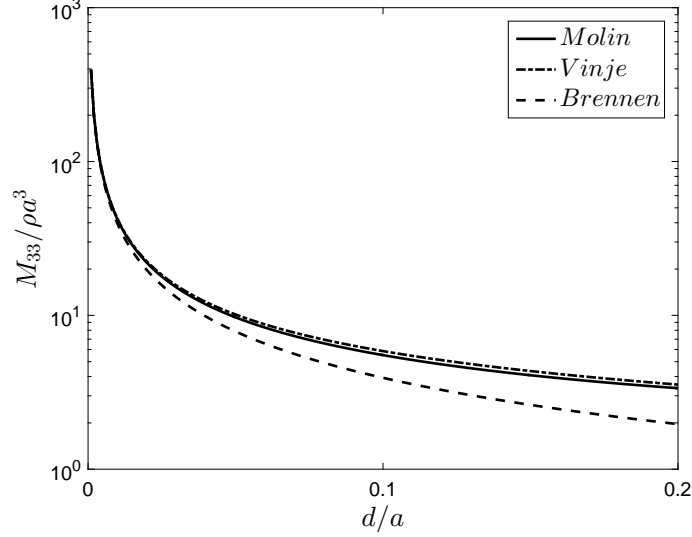


Figure 3.4: Comparison between three different analytical heave added mass for a circular disc

Previously stated, the difference between Vinje and Molin is negligible due to large radius-to-gap ratio. This is not entirely true with Brennen as it lacks the second term in Molin or Vinje. One possible explanation on the lack of second term for Brennen is that during derivation, no contribution from the outer domain is included, whereas at Molin and Vinje, matched asymptotic methods guaranteed the inclusion of influence from outer domain in an interactive way. The above statement can be demonstrated by the Fig. 3.4.

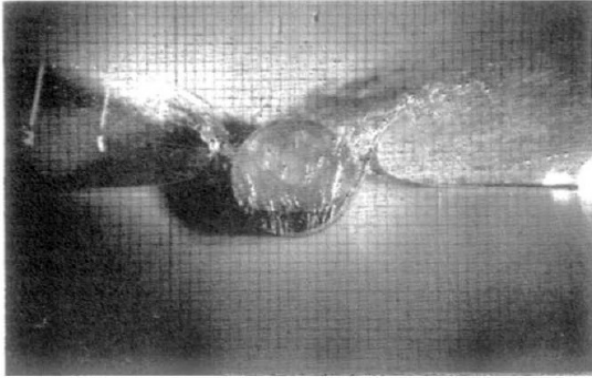
With identified heave added mass, based on Eqs. 3.3 & 3.17, the total inviscid force for heaving circular disc close to seabed can be determined. The first term  $M_{33} \frac{dU}{dt}$  indicates the inertial force and second term  $\frac{1}{2} U \frac{dM_{33}}{dt}$  represents the force due to time variation of added mass. Specifically for the second term, an observation for all three added masses from Tab. 3.1 shows that added mass is a function of gap height  $h$ , thus reducing the second term to:

$$-\frac{1}{2} \frac{dM_{33}}{dh} U^2 \quad (3.24)$$

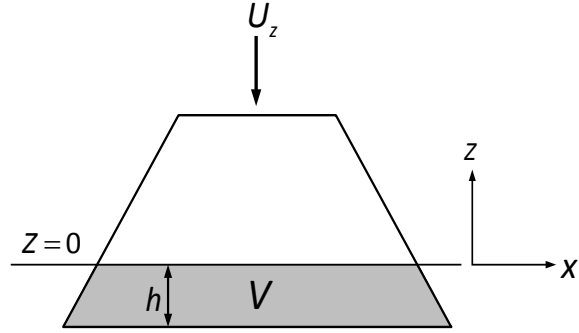
Consequently, the second term is proportional to the velocity squared with the cushioning coefficient  $\frac{dM_{33}}{dh}$ . It must be noted here that this second term is not Morison-drag force. Nielsen [12] addressed this term as 'cushioning' load, analogous to the water entry problem [13] during subsea deployment operations for templates:

The physic interpretation for the cushioning force in this thesis is that the body will experience a force associated with the sudden change of added mass due to change of gap height.

The disc approaching the seabed will gain added mass. Then this process can be illustrated as a marching snow ball growing bigger while keeping the constant velocity  $U$ , as illustrated in Fig. 3.6.



(a) Water-entry of a horizontal circular cylinder [13]



(b) Water entry for subsea template installation

Figure 3.5: cushioning load for water entry problem

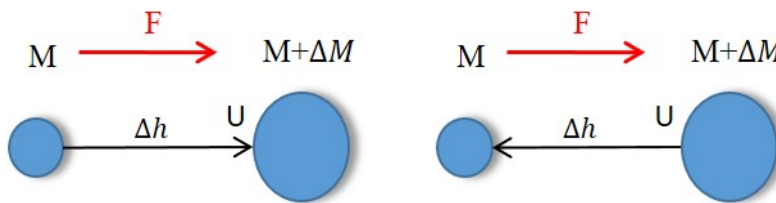


Figure 3.6: force changing added mass due to gap height change

According to work-kinetic energy theorem, we have:

$$\Delta K = \frac{1}{2}(M + \Delta M)U^2 - \frac{1}{2}MU^2 \tag{3.25}$$

$$W_{total} = F \cdot \Delta h \tag{3.26}$$

Thus, the force related to this mass gaining effect is:

$$F = \frac{\frac{1}{2}\Delta MU^2}{\Delta h} \approx \frac{1}{2} \frac{dM}{dh} U^2 \tag{3.27}$$

The positive direction of this force is always downward for the added mass, which causes the upward force for the disc itself. Two important features for this cushioning force are positive directionality regardless of motion direction and proportionality to velocity squared. As add mass is inversely proportional to gap height, its derivative with respect to gap height would be increased with gap height squared. The cushioning force of the heaving cargo close to the seabed can be viewed as a high frequency positive force (twice of the oscillation frequency) added to the inertial force. The cushioning coefficients  $|\frac{dM_{33}}{dh}|$  are obtained by differentiating added mass with gap height, result shown in Tab. 3.2.

Again, to compare the cushioning difference between Molin, Vinje and Brennen, the dimensionless cushioning coefficients are drawn in Fig. 3.7. Still, the difference between Molin and Vinje is negligible as two curves seem to be coincidental for the dimensionless gap-radius ratio range(0–0.2), whereas Brennen has shown a somewhat different cushioning coefficient curve.

### 3.2. TRUNCATED CYLINDER THEORY

The thin disc theory properly deals with the gap flow problem, which is the main source of non-linearity, while omitting the influence from the free surface, as the disc is deeply submerged and

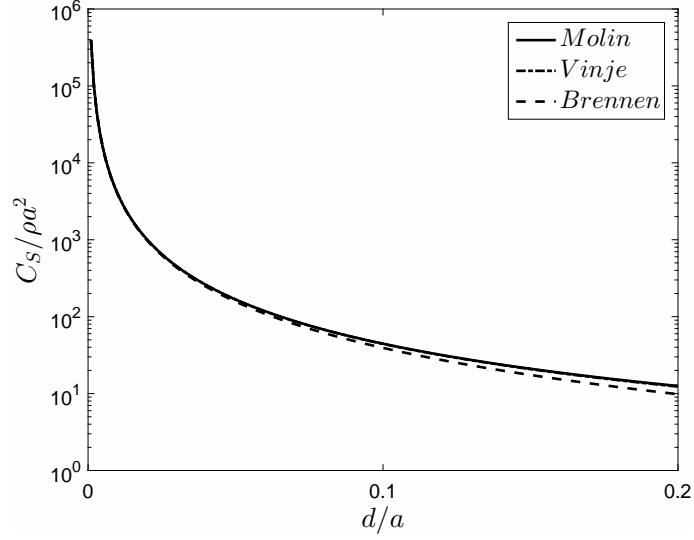


Figure 3.7: Comparison between three analytical cushioning coefficients for a circular disc.

cushioning coefficients $C_S$	
Brennen	$\rho \pi a^2 \left[ \frac{a^2}{8d^2} \right]$
Vinje	$\rho \pi a^2 \left[ \frac{a^2}{8d^2} - \frac{a}{2\pi d} \right]$
Molin	$\rho \pi a^2 \left[ \frac{a^2}{8d^2} - \frac{a}{2\pi d} + \frac{1}{2} \right]$

Table 3.2: Comparison of analytical heave added mass for a circular disc

assumed zero thickness. In our simplified hydrodynamic model 2.1, the cargo-body has a certain draft and is subject to free surface effect. Consequently, more relevant to this simplified hydrodynamic model 2.1 is the classic problem of truncated circular cylinders in finite water depths. This analogy provides a path to solve the more general problems with arbitrary shaped-body with a draft. Another important aspect of circular cylinder theory is that it provides the results for roll/pitch added moment.

For classic problems of truncated circular cylinders, the velocity potential in cylindrical coordinate is expanded by eigenfunctions for interior and exterior solutions, a methodology used by Sabuncu and Calissal [14], Yeung [15].

More recently, Drobyshevski (2004) [16][17] derived theoretical formulations with the structure in extreme shallow water depth conditions and small under-bottom clearance, which is quite consistent with our simplified hydrodynamic model and corresponding hypotheses. Further, he developed a numerical method [18] benchmarked against the theoretical results for circular cylinders, also with the possibility to extend to arbitrary plan bottom.

### DROBYSHEVSKI ANALYTICAL RESULTS

Here we give a detailed introduction of Drobyshevski theory, as it is most relevant to the radiation problem in this thesis. Now, for a truncated circular cylinder of a radius  $a$  and draft  $T$  in water depth  $H$  as illustrated in Fig. 3.8 with a cylindrical coordinate system ( $z$  axis is downward), assuming ideal fluid, the radiation potential is written as:

$$\Phi(x, y, z, t) = \text{Re} \left( \varphi(x, y, z) \cdot e^{i\sigma t} \right) \quad (3.28)$$

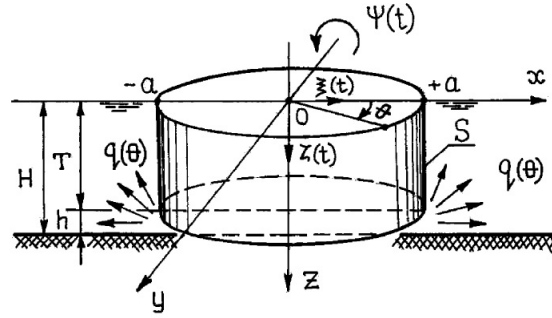


Figure 3.8: Geometric features and coordinate system [17].

The assumptions made in his theory are small gap compared to water depth and same order for radius and water depth:

$$\frac{h}{H} = \varepsilon (\ll 1); \quad \bar{a} = \frac{a}{H} = O(1); \quad \frac{T}{H} = O(1) \quad (3.29)$$

For the spatial potential  $\varphi(x, y, z)$  must be solved through following boundary conditions:

$$\nabla^2 \varphi(x, y, z) = 0 \quad \text{in the fluid domain} \quad (3.30)$$

$$\left( \frac{\partial}{\partial z} + \frac{\sigma^2}{g} \right) \varphi(x, y, 0) = 0 \quad \text{on the free surface } |r| > a; \quad z = 0 \quad (3.31)$$

$$\frac{\partial \varphi}{\partial z} = 0 \quad \text{on the seabed } z = H \quad (3.32)$$

$$\frac{\partial \varphi}{\partial n} = \begin{cases} \cos(n, z) \\ z \cos(n, x) - x \cos(n, z) \end{cases} \text{ for } \begin{cases} i = 3 \\ i = 5 \end{cases} \quad \text{on the body surface} \quad (3.33)$$

To express the Eqs.3.33 in polar coordinates  $(r, \theta)$ , we have:

$$x = r \cos(\theta) \quad y = r \sin(\theta) \quad (3.34)$$

This yields the boundary condition of the body surface assuming a flat rigid bottom:

$$\frac{\partial \varphi}{\partial r} = f_i(z, \theta) = \begin{cases} 0 \\ z \cos(\theta) \end{cases} \text{ for } \begin{cases} i = 3 \\ i = 5 \end{cases} \quad \text{on the side surface} \quad (3.35)$$

$$\frac{\partial \varphi}{\partial z} = g_i(z, \theta) = \begin{cases} 1 \\ -r \cos(\theta) \end{cases} \text{ for } \begin{cases} i = 3 \\ i = 5 \end{cases} \quad \text{on the bottom} \quad (3.36)$$

Indeed, looking from far away, the gap tends to be zero as the cylinder occupies the whole water depth vertically. For the flow just beneath the cylinder bottom and far from the edge, it can be considered as 2D flow. These are defined as outer domain with several unknowns.

In the outer domain, the velocity potential consists of two parts:  $\varphi_1(x, y, z)$  representing the side surface of the cylinder part extending over the whole water depth,  $\varphi_2(x, y, z)$  the under bottom flow part.

$$\varphi(x, y, z) = \varphi_1(x, y, z) + \varphi_2(x, y, z) \quad (3.37)$$

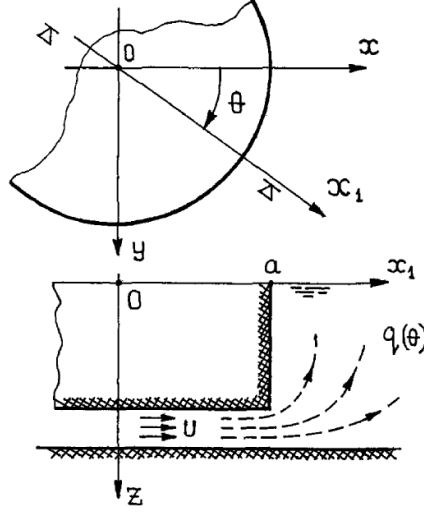


Figure 3.9: Local inner flow coordinates [17]

Each part can be expressed in the following equation, satisfying boundary conditions on the free surface and seabed:

$$\varphi(x, y, z) = G_0(x, y) \cdot Z_0(z) + \sum_{m=1}^{\infty} G_m(x, y) \cdot Z_m(z) \quad (3.38)$$

For the flow under the structure bottom, the velocity potential is expressed as a series of vertical coordinate  $(z - H)$ , which is of small value due to small gap.

$$\varphi(x, y, z) = \varphi^{(0)}(x, y) + (z - H)\varphi^{(1)}(x, y) + (z - H)^2\varphi^{(2)}(x, y) + O((z - H)^3) \quad (3.39)$$

For the inner domain, namely near the cylinder bottom edge. the fluid flow is normal to the cylinder surface with very slow change in  $\theta$ -direction. Thus a constant unknown must be added to properly match the outer domain solutions. To use conformal mapping, a local 'stretched' coordinate is introduced (Fig. 3.9). Similar to 2D problem, the expansions near the edge of cylinder are expressed here:

$$\varphi(x_1, y)|_{(x_1-a) \rightarrow -\infty} = |U(\theta) + f(H, \theta)| \cdot (x_1 - a) - \frac{2U(\theta)h}{\pi} (1 - \log 2) + C(\theta) \quad (3.40)$$

$$\varphi(x_1, y)|_{(x_1-a) \rightarrow +\infty} = \frac{2U(\theta)h}{\pi} \log|w| - \frac{2U(\theta)h}{\pi} \log\left(\frac{2h}{\pi}\right) + f(H, \theta)(x_1 - a) + C(\theta) \quad (3.41)$$

where  $w = \sqrt{(x_1 - a)^2 + (z - H)^2}$ .

To solve inner and outer potentials, their appropriate expansions must be matched. With the small gap assumption, this reminds us of the matched asymptotic technique used in section 3.1 by Molin. The gap height  $h$  for the first order is retained during the asymptotic matching process. After solving all the unknowns of the potentials, the hydrodynamic coefficients are obtained by integrating potential over the surface of the cylinder. For brevity, the added mass for heave and pitch modes are listed in Eqs. 3.42, 3.43.

Heave mode:

$$\mu_{33} = \rho\pi a^3 \left[ \frac{a}{8h} + \frac{1}{\pi} \left[ 1 - \ln\left(\frac{4h}{H}\right) \right] + \frac{J_0(\lambda_0)J_1(\lambda_0) + N_0(\lambda_0)N_1(\lambda_0)}{(u_0 + \sinh u_0 \cosh u_0) (J_1^2(\lambda_0) + N_1^2(\lambda_0))} - F_0 \right] \quad (3.42)$$

where  $F_0 = \sum_{m=1}^{\infty} \left[ \frac{K_0(\lambda_m)}{K'_0(\lambda_m)} \frac{1}{(u_m + \sin u_m \cos u_m)} + \frac{1}{m\pi} \right]$

Pitch mode:

$$\begin{aligned} \mu_{55} = & 2\rho\pi a^2 H^3 \left\{ \frac{1}{2} \left[ \bar{q}^{(1)} \frac{a}{H} + \frac{a^2}{2H^2} + \frac{h}{H} \right] + \frac{a^2}{8H^2} \left[ \frac{7}{24} \frac{a}{h} \frac{a}{H} + \bar{q}^{(1)} \frac{a}{h} \right] \right. \\ & + \frac{(\cosh u_0 - 1) A^{(1)}(\lambda_0)}{(u_0 + \sinh u_0 \cosh u_0)} \left[ \frac{(\cosh u_0 - 1)}{\cosh u_0} + \lambda_0 \bar{q}^{(1)} - \lambda_0 \bar{q}^{(2)} \frac{A^{(2)}(\lambda_0)}{A^{(1)}(\lambda_0)} \right] \\ & \left. + \sum_{m=1}^{\infty} \frac{(1 - \cos u_m)(1 - \cos u_m)/u_m + \lambda_m \bar{q}^{(1)}}{u_m^2 (u_m + \sin u_m \cos u_m)} \frac{K_1(\lambda_m)}{(K_1(\lambda_m) + \lambda_m K_0(\lambda_m))} \right\} \end{aligned} \quad (3.43)$$

We note that for heave and pitch modes, a separation of frequency-dependent added mass is possible essentially because some terms including  $u_0$ ,  $u_m$ ,  $\lambda_0$ ,  $\lambda_m$  ( $u_0 = \alpha_0 H$ ,  $u_m = \alpha_m H$ ,  $\lambda_0 = \alpha_0 a$ ,  $\lambda_m = \alpha_m a$ ) are related to dispersion relations:

$$\alpha_0 \tanh(\alpha_0 H) = \frac{\sigma^2}{g} \quad (3.44)$$

$$\alpha_m \tan(\alpha_m H) = -\frac{\sigma^2}{g} \quad (3.45)$$

where  $\sigma$  is the frequency.

Here we give the result of frequency-independent added mass as a function of gap height. This frequency-independent part is constant given water depth  $H$ , cylinder radius  $a$  and gap height  $h$ . Intuitively, this constant part corresponds to the added mass due to gap flow only. And the total added mass minus the constant part is the frequency part, corresponding to free surface effect.

**Heave mode:**

$$\mu_{33} = \rho\pi a^3 \left[ \frac{a}{8h} + \frac{1}{\pi} \left( 1 - \ln \left( \frac{4h}{H} \right) \right) \right] \quad (3.46)$$

**Pitch mode:**

$$\mu_{55} = \rho\pi a^5 \left[ \frac{7}{96} \frac{a}{h} + \frac{H}{2a} + \frac{hH^2}{a^3} \right] \quad (3.47)$$

Drobyshevski (2006) [18] further investigated a numerical implementation of the fore-mentioned theory for truncated circular cylinder close to seabed. This numerical tool can also be used for vertical sided body with arbitrary bottom shape.

The main technique for this theory requires only discretization the contour line into  $N$  small segments. Then by matching expansions of the potentials for both outer and inner domains, the integral equation for the unknown source strength will be solved numerically (also see [19], [20]). With solved source strengths from two-dimensional integration equation, the potentials will be determined, thus obtaining all hydrodynamic coefficients.

As assumed in 3.29, the accuracy of Drobyshevski theory depends on gap height and radius-to-draft ratio. The smaller the gap height is, the more accurate the results are. The accuracy will also be increased if we have a very wide structure.

### 'NEW METHOD' THEORY

The new method proposed by De Jonge [21] is a combination of Drobyshevski numerical code (AMP, asymptotic matching program) for under bottom domain and potential software Delfrac for the outer domain. Two reasons that we combine AMP and Delfrac:

- AMP computes gap flow part much faster than Delfrac as Delfrac requires a very large number of panels for the bottom of the structure. AMP essentially deals with two-dimensional flow.
- Delfrac can include free surface effect and non-vertical sided structure, thus eliminating the restrictions for AMP. Delfrac essentially deals with three-dimensional flow.

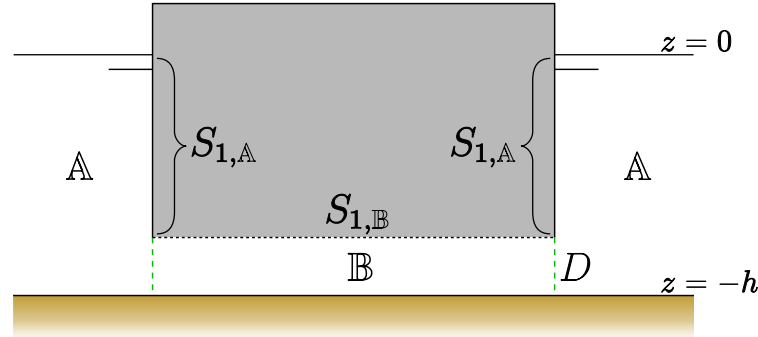


Figure 3.10: Domain boundary definitions [2]

Now, to connect AMP and Delfrac in a interactive way, the technical procedures are outlined here:

1. AMP is used to compute flow velocity due to vertical motions of the structure with a certain gap height. Thus flow velocity anywhere around the contour of the bottom is known as the boundary conditions for  $D$  indicated by Fig. 3.10.
2. Delfrac is used to obtain velocity potential for panels on  $S_{1,A}$  and  $D$ , with velocity input at boundary  $D$  from previous step. Thus, all the hydrodynamic coefficients and loading will be immediately known with pressure for each panel on  $S_{1,A}$  and  $D$ .
3. With pressure input at boundary  $D$  from Delfrac calculation, AMP computes the velocity potential for the under-bottom surface  $S_{1,B}$ , thus obtaining all the hydrodynamic coefficients and loading for  $S_{1,B}$ .
4. Postprocess hydrodynamic data from  $S_{1,A}$  and  $S_{1,B}$ .

### 3.3. TIME DOMAIN THEORY

The convolution method is introduced here as it is used to compute radiation force in time domain. It is a more general method taking into account the non-linear response and requiring no de-couple at wave frequency for a time history solution. Basically, with convolution method, the approximation for the linear response at wave frequency will be overridden by non-linear response with instantaneous amplitude. For the gap problem in this thesis, it is necessary to use convolution method for a time domain simulation. Moreover, by using the convolution method, the relationship between added mass at infinite frequency and at maximum frequency will be understood.

The general motion equation in time domain with convolution has the following expression:

$$\{m + A_{\infty}\} \ddot{X}(t) + c\dot{X}(t) + kX(t) + \int_0^t h(t-\tau) \ddot{X}(\tau) d\tau = F(t) \quad (3.48)$$

where  $m$  is the body mass and  $A_{\infty}$  is the added mass at infinite frequency,  $c$  is the damping matrix and  $k$  is the stiffness matrix.

The radiation force is expressed as the convolution form, in which  $h(t-\tau)$  is the Convolution Integral Function (CIF):

$$h(t) = -\frac{2}{\pi} \int_0^{\infty} B(\omega) \frac{\sin(\omega) t}{\omega} d\omega = \frac{2}{\pi} \int_0^{\infty} \{A(\omega) - A_{\infty}\} \cos(\omega t) d\omega \quad (3.49)$$

With zero forward speed, the damping  $B$  and added mass  $A$  are mutually derivable. This indicates that if damping is known, the added mass can be derived via Kramer-Konig relations (or, Hilbert transform) and vice versa. By Hilbert transformation, the imaginary part (damping) and real part (added mass) can be obtained from each other as the complex function is in the upper half-plane:

$$\begin{aligned} \{A(\omega) - A_{\infty}\} &= \frac{1}{\pi} c\nu \int_{-\infty}^{\infty} \frac{[B(f)]}{f(f-\omega)} df \\ \left[ \frac{1}{\omega} B(f) \right] &= -\frac{1}{\pi} c\nu \int_{-\infty}^{\infty} \frac{\{A(\omega) - A_{\infty}\}}{(f-\omega)} df \end{aligned} \quad (3.50)$$

where  $c\nu$  is the Cauchy principle value.

Now, we will brief discuss why the **separation of frequency** is needed for time domain simulations.

To include time-varying, i.e., gap-height-varying, added mass in the time domain simulation, the separation of frequency must be done due to two things:

- The impulse function will remain untouched as the kernel  $\{A(\omega) - A_{\infty}\}$  is mainly dependent on frequency and independent of gap flow.
- The added mass at infinite frequency  $A_{\infty}$  for the first left term of the equation 3.48 is time-variant because for instance if the gap height reduces when the body moving downward, the added mass due to gap flow is significant larger.

Constant part	Frequency-dependent part
$A_{\infty}(t)$	$A(\omega) - A_{\infty}$

### 3.4. NON-LINEAR MODEL FOR GAP PROBLEM

#### 3.4.1. ASSUMPTIONS

The hydrodynamic properties of a cargo during HTV offshore charge and loading are dependent on a large group of various parameters, making it implausible to exhaust all the possible combinations due to theoretical difficulties and the sheer amount of work involved. Thus, along with the simplified physical model, several assumptions have been proposed based on engineering practice and related works.

- The deck of HTV is horizontally flat and water depth above the deck is fixed and extremely shallow. The vertical motions of the cargo shall represent relative vertical motions between HTV and the cargo, treating HTV deck as a fixed and horizontal seabed, namely, the 'artificial' bottom;
- The gap between the cargo and HTV is comparably much smaller than the cargo bottom size;

- The bottom of the cargo is flat without protuberance and simply connected. The sides of the cargo are largely vertical and enclosed, indicating no 'holes' exist on the submerged part;
- Diffraction force is independent of gap flow, thus subject to linearization.(Diffraction)
- The influence of oscillation amplitude is linearized. (KC Influence)

#### DIFFRACTION

The general equation describes the forces associated with radiation problem. In principle, by applying Haskind-Newman formula, the diffraction part can be obtained immediately. In this thesis, the diffraction problem is linearized, largely independent of gap height. Thus, it can be handled in the standard diffraction programme.

#### KC INFLUENCE

The influence of oscillation amplitude on added mass, indicated by KC number, is linearized with the assumption that the oscillation at each time step is considerably small that added mass remains constant within that time step. Thus, for each time step, it corresponds to a new gap height, leading to a new added mass, eliminating the influence of KC number.

#### 3.4.2. MODEL INTERPRETATION

Starting from time-domain equation, the prediction of non-linear behaviour, in which gap flow is involved, can be improved by implementing a gap-dependent function in the time-domain solution, where the gap flow characteristics are separated in a frequency-dependent part and gap-dependent (frequency-independent) part.

Hydrodynamic components	Physical phenomenon	Variables
Frequency-dependent part	Free surface effect	Frequency
Frequency-independent part	Gap flow	Gap height, asymmetry, shape factor

Table 3.3: Dichotomy of hydrodynamic coefficients

**The main line of this thesis work will be two-fold: first, to prove that free surface effect is independent of gap flow; second, to quantify the gap flow part with variables.**

#### FREE SURFACE EFFECT

The general equation by Molin is derived for the deeply submerged disc, disregarding the free surface effect. Thus the general equation contains no information on frequency.

For our cargo system, the free surface effect cannot be ignored as the cargo piercing out of water, has a certain draft. Physically, as the cargo oscillates, it will generate radiated waves, which are frequency dependent. The circular cylinder theory from Drobyshevski is more relevant to the cargo problem in this thesis.

Take analytical heave added mass from Drobyshevski for instance: the last two terms in Eqs. 3.51 are frequency dependent. But in Molin, his heave added mass is frequency independent.

$$\mu_{33} = \rho \pi a^3 \left[ \frac{a}{8h} + \frac{1}{\pi} \left[ 1 - \ln \left( \frac{4h}{H} \right) \right] + \frac{J_0(\lambda_0) J_1(\lambda_0) + N_0(\lambda_0) N_1(\lambda_0)}{(u_0 + \sinh u_0 \cosh u_0) (J_1^2(\lambda_0) + N_1^2(\lambda_0))} - F_0 \right] \quad (3.51)$$

With frequency-independent hydrodynamic coefficients in the general equation accommodated in time-domain simulations, the separation of frequency-dependent part should first be made properly.

Consequently, the frequency-dependent hydrodynamic coefficients must be assessed to prove that the frequency-dependent part will be largely independent of gap flow part.. This topic will be handled in the next chapter.

#### GAP FLOW

As mentioned in the introductory Chapter 1, the key objective of this thesis is to investigate offshore discharge and loading problem in time domain. For time domain simulation, the hydrodynamic coefficients, for instance, added mass, are input as the constant matrix. This is more or less true for conventional time-domain hydrodynamic analysis as the input added mass matrix in most cases are time independent. But in this thesis, the added mass will be time-varying, which must be updated in time domain equation. It should be noted that here the added mass is at infinite frequency with a constant value.

Below is the list of three important parameters associated with gap flow part:

- **Gap Height:** for our physical model, the gap height has a significant influence on added mass, thus leading to a time-variant added mass during time-domain simulation as the gap height varies due to cargo vertical motions. For instance, in time domain, if the gap height is diminished from 1[m] to 0.5[m], the heave added mass for a circular disc is twice larger, based on 3.23,  $M_{33} = \rho\pi a^3 \left[ \frac{a}{8d} \right]$ . This time-variant added mass w.r.t gap height must be considered in the time domain model. Moreover, the cushioning load  $-\frac{1}{2} \frac{dM_{33}}{dh} \dot{X}^2$  is an unconventional force which is not included in time domain programme.
- **Asymmetry:** the general equation implicitly assumes a parallel cargo and seabed, i.e constant gap height w.r.t  $(x, y)$  coordinates. This omits the situation that when the cargo is inclined to a certain angle, the added mass term might be different from parallel cases. It will not be a rare case as the cargo subject to waves often has some inclined angles.
- **Arbitrary Shape:** the theoretical efforts made in this chapter focus on the very simple geometry, namely circular shape. For a cargo with arbitrary bottom shape, the form of the general equation might be different. New method can be used for this issue.

With calculated constant added mass for gap flow part, the general force equation given in thin disc theory [4] can be used to formulate external force for the model here. This general equation 3.52 is fundamental to describe the hydrodynamic properties of one-body (cargo) in extremely shallow water depth with very small gap height.

$$F = -M_{33}\ddot{X} - \frac{1}{2} \frac{dM_{33}}{dh} \dot{X}^2 - F_b \quad (3.52)$$

Three components are identified for forced heave motions, each corresponding to a different physical mechanism.

- $-M_{33}\ddot{X}$  is the inertial force with heave added mass  $M_{33}$ .
- $-\frac{1}{2} \frac{dM_{33}}{dh} \dot{X}^2$  is the cushioning force due to variation of added mass w.r.t gap height. The cushioning force is associated with velocity squared.
- $-F_b$  is the damping force, secondary to dominant inertial force.

The damping force  $F_b$  is non-dominant compared to the inertial effects. Molin proposed a Morison-like drag force to compensate for the discrepancy between model test data and the theoretical formulation:

$$F_D = -\frac{1}{2}\rho C_D (2\pi R d) \frac{R}{2d} \left| \frac{UR}{2d} \right| = -\frac{\pi}{2}\rho C_D \frac{R^3}{d} U|U| \quad (3.53)$$

Molin used  $C_D = 1$  for his circular disc case. Peters [2] found from model test that the drag coefficient in Eqs. 3.53 is inversely proportional to heaving velocity:  $C_D = \frac{1.5}{|U|}$ . Then we have the drag force:

$$F_D = -\frac{3\pi}{4}\rho \frac{R^3}{d} U \quad (3.54)$$

The evaluation of damping force is not within the scope of this thesis. For time domain simulation, the empirical value from the above will be used.

# 4

## SEPARATION OF FREQUENCY

This chapter tackles the problem on frequency separation, as shown in Tab. 3.3. Two merits should be achieved by the separation:

- Understand further the hydrodynamics of gap part.
- Prepare for the time domain simulations in AQWA.

A more direct explanation for why separation of frequency is needed lies in the fact that since free surface effect is largely linearized and well accommodated in 3D potential theory and gap flow part is strong influenced by non-linearity, by separation, this non-linearity of gap part can be treated in time-domain.

The main numerical tools used in this chapter are AQWA and New method. First, before doing the separation, the key prerequisite is to validate the use of New method and AQWA. Second, if the prerequisite is satisfied, care must be taken to assess the interaction between gap part and free surface part. A complete separation is only possible when the use of New method is allowed and the interaction between gap and free surface is negligibly small.

### 4.1. APPLICABILITY OF NEW METHOD

Both AQWA and New method are employed here to evaluate the hydrodynamic coefficients. Ideally, the use of New method is more relevant as far as gap part concerned. This is due to following reasons: first the computation time can be greatly saved by use of New method, second the New method is more suitable to deal with situations for extreme small gap height. For instance, with a gap height of  $0.25[m]$  case calculated by the same computer, it took AQWA two hours to get all the hydrodynamic coefficients while only taking New method a few minutes. The meshing efforts for the body bottom are also immense for AQWA with such small clearance to seabed, thus leading to very fine panels. For New method, it only requires a 2D mesh of contour line for the body bottom.

It must also be noted that New method, similar to AMP, is subject to limitations or hypothesis of Drobyshevsky theory for truncated circular cylinder.

All these advantages associated with New method are only necessary when results from New methods are sufficiently accurate. To assess this, comparing AQWA and New method is the theme of the section here. In a way, AQWA and New method are mutually verified against each other.

#### 4.1.1. EVALUATION DEFINITION

The evaluated cases are defined here as two truncated circular cylinders, with the same radius of 20[m] for both. The draft is taken as 5[m] and 15[m], respectively. With draft unchanged, the gap heights are created by varying the water depth. Below is a brief summary of all the relevant definitions:

Cylinder case	Draft [m]	Radius [m]	Gap height range[m]	Water depth range[m]
case 1	5	20	0.25 – 4.0	5.25 – 9.0
case 2	15	20	0.25 – 4.0	15.25 – 19.0

Table 4.1: Evaluation cases

The frequencies will be dimensionalized as  $k_0R$ , where  $k_0$  is the wave number. Dimensionless added mass for heave and pitch modes are expressed with draft  $T$  and radius  $R$ :

$$\overline{M}_{33} = \frac{M_{33}}{\rho\pi R^2 T} \quad (4.1)$$

$$\overline{M}_{55} = \frac{M_{55}}{\rho\pi R^2 T^3} \quad (4.2)$$

The relative error is computed for the largest frequency ( $2.5rad/s$ ):

$$RD = \frac{AQWA - Drobj}{Drobj} \times 100\% \quad (4.3)$$

#### 4.1.2. HEAVE MODE

Comparison between AQWA and New method for heave mode shows that the total added mass compares quite well for almost all the gap heights for both case 1 and case 2, see Fig. 4.1a and 4.1b. The minor difference for extreme small gap height 0.25[m] in both cases indicate the relative inaccuracy of AQWA due to difficulties aroused by the small clearance to seabed. The immediate question about relative accuracy of AQWA and New method is answered in Fig. 4.2.

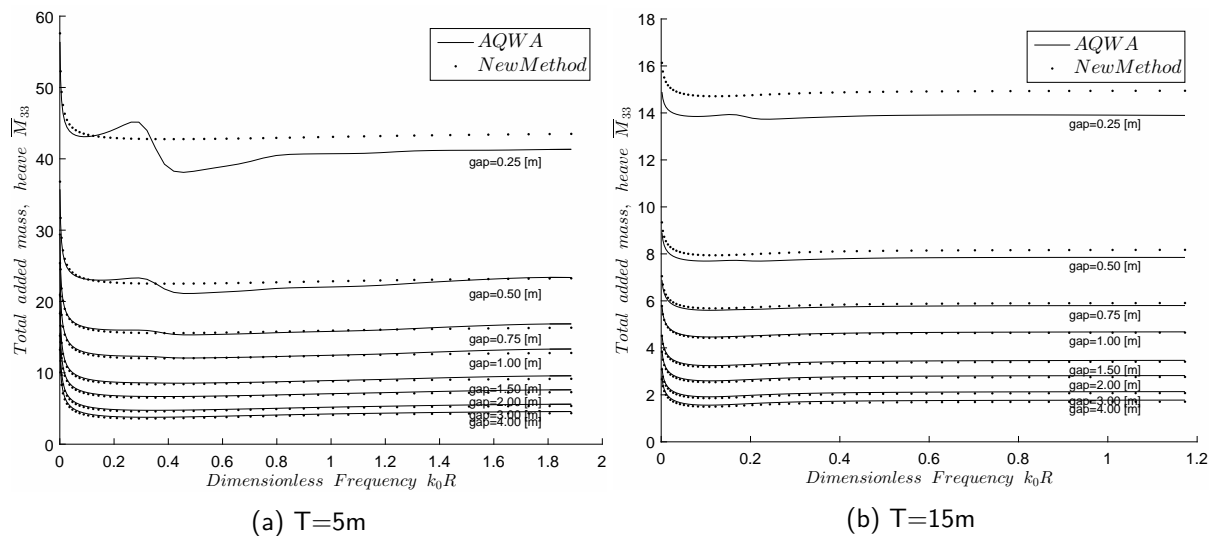


Figure 4.1: Comparison for heave added mass

The curve trend in Fig. 4.2 shows that with gap height increased from 0.25[m] to 4.00[m], relative errors also increase from negative to positive values. Remind that New method is mainly developed to compute hydrodynamic coefficients for very small gap heights whereas AQWA is more accommodating with large gap heights. This explains the relatively accurate New method over AQWA for small gap heights and vice versa for large gap heights. Besides, for both cases, AQWA and New method are almost identical around 1.00[m] gap height, which can be seen as the critical point in Fig. 4.2.

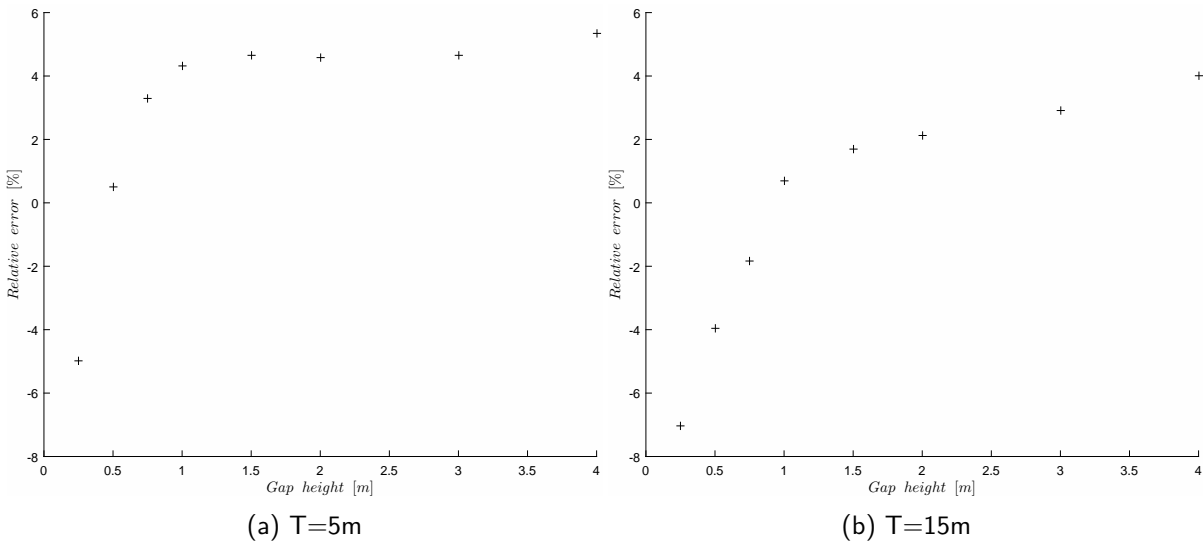


Figure 4.2: Relative difference between AQWA and New method, heave

4.1.3. PITCH MODE

Analogous to heave mode, the comparison between AQWA and New method for pitch mode has shown the same characteristics for both cases in Fig. 4.3a and 4.3b. The relative error range for pitch mode is even smaller than that of heave mode and relative error trends are consistent for both heave and pitch, shown in Fig. 4.2 and 4.4.

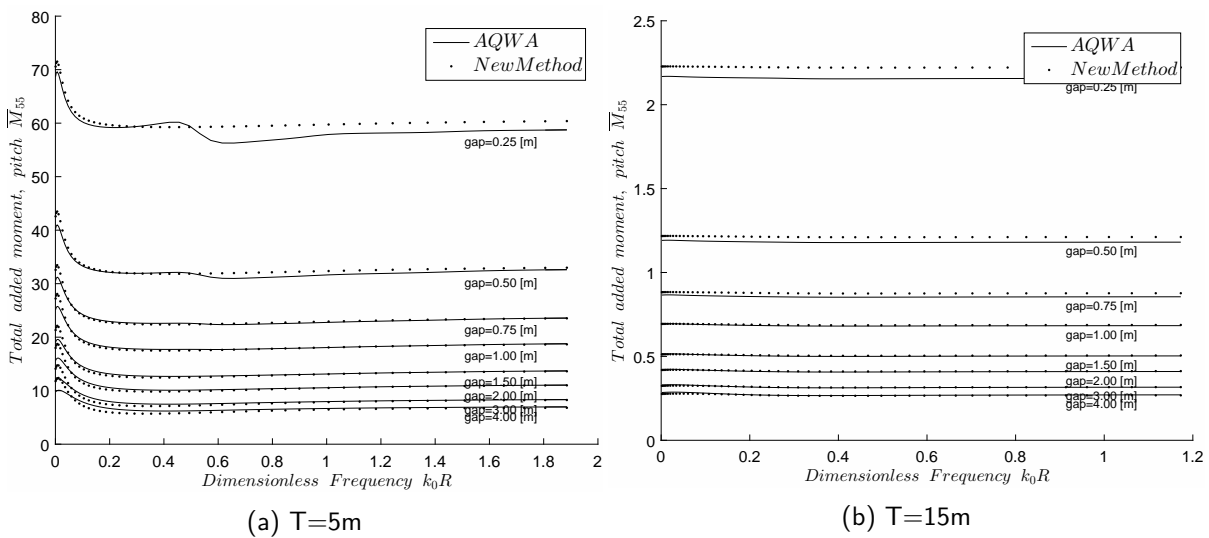


Figure 4.3: Comparison for pitch added mass

It should be worth noting that for both case 1 and case 2, the rotation axis is on the free surface with origin at the center of the circular cylinder. Unlike heave mode in Fig. 4.1a and 4.1a where the change of draft does not change the curve shape of total added mass, for pitch mode, its curve shape for case 1 with the draft of 5[m] gives a marked difference from that of case 2 with the draft of 5[m]. For the latter, the curve is almost constant for all frequencies, see Fig. 4.3b.

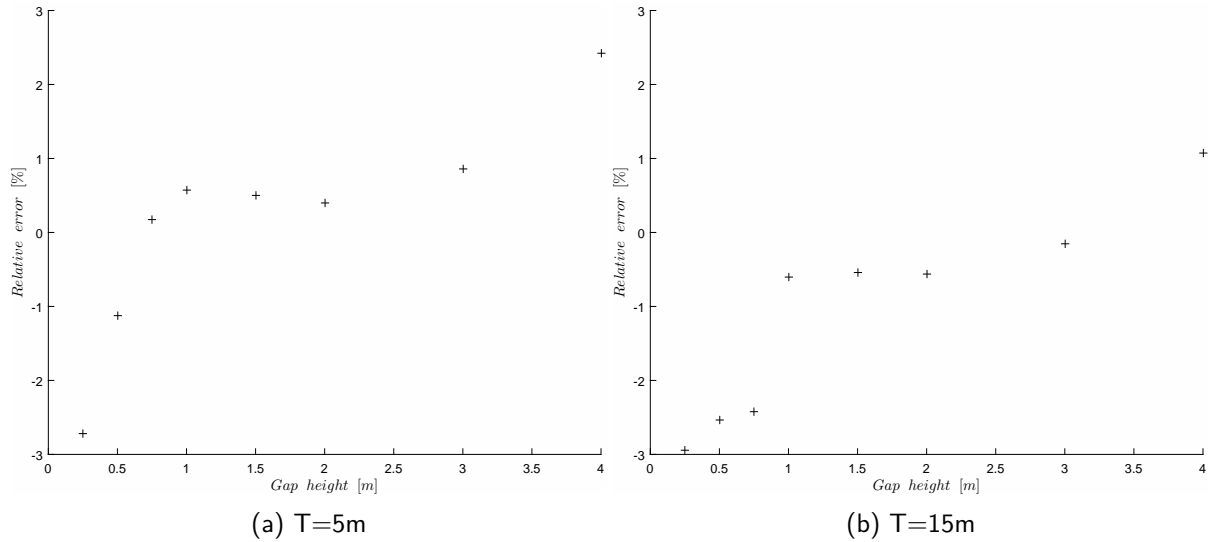


Figure 4.4: Relative difference between AQWA and New method, pitch

## 4.2. SEPARATION METHODS

### 4.2.1. USE OF NEW METHOD

The outline of New method is described in Chapter 2. In new method, the contributions from different potential terms will be divided into two categories: frequency part and constant part. Remind that these two parts corresponds to two distinct mechanisms: frequency part for free surface effect and constant part for gap flow problem, see Tab. 3.3. Identifying any one of the two parts will make separation of frequency possible. This method can be used for any arbitrary shape.

The previous section has validated the use of New method as an accurate way of evaluating hydrodynamic coefficients in this thesis. New method is considerably faster than AQWA and more reliable for small gap heights, which are most relevant to the thesis topic,. Now using New method solely, the next step is to tackle the focus of this chapter: separating the frequency part.

### 4.2.2. EVALUATION OF FREE SURFACE EFFECT

The evaluation of free surface effect with varied gap heights help to assess the non-linearity of frequency part. The implicit assumption for complete separation is that free surface effect is virtually independent of what happened inside the gap. If the interaction between free surface and gap flow is strong, the distinct separation will not be feasible. If the weak non-linearity is found, the frequency part shall be conveniently handled as a fixed initial input in time domain.

The added mass evaluated in New method can be decomposed into two parts: frequency part and constant part. The frequency part corresponds to free surface effect and the constant part gap flow problem. Remind that New method is not a stand-alone program but a synthesis of AMP and Delfrac, as explained in Chapter 2. AMP deals with the gap flow part and Delfrac is

more about frequency-dependent part. In New method, the total added mass consists of 6 terms, of which the first four terms are identified as constant part, which and the last two terms are frequency-dependent, computed in Delfrac.

In this section, the free surface effect with varied gap heights will be assessed, i.e., to examine the influence of gap flow on free surface. Again, the two circular cylinders cases are used here.

As shown in Fig. 4.5-4.8, the frequency part is varying with gap height. The added mass of frequency part with the smallest gap height has the largest value.

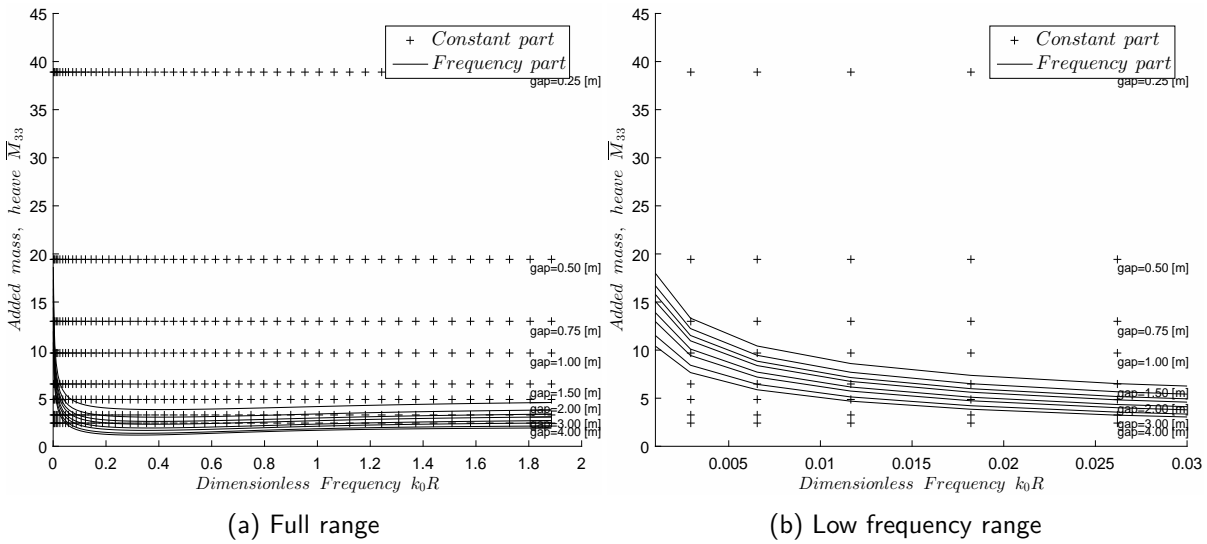


Figure 4.5: Comparison between constant and frequency part, Heave, T=5m

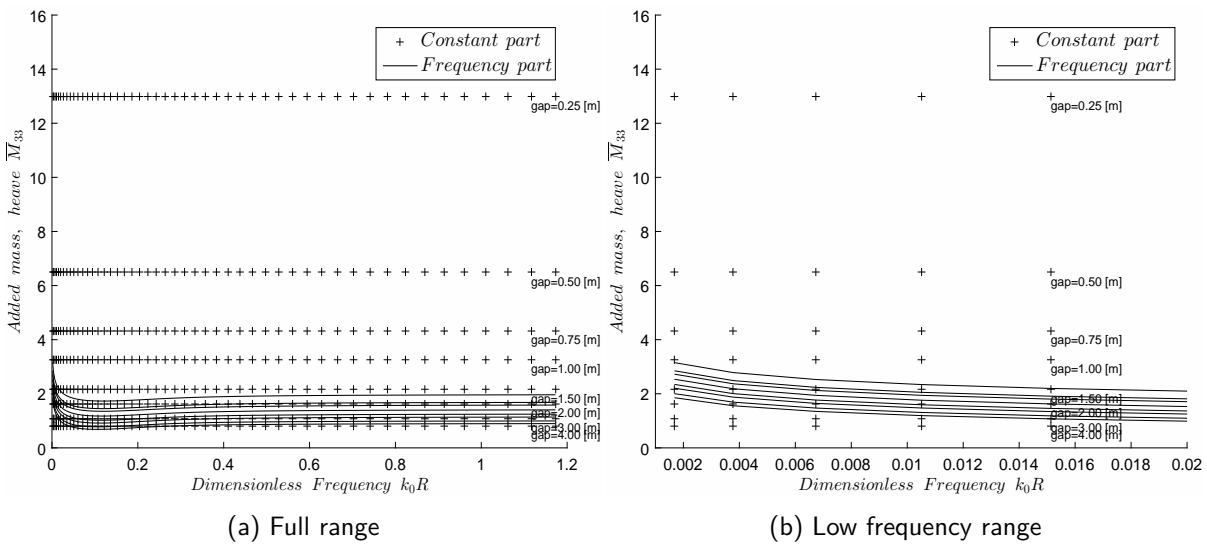
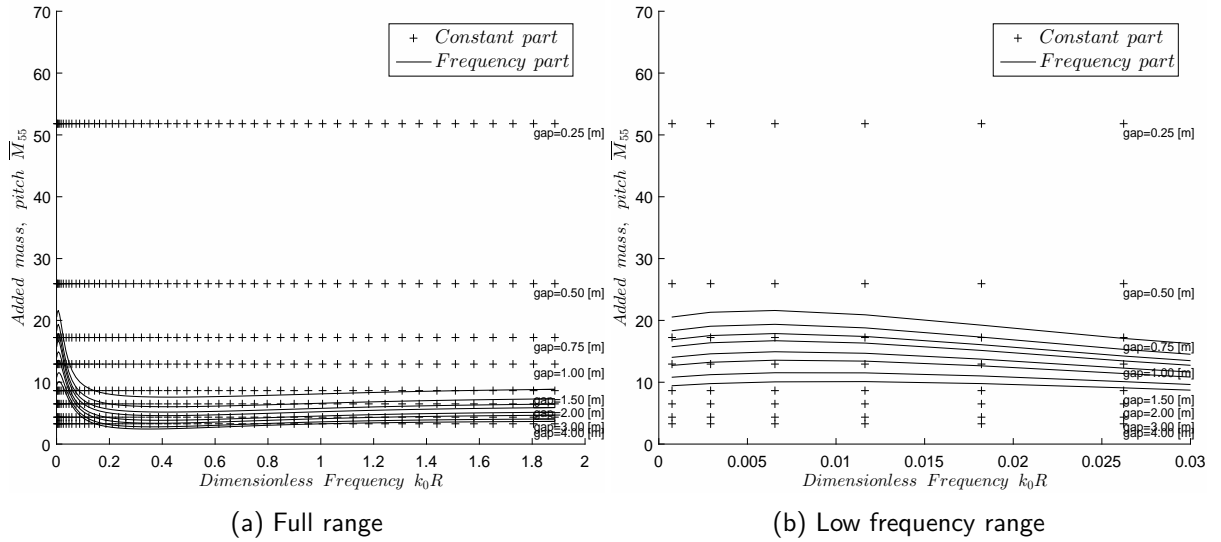
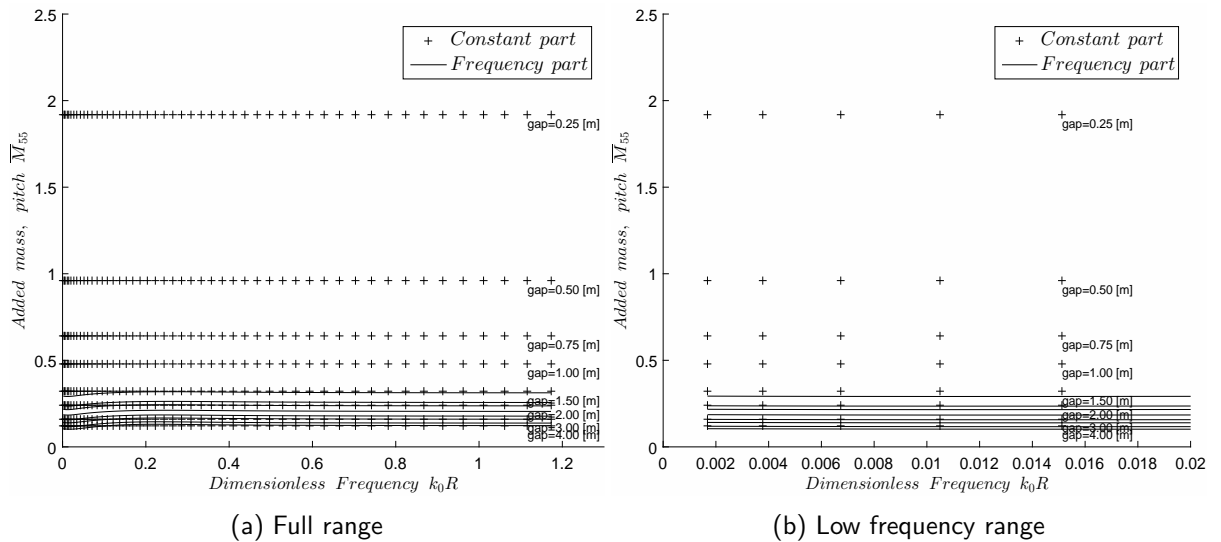


Figure 4.6: Comparison between constant and frequency part, Heave, T=15m

For the full range, the frequency part will not converge for different gap heights. For the low frequency range, the difference between frequency parts from varied gap heights is further enlarged. A deeply-drafted cylinder as in case 2 shows less variational frequency part than that in case 1. Nevertheless, the emphasis here is that the variation of frequency part is only weakly non-linear with gap height. Clearly, the frequency part slightly varies with different gap heights.

Two things must be understood here as the separation is done via New method:

Figure 4.7: Comparison between constant and frequency part, Pitch,  $T=5m$ Figure 4.8: Comparison between constant and frequency part, Pitch,  $T=15m$ 

- For small gap heights, the contribution of frequency part to total added mass is much smaller than that of constant part.
- For very low frequency range, the frequency part's contribution to total added mass becomes significant, especially for the case 1 with a smaller draft, shown in Fig. 4.5b and 4.7b.

It must be noted that the constant part for both heave and pitch modes is inversely proportional to gap height:  $M_A \propto \frac{1}{h}$ , according to the theory of New method.

#### 4.2.3. SEPARATION AT INFINITE FREQUENCY

Instead of doing the separation in strict physical terms as shown in previous Section 4.2.2, the separation here will be at infinite frequency, as consistent with convolution method in time domain solver..

It is worth noting that here the added mass at maximum frequency (i.e.,  $2.5 \text{ rad/s}$ ) is used instead of added mass at infinite frequency. The difference is negligible. In principle, it is also possible to obtain added mass at infinite frequency in convolution integration method, as introduced with more details in Chapter 3.

The immediate question on how to evaluate added mass at infinite frequency arises as the added mass obtained from frequency-domain analysis has only a limited range of frequencies because the upper limit of frequency is restricted by panel size and wave length. In AQWA time domain solver, the upper limit is around  $\omega_u = 10 \text{ rad/s}$ . To guarantee an accurate evaluation for  $A_\infty$ , a 'best' fit technique is employed:

- First, radiation damping in the frequency range  $[\omega_0, \omega_n]$  is computed in conventional frequency domain hydrodynamic analysis.
- For radiation damping, the total needed frequency range should be  $[0, \omega_u]$ . An extra observation indicates that radiation damping at zero and infinite frequency are virtually zero.
- By extrapolating the damping coefficients, expressed as a set of exponential functions and polynomials, to the low frequency range  $[0, \omega_0]$  and high frequency range  $[\omega_n, \omega_u]$ , the radiation damping in the full range from 0 to  $\omega_u$  is obtained.
- With the obtained damping in previous step, the added mass is then transformed by the Kramer-Konig relations Eq. 3.50.
- The transformed added mass will fit the computed added mass in the range  $[\omega_0, \omega_n]$  with a polynomial smoothing function, thus updating the transformed added mass for the low frequency range  $[0, \omega_0]$  and high frequency range  $[\omega_n, \omega_u]$ . Then the added mass at infinite frequency is obtained.

In principle, in time domain simulations,  $A_\infty$  should be used. For the computed cases for gap part in this thesis, we use added mass at the maximum frequency  $2.5 \text{ rad/s}$ , from the frequency domain results. The difference is completely negligible, at least for those computed cases. But it is often safer to check the consistency between  $A_\infty$  and  $A_{max}$ .

The separation at infinite frequency is required for time-domain simulations. For calculation purpose, the frequency part is obtained by subtracting the total added mass at each frequency with the added added mass at infinite frequency. In our cases, the largest frequency defined in the input file will be used. The difference between largest frequency and infinite frequency is negligible.

It must also be noted here that the separation is done via New method as it is much more efficient and has no limitations on very small gap heights. For heave and pitch modes, results for case 1 & 2 are shown in Fig. 4.9-4.12.

#### HEAVE MODE

For heave mode, comparisons between frequency part and constant part at infinite frequency are made for both case 1 and case 2. The variational range of constant part at infinite frequency is significantly larger than the range of frequency part. It has been shown in Fig. 4.9a and 4.10a that the main contribution to total added mass comes from constant part except for low frequency range, which can be seen more clearly in Fig. 4.9b and 4.10b. For case 1 in Fig. 4.10b, the frequency part is only slightly influenced by gap height variations for the first few frequencies.

For case 2 in Fig. 4.10b, the influence on frequency part due to gap height variations is negligible. This can be explained by the fact that for the 15-meter-drafted circular cylinder, the gap part can hardly influence the frequency part.

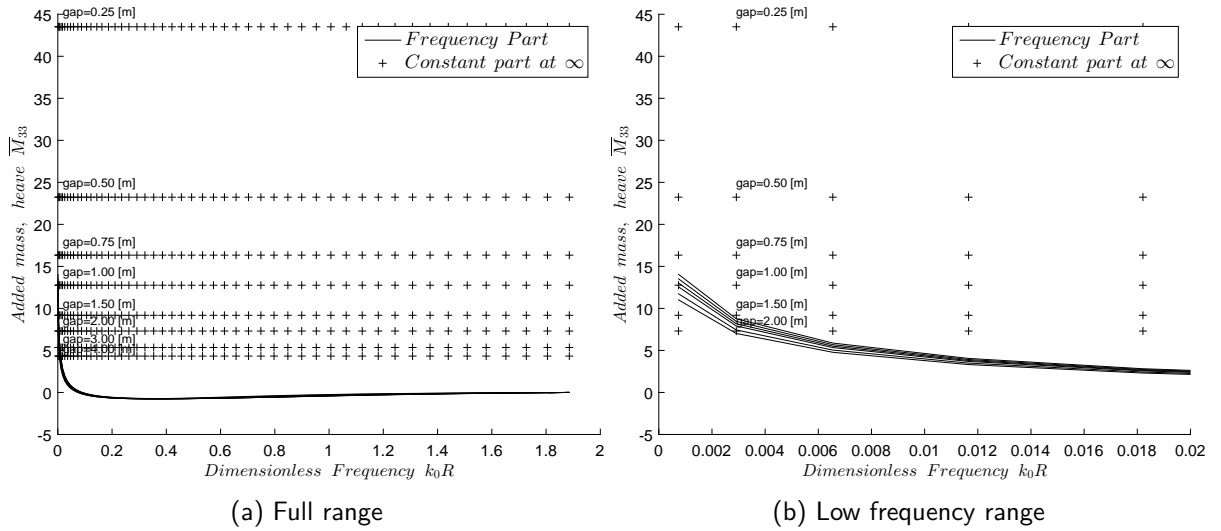


Figure 4.9: Comparison between constant and frequency part, Heave, T=5m

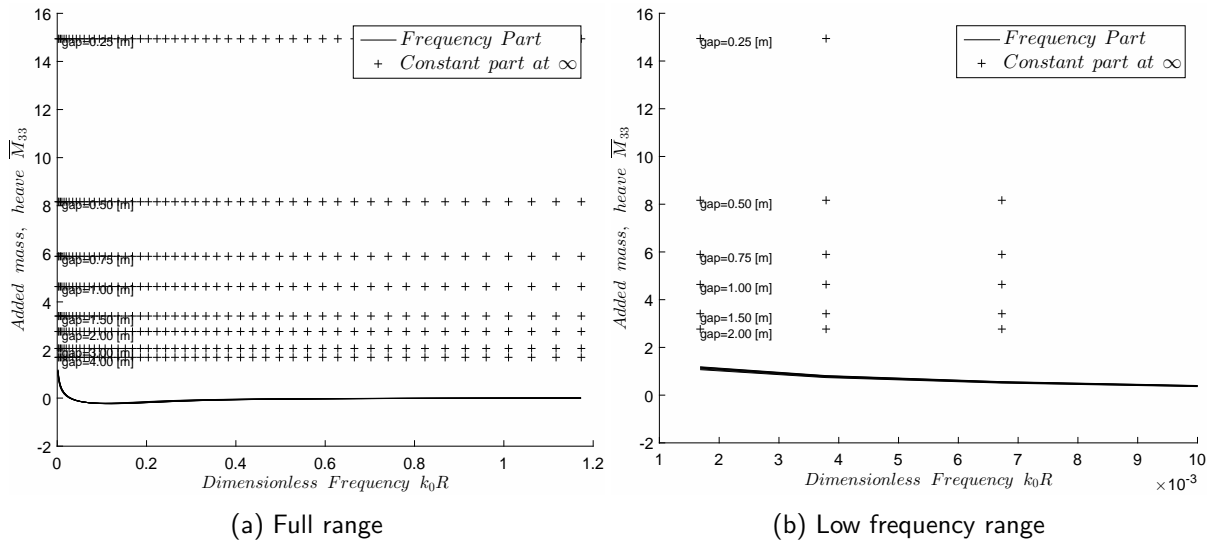


Figure 4.10: Comparison between constant and frequency part, Heave, T=15m

PITCH MODE

Analogous to heave mode, for pitch mode shown in Fig. 4.11 and 4.12, the influence of gap height variations on frequency part is only reflected on low frequency range, where the influence is negligibly small compared to the magnitude of variation for constant part.

Again, the deep-drafted cylinder in case 2 shows an even more negligible influence of gap height variations on frequency part, see 4.12.

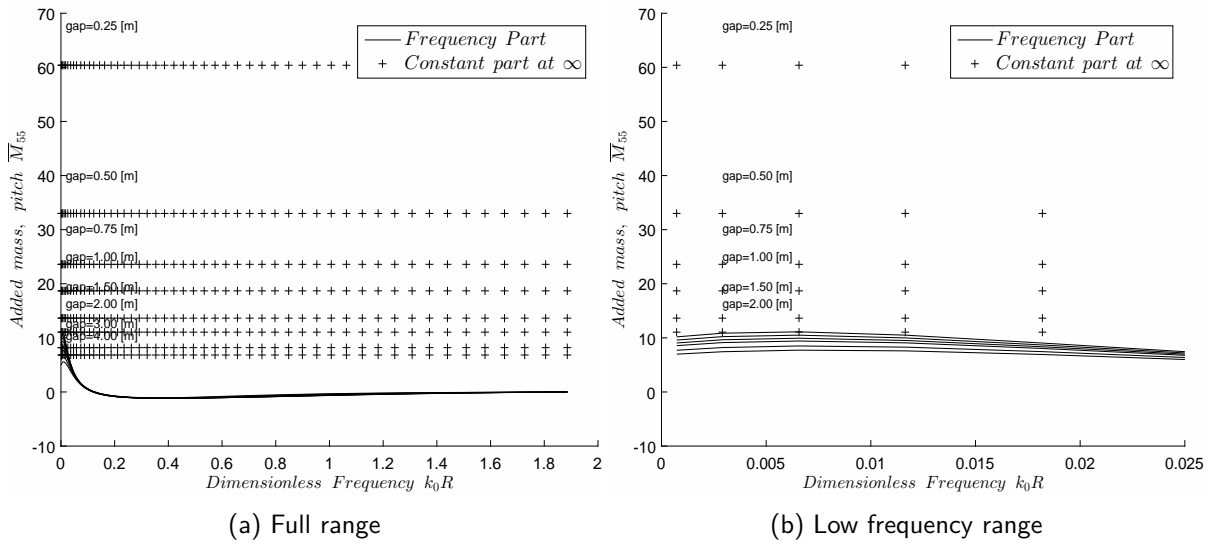


Figure 4.11: Comparison between constant and frequency part, Pitch,  $T=5m$

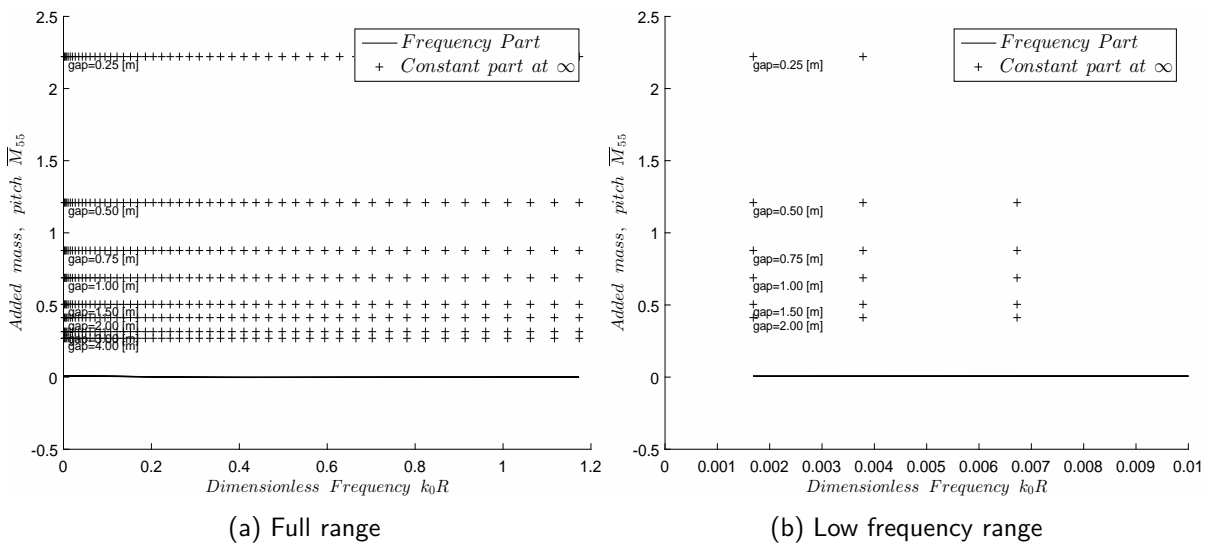


Figure 4.12: Comparison between constant and frequency part, Pitch,  $T=15m$

### 4.3. CONCLUSIONS

In this chapter, separation of frequency is sought to lay the foundation for finding formulations for further time-domain analysis. The core idea is to verify that the frequency part will remain unchanged in radiation convolution, leaving the time-variant-nonlinear constant part to be formulated in next chapter.

The single most important conclusion in this chapter is that **the frequency part will be considered unchanged in radiation convolutions.**

Detailed conclusions associated with calculated cases are listed here:

- AQWA and New method are both available to predict hydrodynamic properties of the simplified hydrodynamic model 2.1 for offshore discharge and loading.
- To separate frequency part, New method is selected due to efficient computational time and relative accuracy for extremely small gap heights.

- For larger gap heights, AQWA is considered to be more accurate as AQWA has no limitations on large gap heights and New method is assumed to be used mainly for small gap heights.
- Separation made by New method shows that frequency part contribution to total added mass is secondary to constant part at infinite frequency.
- The frequency part is largely independent of gap height variations. At very low frequencies, the influence of increasing gap height will only have a slight increase of frequency part compared to the increase of constant added mass.
- The independence of frequency part from gap height is also relying on draft. For a deeper draft, the influence is much more negligible than that of a shallower draft.

To delimit the work between gap flow (constant part) and free surface effect (frequency part), a flowchart is made with the complete separation of frequency, as proved in this chapter. With constant part singled out, the task to find the proper formulations to accommodate non-linearity of gap flow in time domain is taken in Chapter 5.

# 5

## QUANTIFICATION FOR GAP FLOW PART

The separation of frequency part from total hydrodynamic part enables the subsequent investigation on properties for frequency-independent or constant part at infinite frequency, i.e., gap flow part. The significance of comprehending gap flow part lies in the fact that it is the prerequisite for non-linear time domain simulation as the external force associated with gap varies with time. The external force takes the form of Eq. 3.3 as stated in the thin disc theory of chapter 2.

To describe this time-variant external force, we shall look for the proper formulations with variables such as gap height, inclined angle and shape factor. Consistent with chapter 3, the main calculated cases are circular cylinders.

### 5.1. INFLUENCE OF GAP HEIGHT

The most relevant parameter of gap flow problem for hydrodynamic coefficients is gap height. The relations between added mass and gap height will throw light on how the external force changes over time. Analytical results given by Drobyshevsky and AQWA are discussed in B. Here New method is more relevant as demonstrated in chapter 3 that constant part at infinite frequency can be obtained efficiently. Thus, New method is adopted to extract added mass.

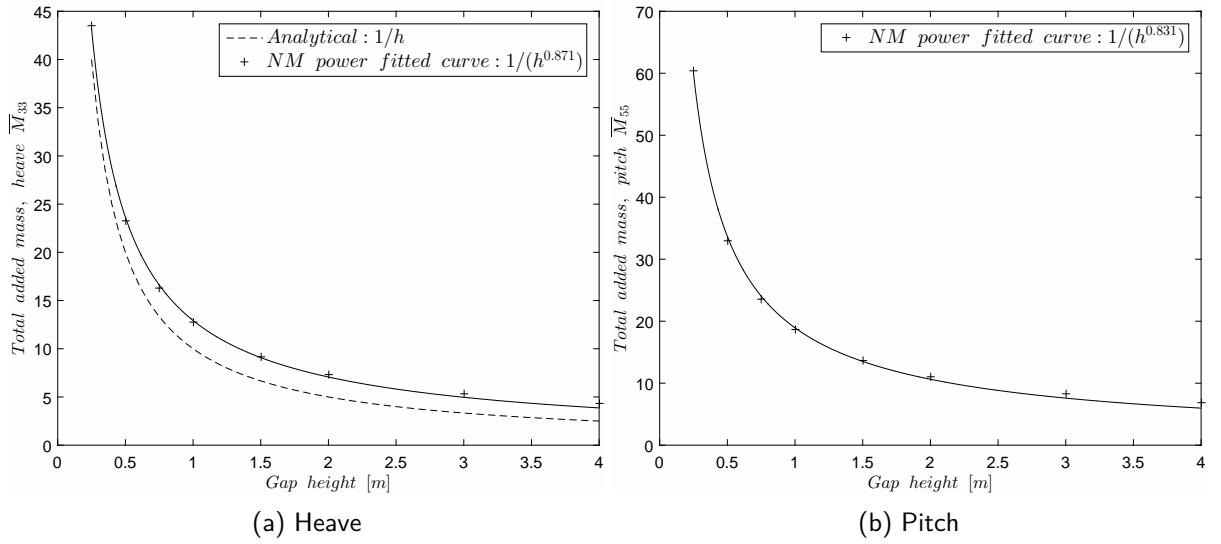
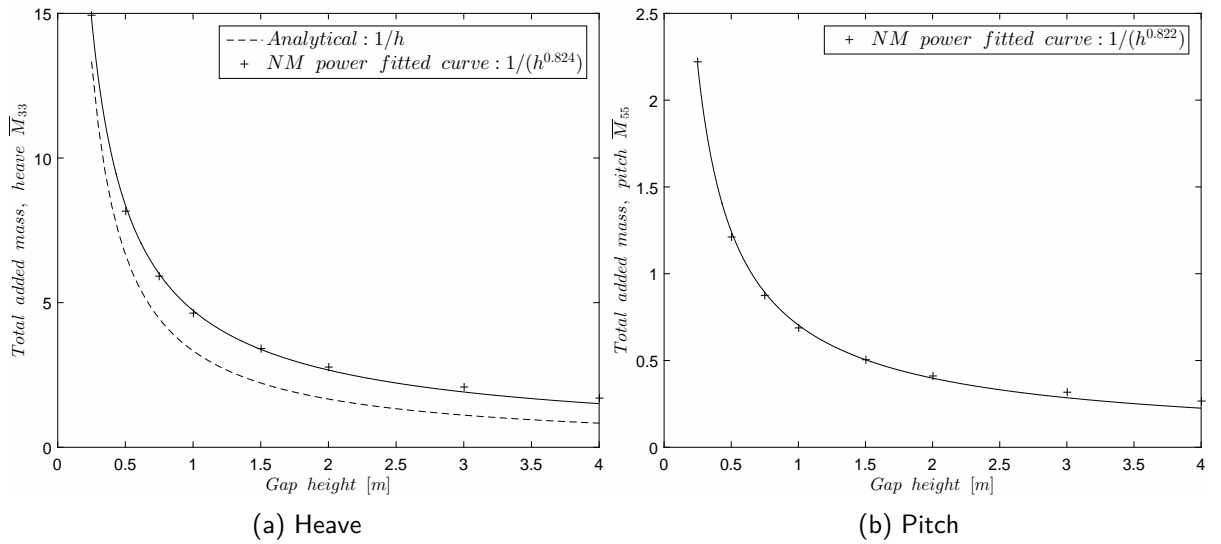
The focus here is to construct the relation between constant added mass at infinite frequency and gap height. The expression of the relation contains a certain term with inverse gap height, as shown in Molin 3.12 and Drobyshevsky 3.42 & 3.43. Following the same spirit, with constant added mass for varied gap heights calculated in New method, an empirical formulation can be constructed via power fitting function:

$$M_A = a \cdot h^b \quad (5.1)$$

By fitting the calculated added mass values from New method, coefficients  $a$  and  $b$  are obtained, thus establishing the empirical formulations for constant added mass at infinite frequency.

Cylinder case	Coefficient $a$	Gap Coefficient $b$
case 1 heave	12.93	-0.871
case 1 pitch	18.93	-0.831
case 2 heave	4.73	-0.824
case 2 pitch	0.704	-0.822

Table 5.1: Fitting coefficients

Figure 5.1: Curve fitting results for case 1,  $T=5$ [m]Figure 5.2: Curve fitting results for case 2,  $T=15$ [m]

In Fig. 5.1 & 5.2, added mass for both heave and pitch modes at two different drafts will monotonically decrease as the gap height increases. In fact, the slight variation of gap height around, for instance,  $0.5m$  will lead to a significant change of added mass. Much less so when the variation is around large gap height, for instance,  $3.0m$ . Consequently, this change of added mass due to gap height variations must be considered and included in time-domain simulations.

The empirical power function is evaluated with added mass data from New method, which is fairly accurate for the gap flow problem as shown in Chapter 3. Consequently, empirical coefficients  $a$  and  $b$  are reliable. It is also worth noting that the value of coefficient  $b$  in two cases is around 0.82, where the theoretical value is 1 from Molin 3.12 and Drobyshevsky 3.42 & 3.43. For Molin, the model is a deeply submerged disc and an extra term other than power function also exists. For Drobyshevsky, though the model being cylinder, an extra term also exists. These cause the different  $b$  values in cases here.

## 5.2. INFLUENCE OF ASYMMETRY

The asymmetry problem should be interpreted as that the body bottom is not parallel to the seabed but with an inclined angle. The moving body with a slight inclination can be a dangerous situation because when the cargo subject to adverse seastate inclines, the tipping point might touch the seabed. In this section, we will investigate its influence on hydrodynamic coefficients.

Only case 1 (draft=15[m]) is studied in this section. Due to limitation of New method that the cargo bottom must be parallel to seabed, all the computation here are done in AQWA instead of New method. This will not create much discrepancy as AQWA is also capable of evaluating added mass for gap problem, as shown in Chapter 3.

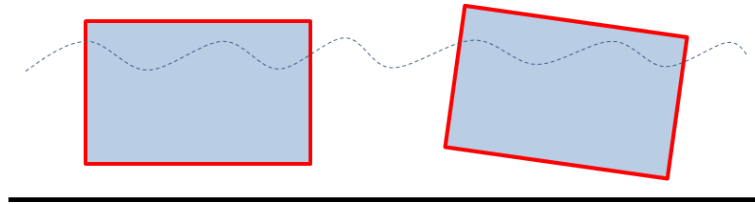


Figure 5.3: Asymmetry problem with an inclined angle

The influence from inclination will be assessed via a matrix of gap height ranging from 0.5[m] to 4[m] and inclination percentage from 0% to 95%. The larger the inclination percentage is, the more inclined the structure is. The dimensionless inclination percentage indicated the extent of inclined angle w.r.t gap height:

$$\text{inclination percentage [\%]} = \frac{\text{gap height} - \text{inclination edge clearance to seabed}}{\text{gap height}}$$

The constant added mass for both heave and pitch modes is monotonically increasing with inclination percentage, i.e., that the larger the inclination angle is, the greater the added mass will be, as shown in Fig. 5.4. This monotonicity of increase can be explained by the fact that when the cylinder is inclined, the gap height at the inclined tipping edge is smaller and the other edge is larger than the original gap height without inclination. As known in previous section, the decrease

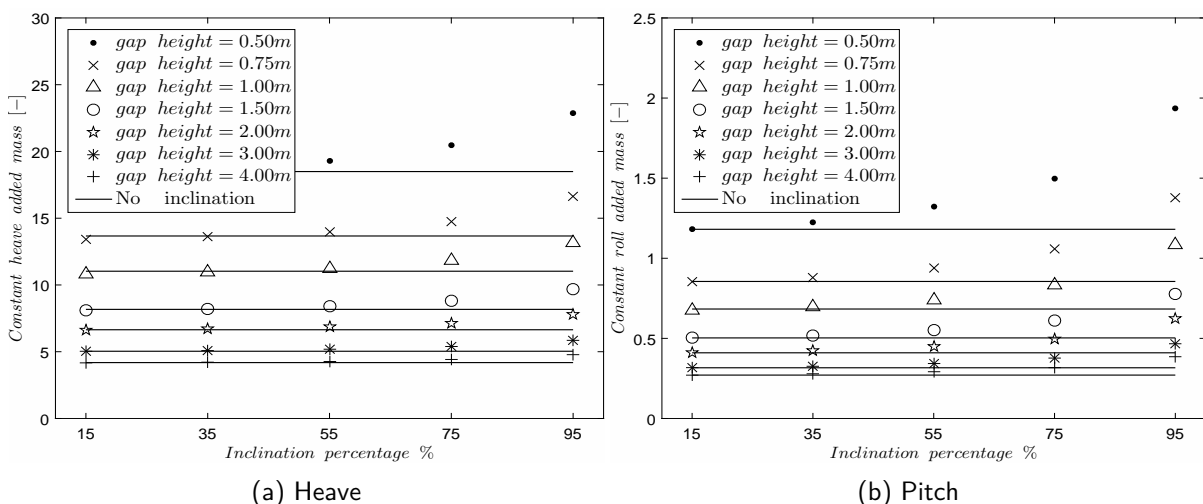


Figure 5.4: Constant added mass with different inclination percentages

of gap height will lead to the increase of added mass and vice versa. However, the magnitude of added mass increase due to decreased gap height will much exceed the magnitude of the added

mass decrease due to increased gap height. Overall, the effect is to increase the added mass with inclination. As shown in Fig. 5.5, the increase due to inclination percentage also depends on gap height; with smaller gap heights, the increase is more obvious. Also noted here is that for

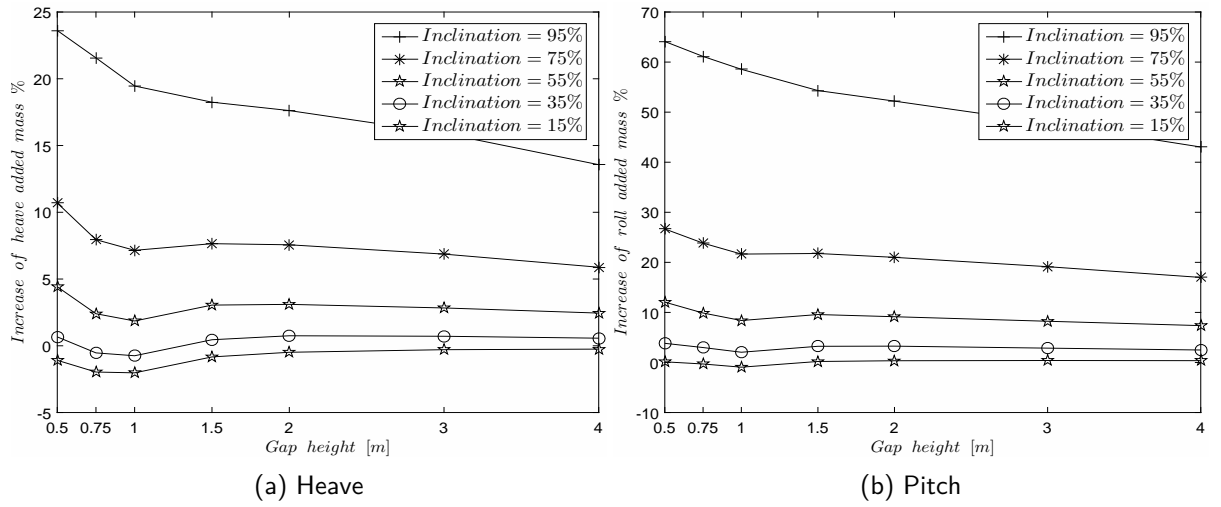


Figure 5.5: Increase of added mass due to inclination for different gap heights

inclination percentage from 15% to 55%, the increase of heave added mass is negligible or even negative. Further, we study the increase of added mass due to inclination percentage with varying gap height for both heave and pitch modes. Compared to heave mode, the pitch mode has seen a much larger increase of added mass for inclination percentage 75% and 95% in Fig. 5.5.

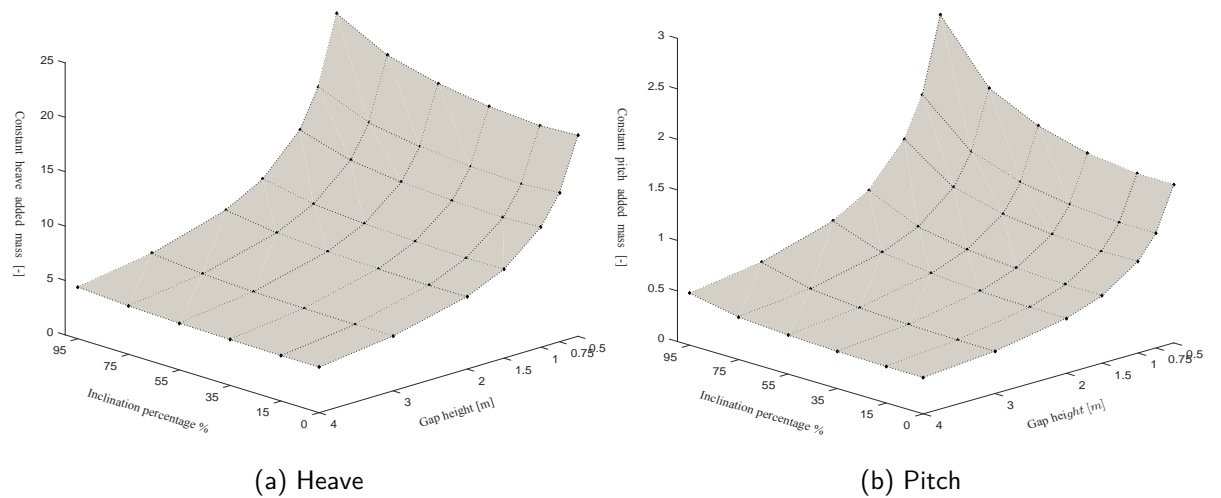


Figure 5.6: 3D plot w.r.t gap height and inclination percentage

Recall that the added mass is highly dependent on gap height for parallel cases. And here it is also related to inclination angles. Thus, a 3D plot showing the relations between added mass and gap height with inclination percentage is shown in Fig. 5.6. In brief, the asymmetry problem should be viewed as interactive added mass for pitch-heave, pitch-pitch and pitch-roll, see Eq. 5.2. A more complete result for asymmetry problem is illustrated in Appendix A.

$$M_{add} = \begin{bmatrix} M_{33}(h, \theta_1, \theta_2) & & \\ & M_{44}(h, \theta_1, \theta_2) & \\ & & M_{55}(h, \theta_1, \theta_2) \end{bmatrix} \quad (5.2)$$

### 5.3. INFLUENCE OF SHAPE

Consistent with different cargo types, shape factor must also be considered as this thesis seeks to tackle a general cargo-HTV problem. Previous calculations are all based on the shape of circular cylinder. To expand, different shapes are investigated in this section in terms of gap height influence. Except for circular shape, here an equilateral triangle, a square and a rectangle with a ratio 1:6 are listed below. To compare shape factors, all these shapes have the same bottom area as circular cylinder in case 1 and 2, i.e., a radius of  $20m$ . A draft of  $15m$  is chosen for all cases.

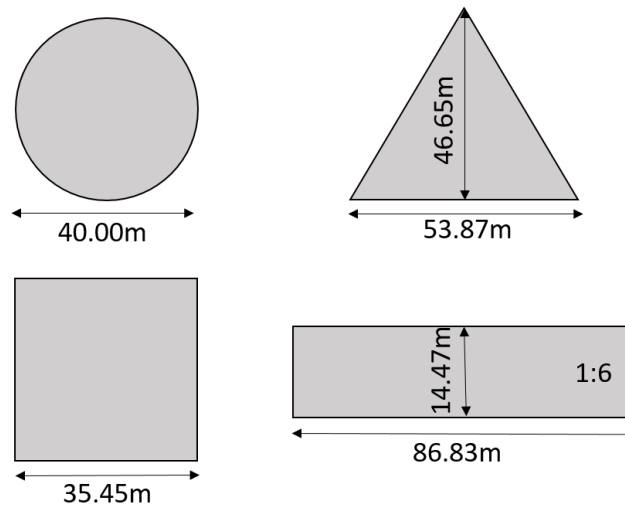


Figure 5.7: Basic shapes

Essentially, the shape factor will not change the methodology we use to predict hydrodynamic coefficients. Influence of shape can be generically tackled using AQWA or New method, as shown in circular cylinder cases. Results from AQWA are summarized in Appendix C.

It is shown in Appendix C. that added mass for circle, triangle and square will not vary much, as also verified by the model test results in [2]. For rectangle, the added mass would be considerably different from other shapes. The outline is first check the validity of AQWA and New method to be used for evaluating added mass for rectangle case, followed by comparison between rectangle and circle cases.

#### AQWA VS NEW METHOD

First, for rectangle case with a draft of  $15m$ , comparison between AQWA and New method is shown in Fig. 5.8. As predicted in circular cylinder cases, both AQWA and New method can also be used for evaluating added mass of rectangular case. Again, analogous to circle case in Chapter 3, at very small gap heights, New method is more accurate than AQWA and at large gap heights the other way round.

#### CIRCLE VS RECTANGLE

To examine the influence of circle and rectangle on added mass, AQWA is used to show constant added mass at infinite frequency comparison in Fig. 5.9.

For heave added mass, the value from circle case is considerably larger than that from rectangle case, especially at very small gap heights. This means that forced oscillation for circle case can

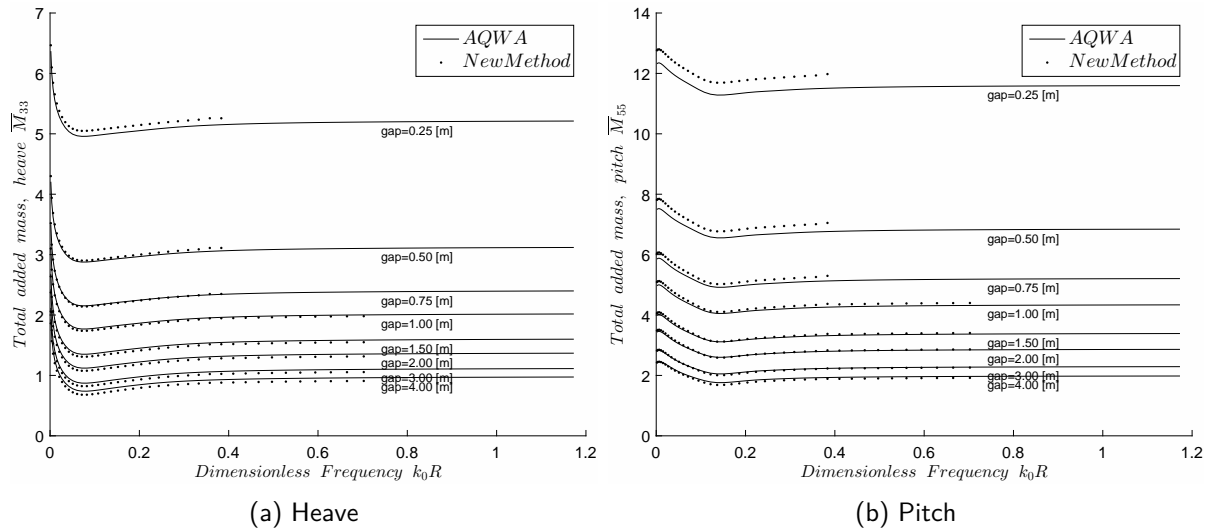


Figure 5.8: AQWA vs New method for rectangle case

produce larger radiation force as it is easier to disturb the fluid around it whereas for rectangle case it's less influenced by the surrounding fluid due to its small width-length-ratio.

Different from heave mode, for pitch added mass, the value from circle case is considerably smaller than that from rectangle case as the long arm of rectangular bottom could easily pass rotation momentum to the fluid around it.

In the same manner as the circle case, the influence of gap height and asymmetry on rectangle case can also be quantitatively assessed via New method and AQWA.

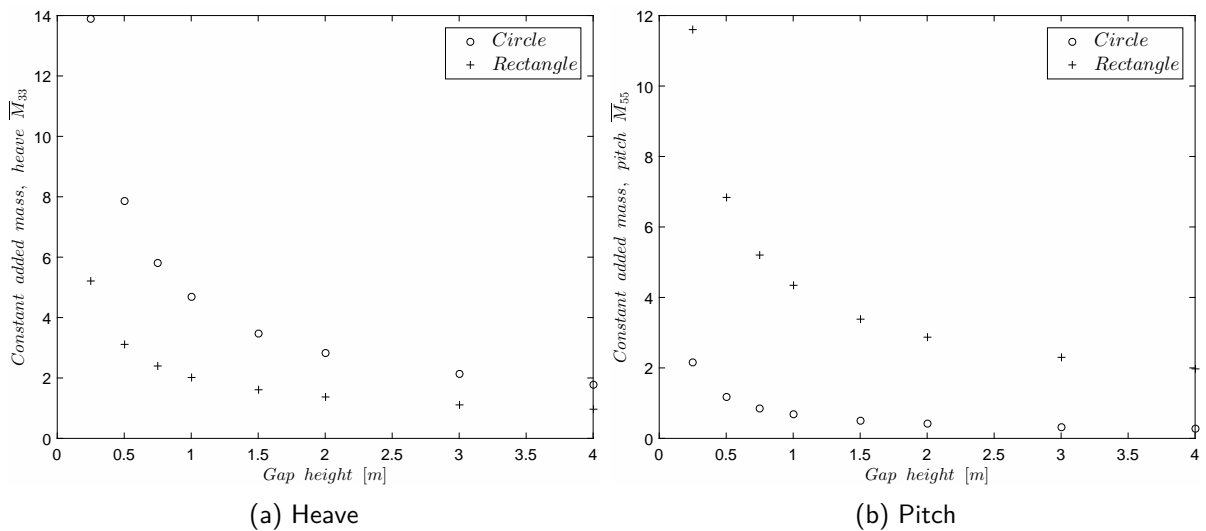


Figure 5.9: Circle vs Rectangle

## 5.4. SUMMARY

In this chapter, the quantitative analysis of constant added mass w.r.t gap height, inclination angle and shape factor is investigated. With evaluated added mass, the external force to be coded in DLL, made up of inertial and cushioning force, can be calculated.

### 5.4.1. FORMULATIONS FOR EXTERNAL FORCE

The purpose of this chapter is to formulate relations between external force and influencing factors, i.e., gap height, inclination angle and shape. For gap height and inclination angle, the formulations can be constructed empirically. For shape factor, it is implicitly solved by AQWA or New method, thus excluded in the subsequent analysis.

In line with Molin [4] and Nielsen [12], the general equation describing heave external force is extended to angular motions. Essentially, the general external force(moment) is made up of two terms: inertial force and cushioning force.

$$\begin{aligned} F_{ext}(t) &= -A(h, \theta_1, \theta_2) \cdot \ddot{h} - \frac{1}{2} \frac{dA(h, \theta_1, \theta_2)}{dt} \cdot \dot{h} \quad (\text{heave}) \\ M_{ext}(t) &= -J(h, \theta_1, \theta_2) \cdot \ddot{\theta} - \frac{1}{2} \frac{dJ(h, \theta_1, \theta_2)}{dt} \cdot \dot{\theta} \quad (\text{roll/pitch}) \end{aligned} \quad (5.3)$$

where  $A$  and  $J$  are added mass (moment) for heave and angular motions with three variables  $h$ ,  $\theta_1$  and  $\theta_2$  represent gap height, roll and pitch inclination angles respectively. It should be noted here that only diagonal terms in the added mass matrix are used in the external force formulations as the non-diagonal terms are not as relevant as diagonal ones.

The above equation can also be generalized as the form:

$$F_{ii} = -M_{ii} \ddot{X}_i - \frac{1}{2} \frac{dM_{ii}}{dt} \dot{X}_i \quad (5.4)$$

where  $M_{ii} = f(h, \theta_1, \theta_2)$ . The subsequent efforts will be shifted to implement the above equation in DLL prepared for time-domain simulations. We provide two approaches to accommodate this issue.

#### INTERPOLATION OF DATABASE APPROACH

This approach is based on the availability of large quantities of added mass data at discrete gap heights and discrete inclination angles for a given shape. After collecting all the discrete data, we can make a database to be searched for each time step in time domain simulations. Subsequently, the approximate added mass value will be interpolated from these discrete data. Naturally, the accuracy of the interpolation relies on the accuracy and volume of added mass database. Much effort will be made to build a reliable and adequate database including all the necessary parameters, specifically for a certain cargo.

With backward Euler method, the external force in DLL at  $n+1$  time step can be expressed as:

$$F_{ii}(t_n) = -M_{ii}^n \ddot{X}_i^n - \frac{1}{2} \frac{M_{ii}^n - M_{ii}^{n-1}}{\Delta t} \dot{X}_i^n \quad (5.5)$$

The searching function in DLL comes into play when added mass  $M_{ii}^{n+1}$  and  $M_{ii}^n$  at  $n$  and  $n+1$  time steps are interpolated from database. This searching and interpolation procedures will be executed at every time step and can be very time-consuming for the preliminary phase. On the other hand, this interpolation of database approach is very direct to use and implement, even allowing for non-diagonal added mass to be included in DLL.

#### DIRECT FORMULATION APPROACH

The direct formulation approach focuses on constructing the empirical formulations that give the expression of external force. The advantage is that once the formulations are constructed, interpolation will not be needed and can be much faster than database approach as it requires no searching and interpolation procedures at every time step. But curve-fitting preparations for this approach will be intensive.

Similar to the database approach, first large quantities of added mass data w.r.t varied gap heights and inclination angles are obtained. Then empirically by curve-fitting, the fitted formulations will be known. For instance, the added mass w.r.t gap height only can be fitted into a power function as shown in 5.1. The fitted formulations might not be unique as long as they cover all the data for different parameters. Ideally, formulations for added mass can be expressed as functions with two variables: gap height and inclination angle.

In DLL, the expression used for this direct formulation approach is:

$$F_{ii}(t_{n+1}) = -M_{ii}^{n+1} \ddot{X}_i^n - \frac{1}{2} \left[ \frac{\partial M_{ii}}{\partial h} \frac{\partial h}{\partial t} + \frac{\partial M_{ii}}{\partial \theta_1} \frac{\partial \theta_1}{\partial t} + \frac{\partial M_{ii}}{\partial \theta_2} \frac{\partial \theta_2}{\partial t} \right] \Bigg|_{t=t_n} \dot{X}_i^n \quad (5.6)$$

#### 5.4.2. CONCLUSIONS

Some main conclusions obtained from this chapters are listed below.

- For constant added mass, most relevant parameters are gap height and inclination angle.
- Variations of gap height cause considerable change of constant added mass. This can be described by power function as constant added mass is inversely proportional to gap height. New method is faster and more accurate than AQWA for evaluating added mass at very small gap heights.
- Large inclination angles will lead to the increase of constant added mass for both heave and pitch modes. This asymmetry problem must also be incorporated in time-domain simulations. Due to limitations of New method, asymmetry problem is tackled via AQWA.
- Shape factor will not change the basic methodology we use to predict added mass. Comparisons show for circle and rectangle shapes, their added mass difference is very large at small gap heights.
- With evaluated added mass, the external force is coded in DLL either by interpolation of database approach or by direct formulation approach.
- With separation of frequency from Chapter 4 and parametric study of constant added mass from this chapter, the preparatory work towards time-domain simulations is well established.

With all these work so far, it is possible to simulate the response of physical model in time domain, which is dealt with in next chapter.

The development of an external program to incorporate time-variant hydrodynamic coefficients is the starting point for real time-domain simulations. Work on this will be elaborated in Chapter 6.

# 6

## TIME DOMAIN SIMULATION

The time domain simulations for offshore discharge and loading problems are central to understand the workability of these operations. In this chapter, firstly convolution theory is introduced to provide the basic motion equations in time domain. Then the summary of computational scheme is outlined for one-body physical model. Subsequently, the verification of external force coded in DLL with measurement from forced oscillation tests is made. The foundation of real time series for the topic of this thesis is firmly found by previous steps. To illustrate the power of this method, preliminary time domain calculations is executed for regular waves and irregular waves.

### 6.1. EVALUATION SCHEME

The starting point of time domain analysis is to select an initial gap height. This initial gap height can be determined by the relative accuracy of AQWA compared to New method, as shown in Chapter 3 that at a certain gap height, relative difference between AQWA and New Method is almost negligible. For the circular cylinders case 1&2, this initial gap height is 1[m]. If industrial practice or experience regarding initial gap height, which is largely dependent on HTV and cargo submerged drafts, should be considered, the relative accuracy of AQWA compared to New method must be checked.

Another important input to AQWA time domain solver is the external force, which is coded based on constructed formulations in Chapter 4. The prerequisite of these is the separation of frequency, as done in Chapter 3.

To simplify, first we study the one-body problem with heave only mode without inclinations. After separation of frequency, the coding in DLL requires formulating the external force. The external force will be known once the expression for added mass is found. Below are the procedures to be implemented to construct added mass expressions.

- Select the initial gap height for time domain solver.
- Determine the range of gap height around the initial gap height.
- Extract added mass data for this range of gap height from New method or AQWA.
- Fit the added mass data into power function so that fitted added mass and added mass data are equal at initial gap height.

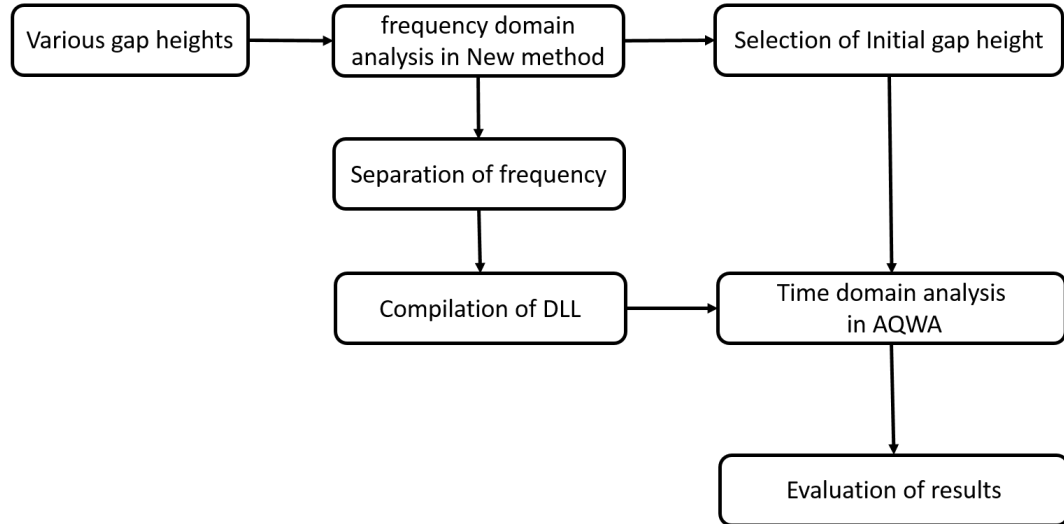


Figure 6.1: Evaluation procedures

- The power coefficient  $\mathbf{b}$  is obtained, thus giving the expression for added mass.

Following the procedures described in 6.1, the constructed formulations in DLL are expressed as:

$$M_A(h) = -A_\infty(\bar{h}) + A(h) = \left[ \left( \frac{\bar{h}}{h} \right)^b - 1 \right] \cdot A_\infty(\bar{h}) \quad (6.1)$$

$$F_{cushioning}(h) = -\frac{1}{2} \frac{dM_A(h)}{dh} \cdot (\dot{x}_3)^2 = \frac{b\bar{h}^b \cdot A_\infty(\bar{h})}{h^{b+1}} (\dot{x}_3)^2$$

where  $\bar{h}$  is the initial gap height,  $h$  the instantaneous gap height and  $A_\infty(\bar{h})$  is the added mass at infinite frequency for the initial gap height, normally obtained in AQWA frequency domain analysis.

## 6.2. VERIFICATION FOR FORCED OSCILLATION TRACES

The external force expressed in 5.3 essentially is the force caused by forced oscillations, i.e., an outcome of radiation problem. Before delving into numerical time-domain simulations, the verification of the external force, obtained from added mass due to gap flow part by AQWA or New method, is necessary.

Model tests of force oscillations were done in the shallow water basin of MARIN (Wageningen) in 2008. The overall description of these model tests is attached in appendix.

Peters [2] compared analytical equations of a deep-submerged circular disc close to seabed from Molin [4] to measurement results. The comparisons lead to an empirical synthesis of drag damping, initially described by Molin as  $F_D = -\frac{1}{2} \rho C_D (2\pi R d) \frac{R}{2d} \left| \frac{UR}{2d} \right| = -\frac{\pi}{2} \rho C_D \frac{R^3}{d} U |U|$ .

Molin used  $C_D = 1$  for his circular disc case. Peters [2] found from model tests that the drag coefficient is inversely proportional to heaving velocity:  $C_D = \frac{1.5}{|U|}$ . Then we have the drag force:

$$F_D = -\frac{3\pi}{4} \rho \frac{R^3}{d} U \quad (6.2)$$

With analytical force equation from Molin combined with empirical drag damping, the result compares quite satisfactorily with measurement. It should be noted here that for model tests, we use

a cylinder geometry while in Molin the analytical equation is derived only from a submerged disc. This is a justifiable simplification as we found that the main contribution to added mass is from under bottom part.

Now, for the external force formulations of circular cylinder, summarized in Chapter 4, comparison to measurement and Molin is also made to verify these external force formulations constructed either by AQWA or New method, as shown in below figures 6.2 and 6.3. A complete comparison for each oscillation test is shown in Appendix D.

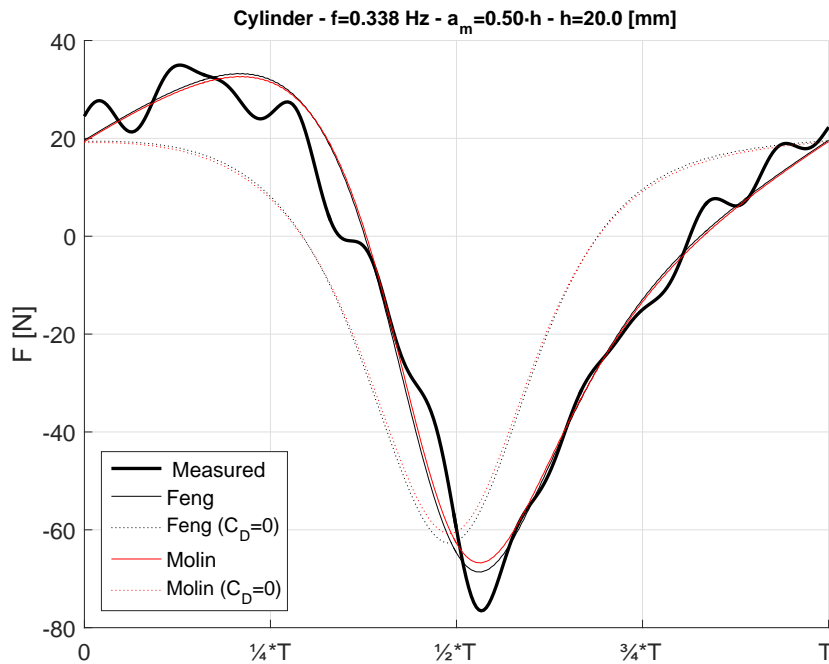


Figure 6.2: Molin, Feng vs measurement, frequency=0.338Hz

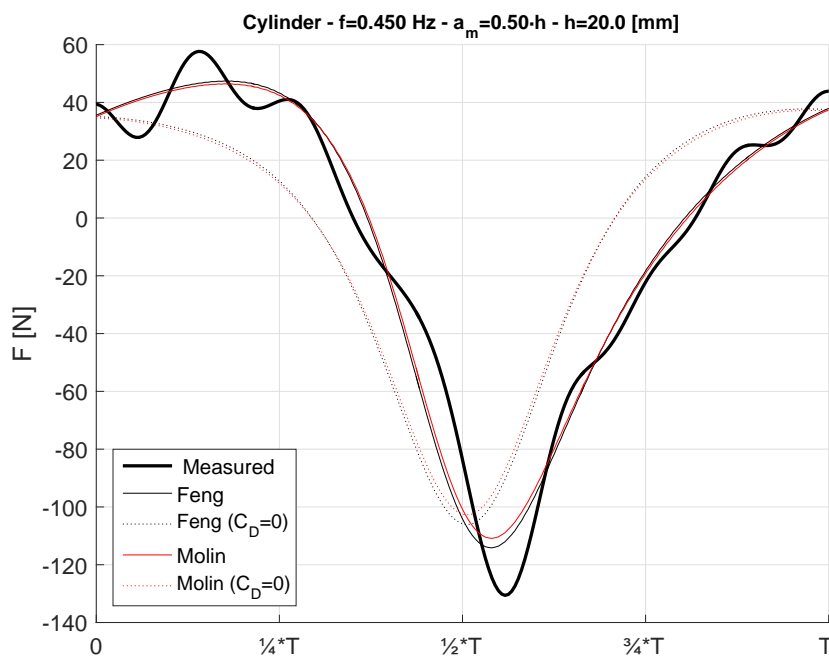


Figure 6.3: Molin, Feng vs measurement, frequency=0.450Hz

It can be seen from these two figures that empirical formulations from Feng (this thesis author) with damping is almost indistinguishable with Molin's and both compares quite well with measurement. This verifies the effectiveness of empirical formulations proposed in Chapter 4. If we only look at external force without damping, a phase shift is noticed. The high frequency oscillations from the measurement at the trough and at both ends might be measurement error due to the vibration of the test facility or disturbance from the sidewalls of the water basin.

Next, we show the influence of different forcing components on total forced oscillation. As explained in the Chapter 2, the dominant force is inertial. This is also reflected in 6.4 with inertial force contributes most to the total force. The cushioning force is always positive (upward) and has a higher frequency (twice of the oscillation frequency). The cushioning force must not be omitted as it is an important part to the total force. The last component, drag damping, will shift the curve to right to match the measurement. The damping force must be included in real time domain simulations as to reflect the phase shift during oscillations.

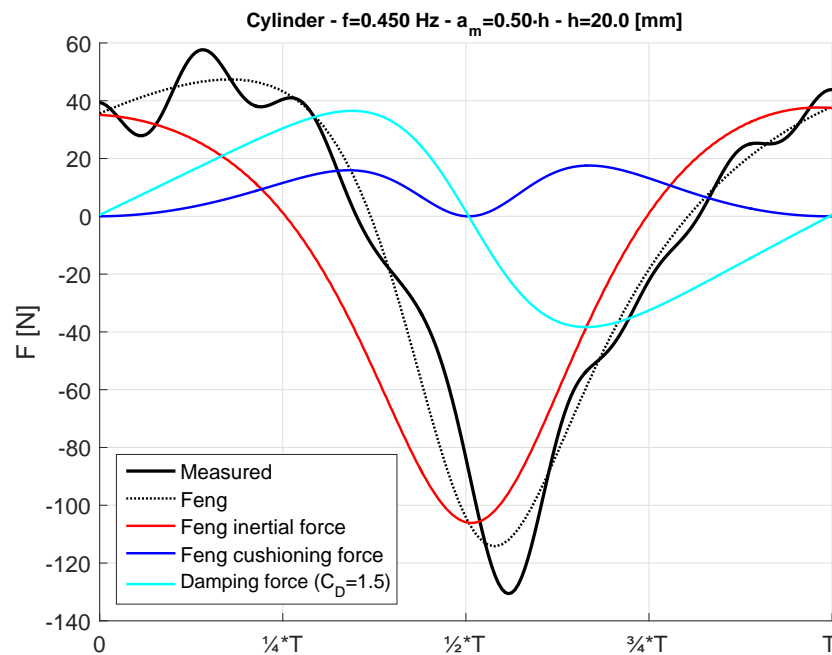


Figure 6.4: Contribution from different components, frequency=0.450Hz

### 6.3. TIME DOMAIN CALCULATIONS

The time domain calculations are carried out in this section with comparisons between conventional linearized results (no DLL) and non-linear results with external forced included (with DLL). The model is a circular cylinder of a draft of 15m and a diameter of 20m. The initial gap height is set as 1m. Drag damping forces are excluded for both cases as the focus is to understand the influence of external force in DLL on vertical motions of cargo in time domain.

#### 6.3.1. REGULAR WAVE CASE

Three regular waves corresponding different wave periods are used here: 8s, 18s(approximate natural period), 60s. Since the purpose is to show the difference between linearized result and non-linear one, the wave heights are chosen only to conveniently illustrate the influence of non-linearity. For simplicity, also note here that only the heave mode is switched on.

As shown in Fig. 6.5, at natural frequency, the linear response is significantly larger than non-linear response. A slight phase shift is also observed. In brief, the linearized result cannot well capture the heave behaviour. This shows that external force must be incorporated in time domain.

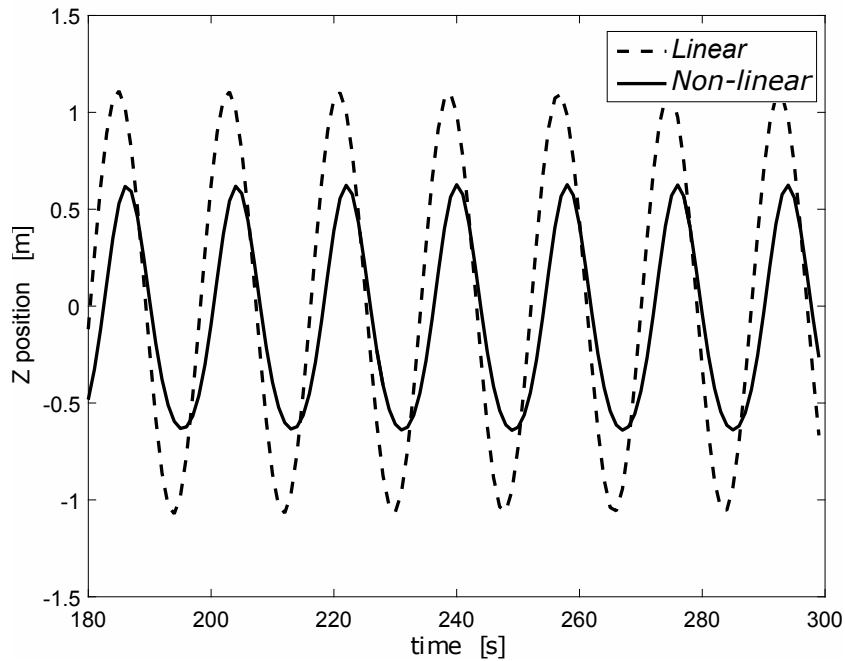


Figure 6.5: Regular wave,  $T=18s$ ,  $H=0.50m$

For wave periods of 8s and 60s in Fig. 6.6 and 6.7, the difference between linearized result and non-linear results is very small. For smaller wave period, the excited heave motion is generally very small, regardless of non-linearity. For larger wave period, its wave length is larger than the diameter

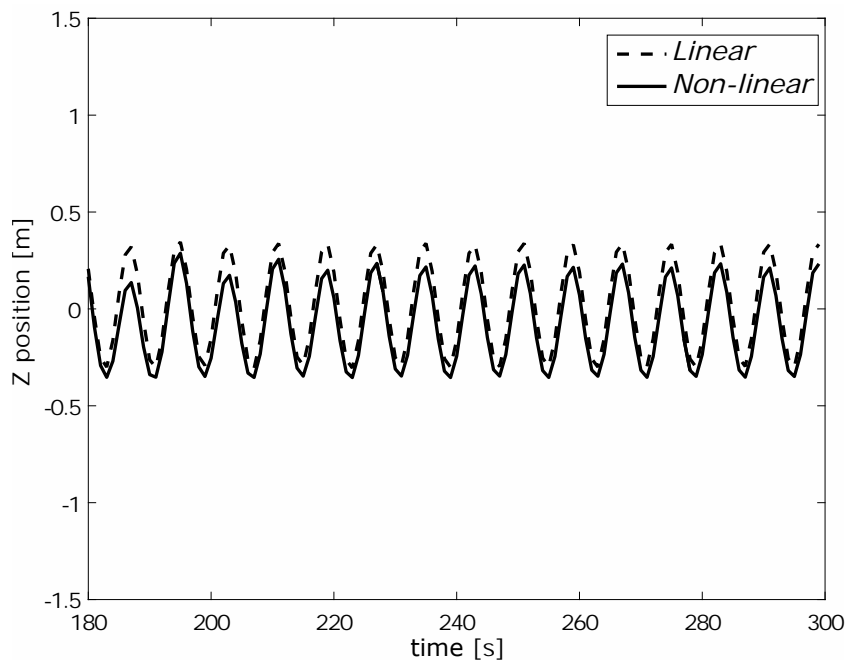


Figure 6.6: Regular wave,  $T=8s$ ,  $H=8.0m$

of circular cylinder, thus leading to a drifting heave motion with the wave, as shown in Fig. 6.7

that the heave amplitude is approximately half of the wave height.

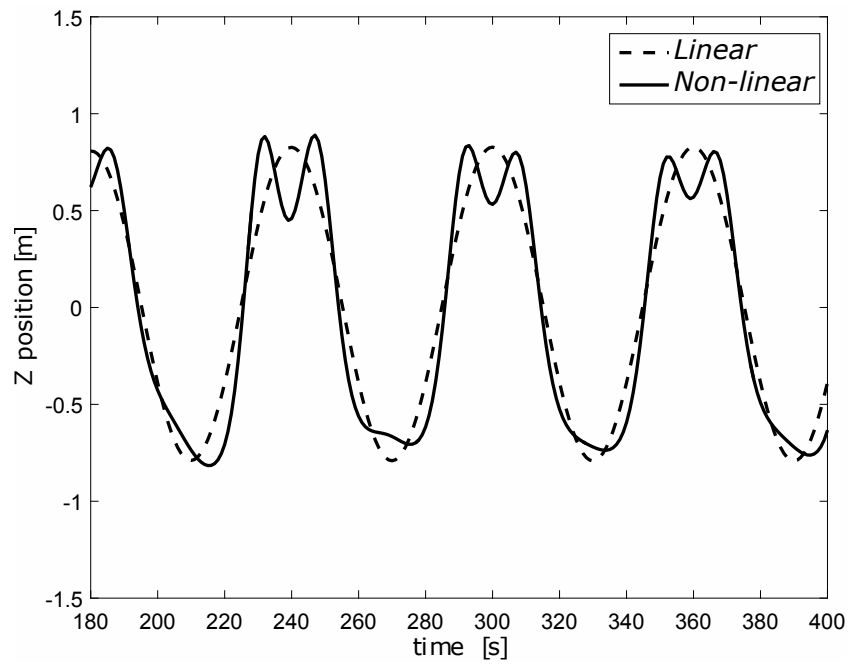


Figure 6.7: Regular wave,  $T=60s$ ,  $H=1.5m$

### 6.3.2. IRREGULAR WAVE CASE

For a defined Jonswap spectrum with a peaked period of 18s, the comparison between linearized result (without DLL) and non-linear one with DLL is shown below. This irregular wave case is only a showcase to indicate the potential for real workability analysis.

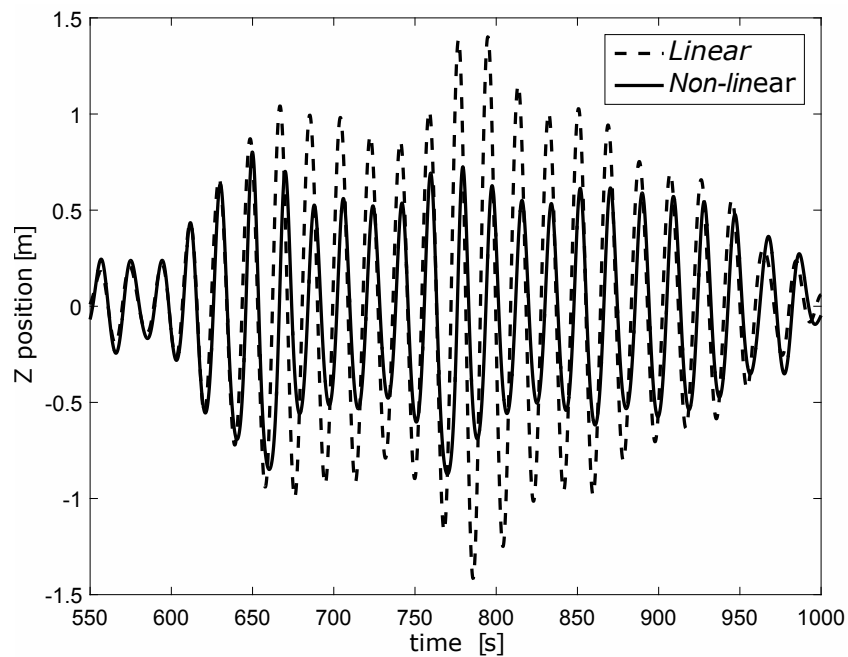


Figure 6.8: Irregular wave,  $T_p=18s$ ,  $H_s=0.45m$

## 6.4. CONCLUSIONS

This chapter deals with the calculations for offshore discharge and loading in time domain. The main purpose is not to give specific calculations for real offshore operations but rather, to illustrate the possibility to do these in future. Associated with this chapter, main conclusions can be drawn as below:

- Results from convolution method show that added mass at infinite frequency can be replaced by added mass at largest frequency computed by 3D diffraction method.
- The computational procedures in time domain are outlined based on analysis from previous chapters.
- The external force formulations associated with gap flow part are verified with model test measurements, and drag damping is empirically found from these measurements.
- Initial time domain simulations in regular waves indicate that the linear response is too conservative at natural period.



# 7

## CONCLUSIONS AND RECOMMENDATIONS

This thesis seeks to address the issue of evaluating hydrodynamic coefficients and behaviour of vertical motions during offshore discharge and loading. Regarding this, this thesis has provided a systematic methodology and basis for time domain simulations and further workability analysis.

The single most important conclusion from this thesis is:

**A systematic methodology is proposed to predict non-linear behaviour associated with gap flow in time domain, where external force is included after separating added mass into frequency-dependent part and gap (constant) part.**

Summarizing all the obtained results, this thesis can be concluded with following statements.

### CONCLUSION

1. Starting from an analytical equation initially derived by Molin [4] for a deep-submerged disc close to seabed, it has been found that the cargo with a small gap above HTV is subject to the external force that is made up of inertial force, cushioning force and drag damping force.
2. To quantify inertial and cushioning forces, added mass must be evaluated. It is found that both New method and AQWA can well capture the total added mass. Specifically, for larger gap heights, AQWA is considered to be more accurate and New method is assumed to be used mainly for small gap heights.
3. As added mass in external force formulations is only gap part dependent (containing no information on frequency), the total added mass must be first split into two parts: constant part and frequency-dependent part. It has been numerically proved that these two parts can be separated via New method or AQWA as the frequency part is largely independent of gap part.
4. The frequency part is mainly caused by free surface effects and constant part due to gap flow. Frequency part contribution to total added mass is secondary to constant part. More importantly, due to separation of frequency, frequency part remains unchanged for computing radiation force by convolution.
5. To formulate expressions for general external force for an arbitrary bottom shape, two key factors on constant added mass are gap height and inclination angle. Shape factor will not change the basic methodology we use to predict added mass.

6. Two approaches have been proposed to obtain general external force: direct formulation approach and interpolation of database approach. The former requires empirical curve-fitting the data w.r.t gap heights and inclination angles. The latter is based on large quantities of discrete added mass data that to be interpolated at each time step.
7. The proposed external force formulation is verified with forced oscillation measurements.
8. A complete scheme to evaluate vertical motions in time domain is outlined.
9. For preliminary time domain simulations, linearized result without DLL has over-predict motions than non-linear result. The external force must be included.

## RECOMMENDATION

1. Multi-domain diffraction method (MDDM) can be promising with matched boundary conditions for velocity and pressure at the gap outflow edge.
2. Drag damping needs to be evaluated physically or be estimated with permissible engineering practice.
3. For basic and detailed designs, double-body simulations should be carried out with all the DOFs, constraints (moorings, control system etc.) and environment conditions (wave, current and wind etc.).

# BIBLIOGRAPHY

- [1] A. Hellings, T. Terpstra, *et al.*, *Offshore dry-docking of fpsos: A response to industry needs*, in *OTC Brasil* (Offshore Technology Conference, 2013).
- [2] O. Peters, *dissertation draft: Offshore Loading and Discharge*, Ph.D. thesis, Delft University of Technology (2016).
- [3] O. Peters, R. H. Huijsmans, M. Seij, *et al.*, *Hydrodynamic behavior during offshore loading and discharge*, in *Offshore Technology Conference* (Offshore Technology Conference, 2012).
- [4] B. Molin, P. Guérin, D. Martigny, and P. Weber, *Etude théorique et expérimentale des efforts hydrodynamiques sur une embase plane à l'approche du fond marin*, Actes 7èmes Journées de l'Hydrodynamique , 291 (1999).
- [5] M. V. Dyke, *Perturbation methods in fluid mechanics*, Applied mathematics and mechanics ( **8** (1964).
- [6] E. Tuck, *Transmission of water waves through small apertures*, Journal of Fluid Mechanics **49**, 65 (1971).
- [7] E. Tuck, *Matching problems involving flow through small holes*, Archive of Applied Mechanics **15**, 89 (1975).
- [8] C. C. Mei, *The applied dynamics of ocean surface waves*, Vol. 1 (World scientific, 1989).
- [9] C. M. Linton and P. McIver, *Handbook of mathematical techniques for wave/structure interactions* (CRC Press, 2001).
- [10] T. Vinje, *Fluid flow through perforated structures.*, Tech. Rep. (MarinConsult Report, 2001).
- [11] C. Brennen, *A Review of Added Mass and Fluid Inertial Forces.*, Tech. Rep. (DTIC Document, 1982).
- [12] F. G. Nielsen, *How to estimate hydrodynamic coefficients applicable for lifting from the sea bed*, Lecture Notes (2007).
- [13] M. Greenhow, *Water-entry and-exit of a horizontal circular cylinder*, Applied Ocean Research **10**, 191 (1988).
- [14] T. Sabuncu and S. Calisal, *Hydrodynamic coefficients for vertical circular cylinders at finite depth*, Ocean Engineering **8**, 25 (1981).
- [15] R. W. Yeung, *Added mass and damping of a vertical cylinder in finite-depth waters*, Applied Ocean Research **3**, 119 (1981).
- [16] Y. Drobyshevski, *Hydrodynamic coefficients of a two-dimensional, truncated rectangular floating structure in shallow water*, Ocean engineering **31**, 305 (2004).
- [17] Y. Drobyshevski, *Hydrodynamic coefficients of a floating, truncated vertical cylinder in shallow water*, Ocean engineering **31**, 269 (2004).

- 
- [18] Y. Drobyshevski, *An efficient method for hydrodynamic analysis of a floating vertical sided structure in shallow water*, in *25th International Conference on Offshore Mechanics and Arctic Engineering* (American Society of Mechanical Engineers, 2006) pp. 147–154.
- [19] L.-S. Hwang and E. O. Tuck, *On the oscillations of harbours of arbitrary shape*, *Journal of Fluid Mechanics* **42**, 447 (1970).
- [20] X.-J. Wu and W. Price, *Evaluation of wave drift forces on vertical cylinders of arbitrary geometry, with application to tension leg platforms (tlps)*, *Ocean Engineering* **18**, 1 (1991).
- [21] J. de Jonge, *An accurate and efficient hydrodynamic analysis for offshore discharge operations*, (2008).
- [22] Ansys Inc., *ANSYS AQWA Theory Manual* (2013).

# Appendices



# A

## ASYMMETRIC CALCULATION CASES

For each gap height ranging from 0.5[m] to 4.0[m], the total heave and roll added mass with different inclination percentages are shown here. The solid curve indicates the non-inclined case. Also, by subtracting the frequency part of Drobyshevski from total heave added mass, we can obtain the constant added mass variations due to inclination percentage.

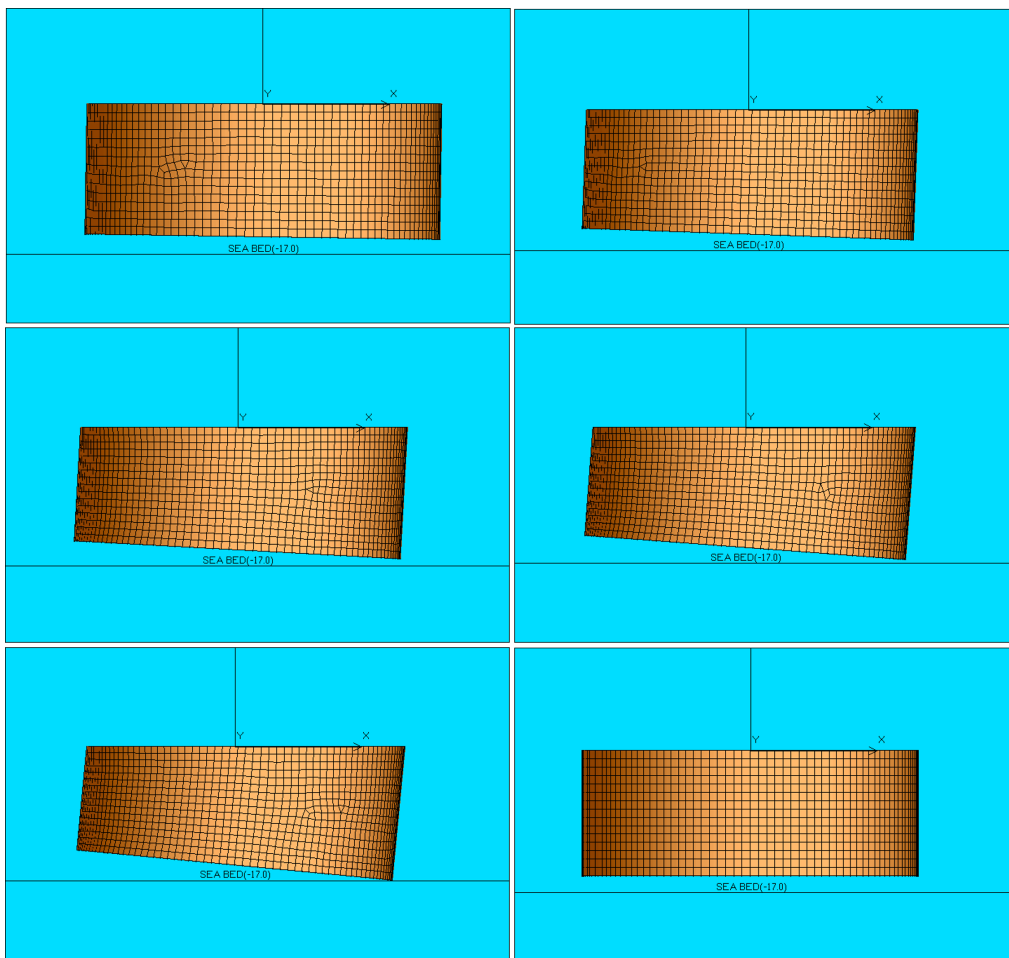
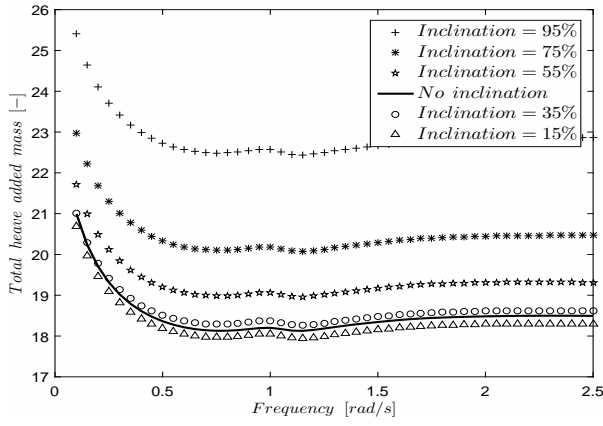
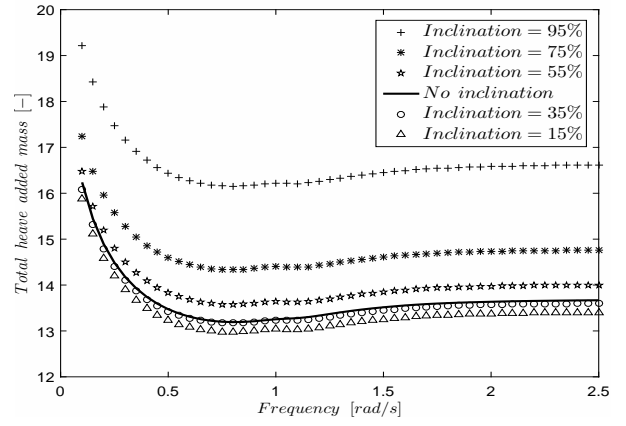


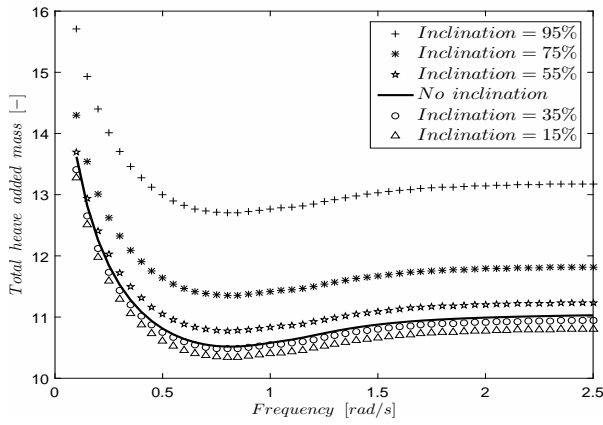
Figure A.1: Cases with different inclination percentages (right corner one is the non-inclined case)



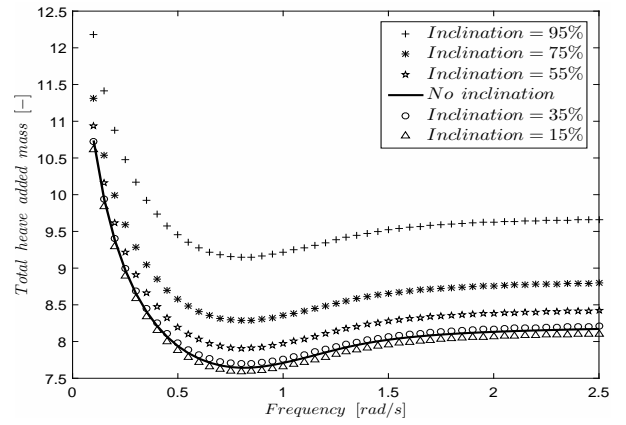
(a)  $GP = 0.50[m]$



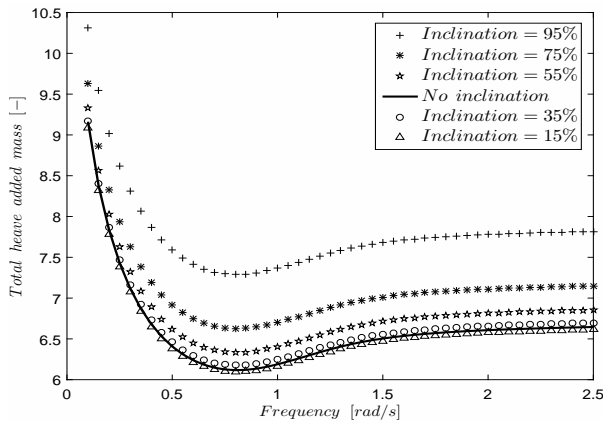
(b)  $GP = 0.75[m]$



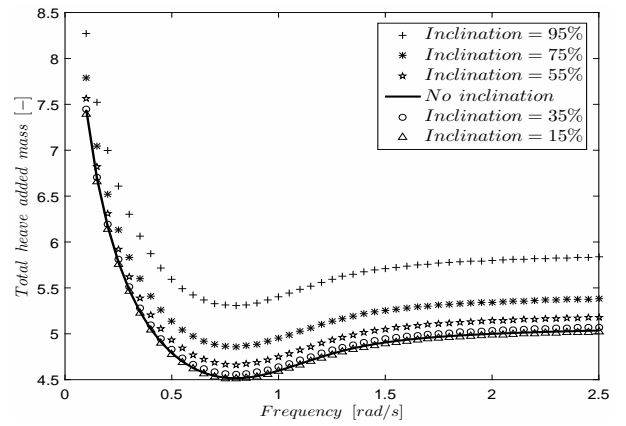
(c)  $GP = 1.0[m]$



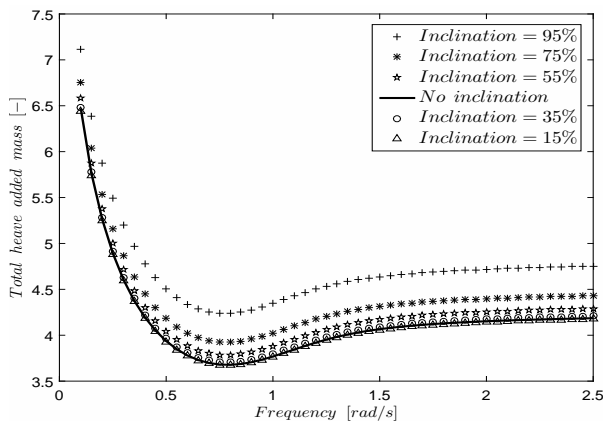
(d)  $GP = 1.5[m]$



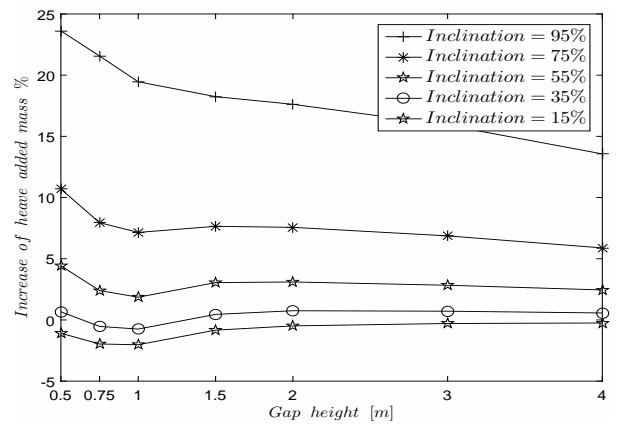
(e)  $GP = 2.0[m]$



(f)  $GP = 3.0[m]$

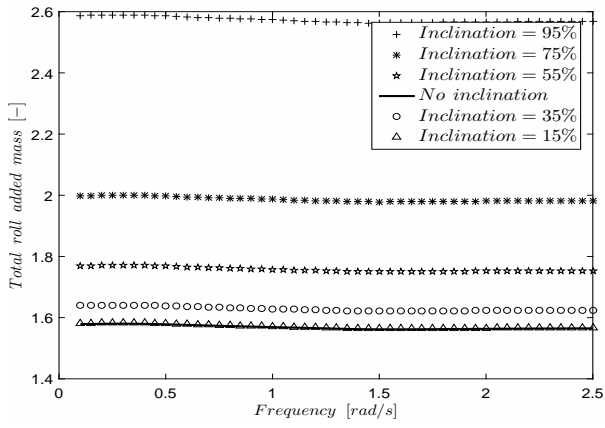


(g)  $GP = 4.0[m]$

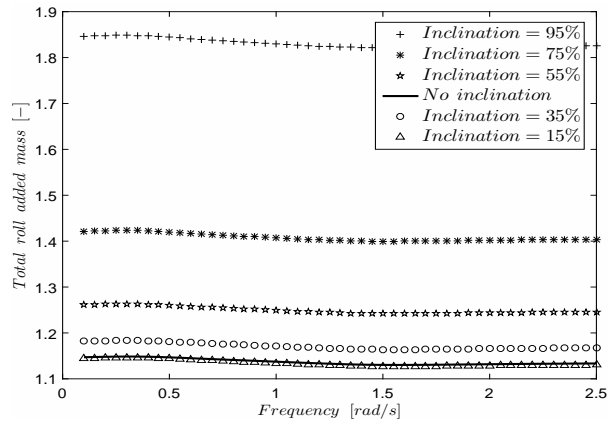


(h) Summary for different gap heights

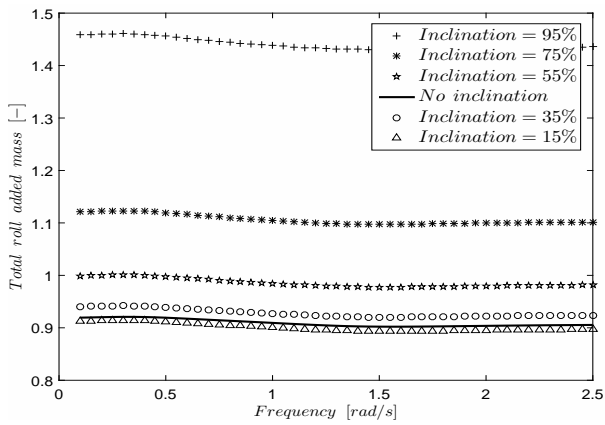
Figure A.2: Total heave added mass with varying inclination angles



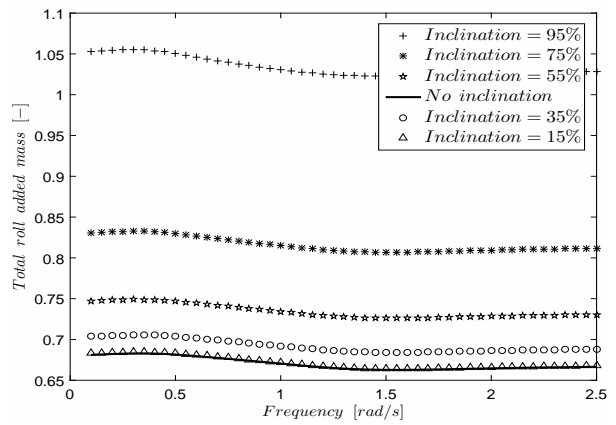
(a)  $GP = 0.50[m]$



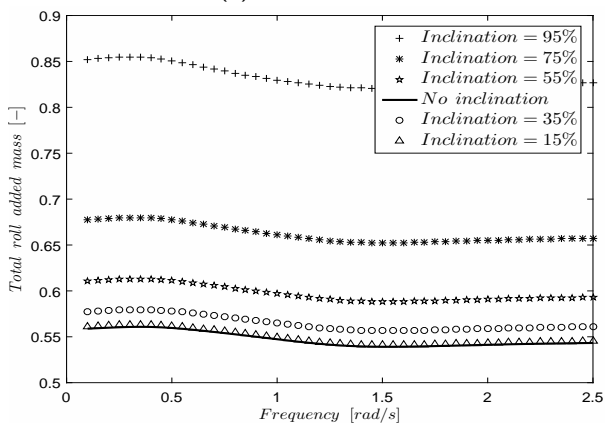
(b)  $GP = 0.75[m]$



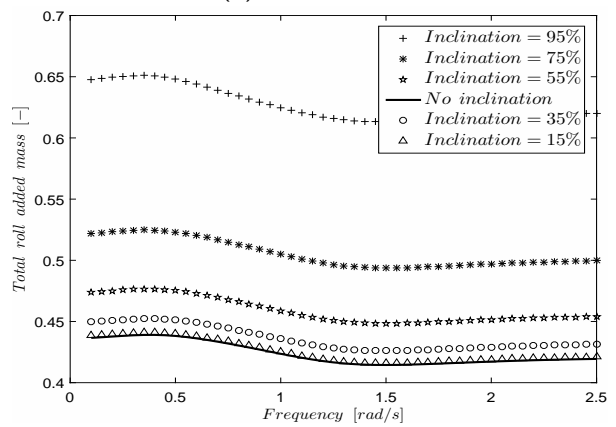
(c)  $GP = 1.0[m]$



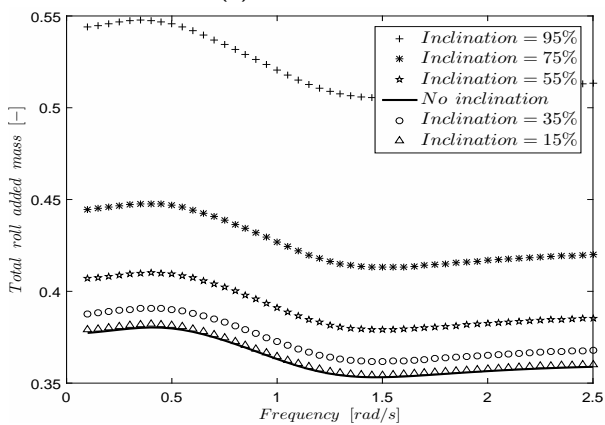
(d)  $GP = 1.5[m]$



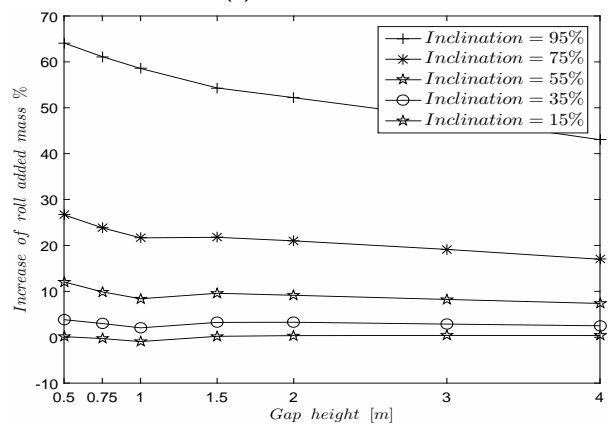
(e)  $GP = 2.0[m]$



(f)  $GP = 3.0[m]$

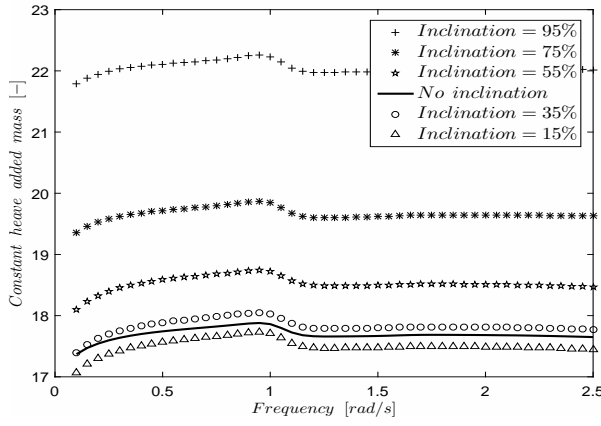


(g)  $GP = 4.0[m]$

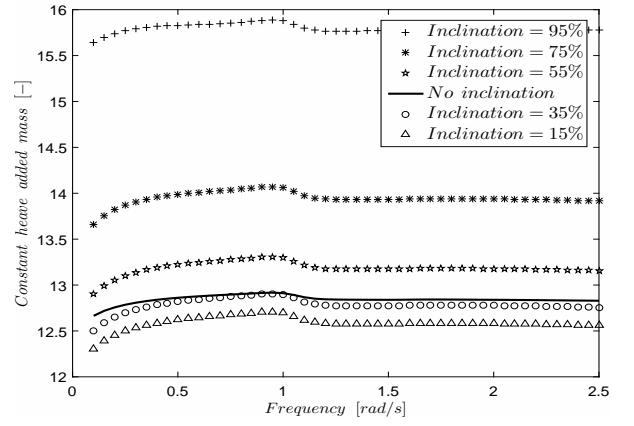


(h) Summary for different gap heights

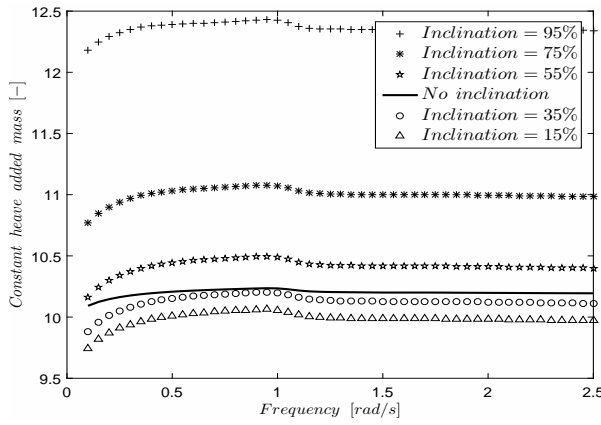
Figure A.3: Total roll added mass with varying inclination angles



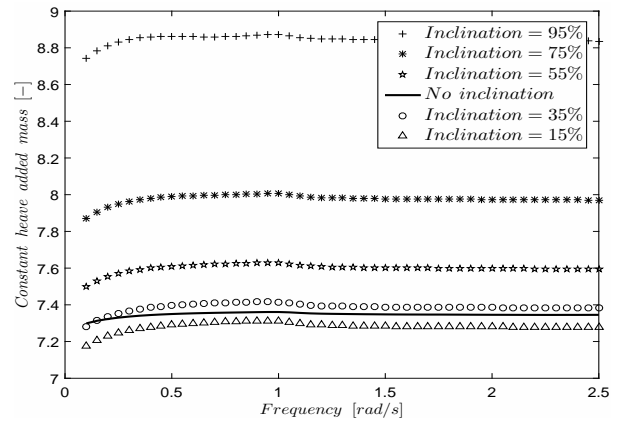
(a)  $GP = 0.50[m]$



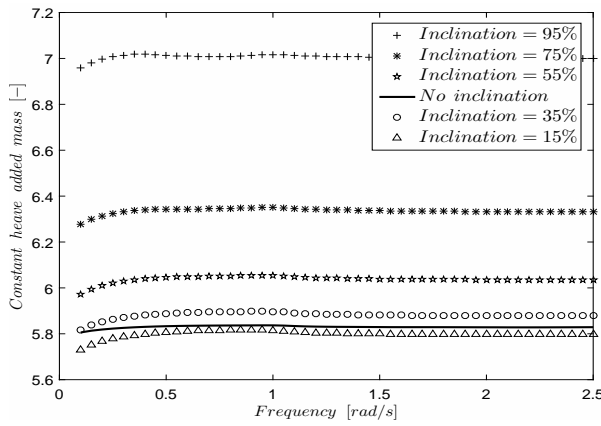
(b)  $GP = 0.75[m]$



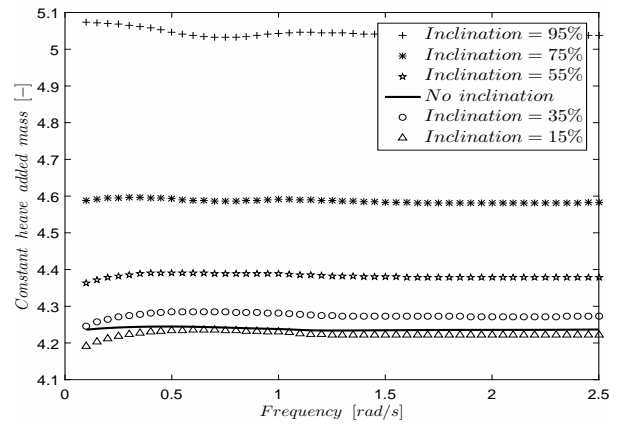
(c)  $GP = 1.0[m]$



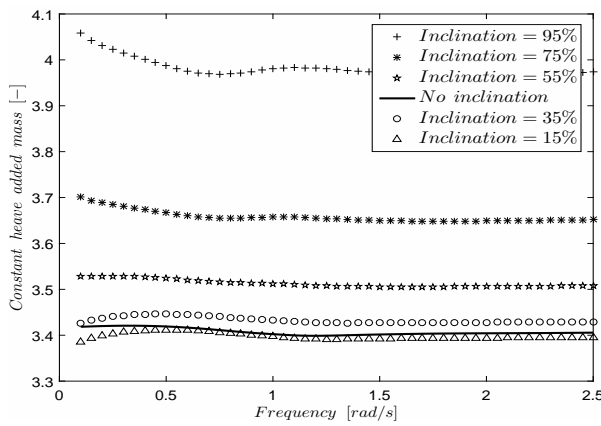
(d)  $GP = 1.5[m]$



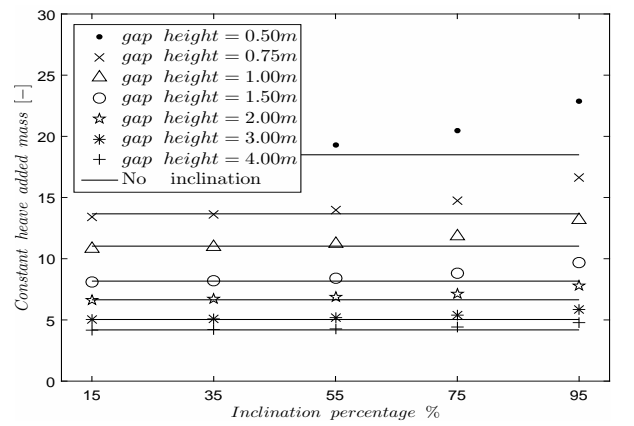
(e)  $GP = 2.0[m]$



(f)  $GP = 3.0[m]$



(g)  $GP = 4.0[m]$



(h) Summary for different gap heights

Figure A.4: Constant heave added mass with varying inclination angles

# B

## ANALYTICAL RESULTS

The analytical equations from Drobyshevsky formed a good basis for new method, in which the external program, AMP (asymptotic matching program), has made possible the calculation for arbitrary bottom shape. Thus, by comparing AQWA and analytical results, it will support the use of AMP in new method. Also, we construct the empirical curve to describe the influence of gap height on added mass, combining AQWA and analytical results, the latter of which can be used for separation of frequency.

### AQWA VS ANALYTICAL DROBYSHEVSKI

For total heave added mass of a circular cylinder, we compare the results from AQWA with analytical equation given by Drobyshevski in Chapter 3. The benchmark case is used for both results with gap heights ranging from  $0.25[m]$  to  $4.0[m]$ . A convergent analysis is done to find the optimal panel size balancing the trade-off between computational time and accuracy.

Comparative results are shown in Fig. B.1, B.2. AQWA can capture total heave added mass fairly well with Drobyshevski. This comparison validates the use of AQWA to compute total heave added mass. Further, the applicability of AQWA for heave mode is slightly dependent on gap height. For very small gap heights, for instance,  $0.25[m]$  and  $0.50[m]$ , the total heave added mass from AQWA shows some discrepancies, whereas for the rest gap heights, AQWA and Drobyshevski compare quite well. To further quantify the difference, the relative error is also evaluated as:

$$RD = \frac{AQWA - Drobys}{Drobys} \times 100\% \quad (B.1)$$

The relative error is larger at both very small gap heights and large gap height. These can be explained in two aspects. For very small gap heights, remember that one key assumption for truncated circular cylinder by Drobyshevski dictates that the gap height is infinitely small compared to radius and AQWA has difficulties calculating very small gap cases due to panel size limitation and precision problems with integral equation. Thus, for very small gap height, the analytical result from Drobyshevski is more trustworthy. For large gap height, the small gap height assumption from Drobyshevski no longer holds and AQWA has no numerical problem handling large gap height. Thus, for large gap height, the AQWA result is more reliable. For gap height in between from  $0.75-2[m]$ , both AQWA and Drobyshevski compare well with each other, with a negligible difference. Overall, regardless of gap height, the relative difference between AQWA and Drobyshevski is small.

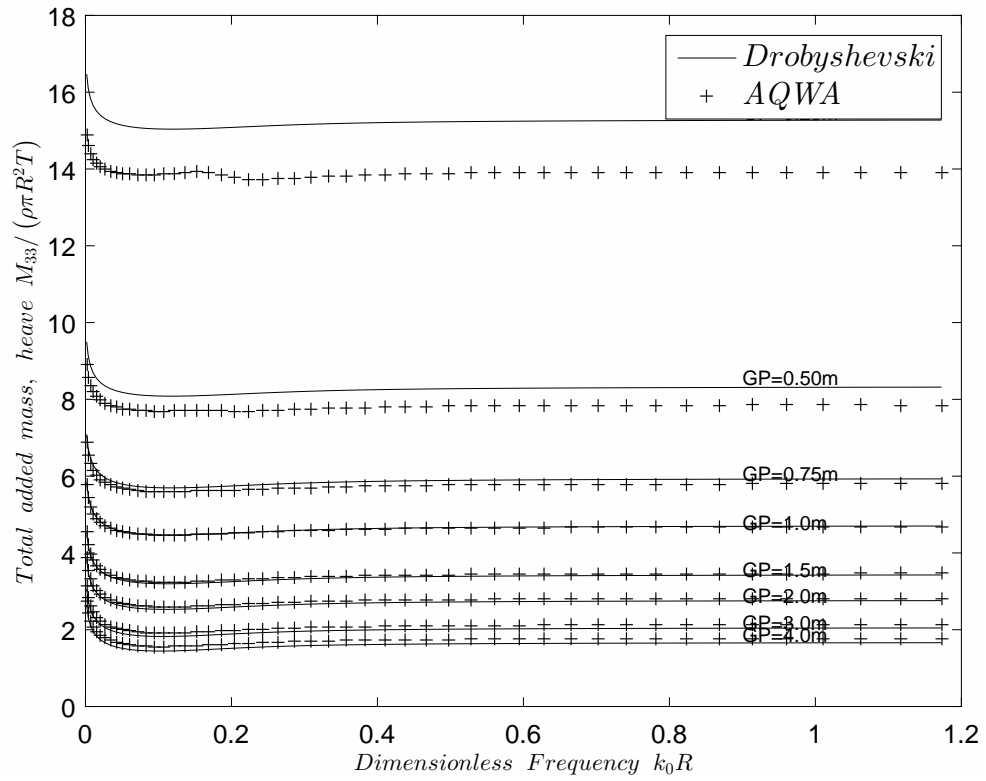


Figure B.1: Heave comparison, Draft=15 [m]

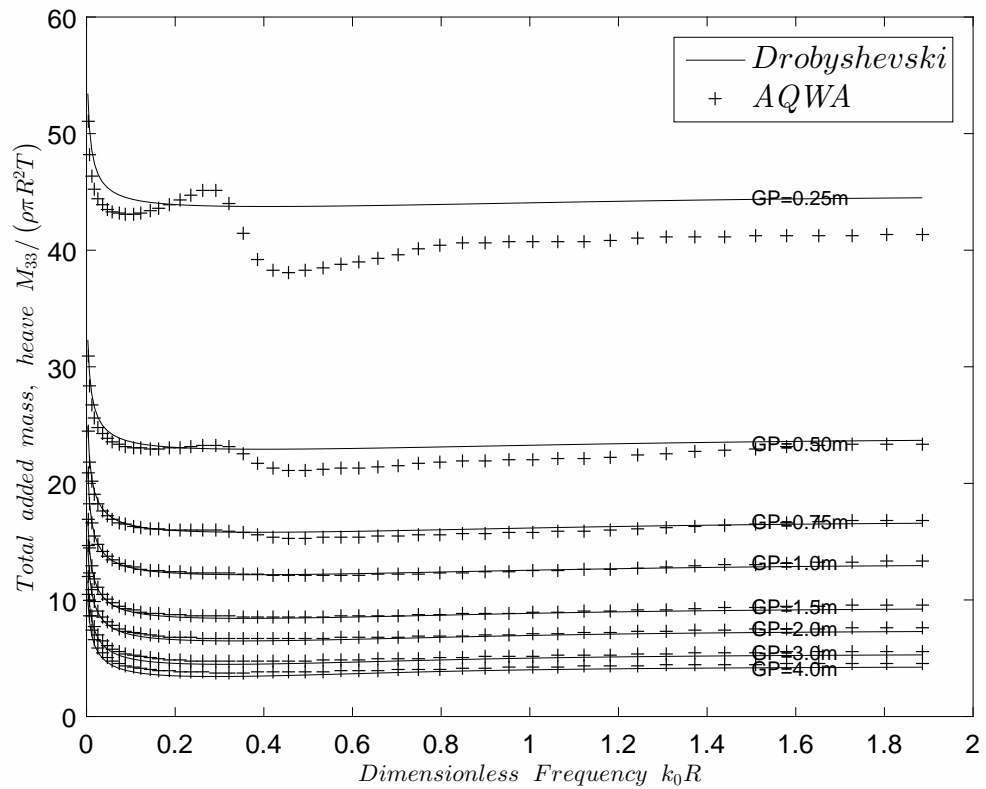
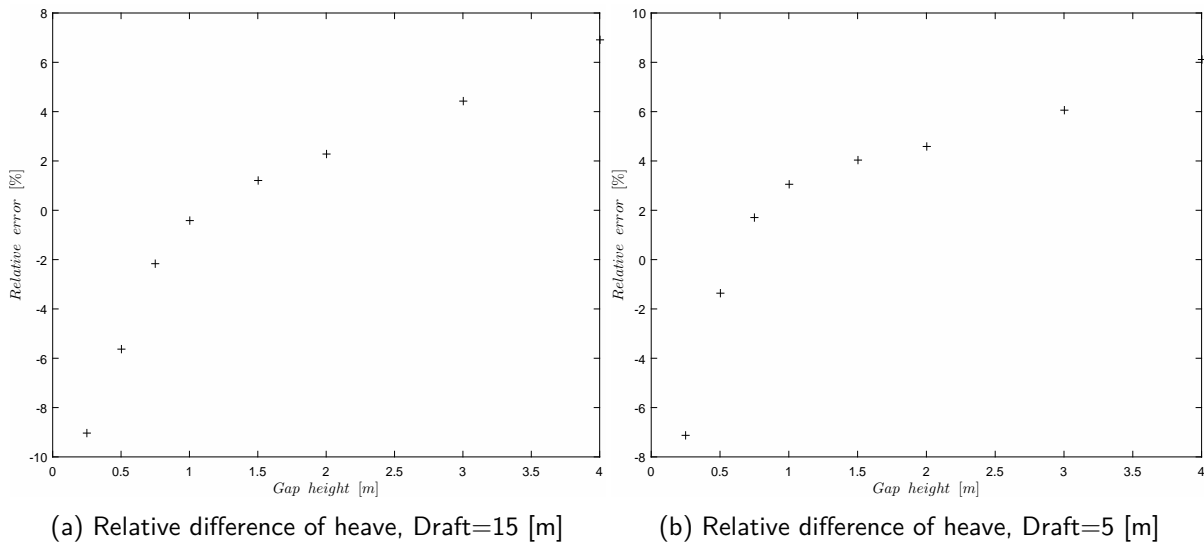


Figure B.2: Heave comparison, Draft=5 [m]



Following the same spirit, total roll added mass is compared here with AQWA and Drobyshevski analytical equation. As seen in Fig. B.4 and B.5, the comparison is generally good except for the low frequency range and large gap heights. The physical explanation for low frequency drop from analytical result is still lacking. The total roll added mass is even negative for large gap heights, which might be erroneous. Analogous to heave, the assumption by Drobyshevski nullifies the use of his analytical equation for large gap heights. In this sense, for total roll added moment, the AQWA result is more reliable. A key characteristic for total roll added mass computed by AQWA is its frequency-independence whereas total heave added mass has not. This will in fact eliminate the need for separation of frequency for roll added mass.

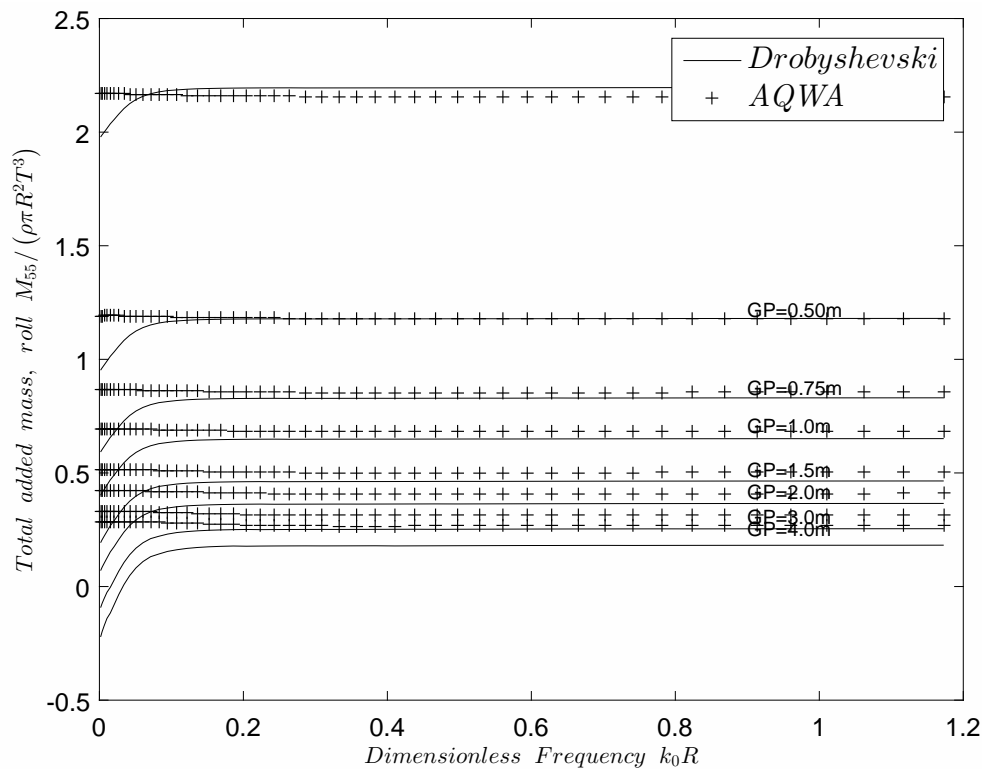


Figure B.4: Roll comparison, Draft=15 [m]

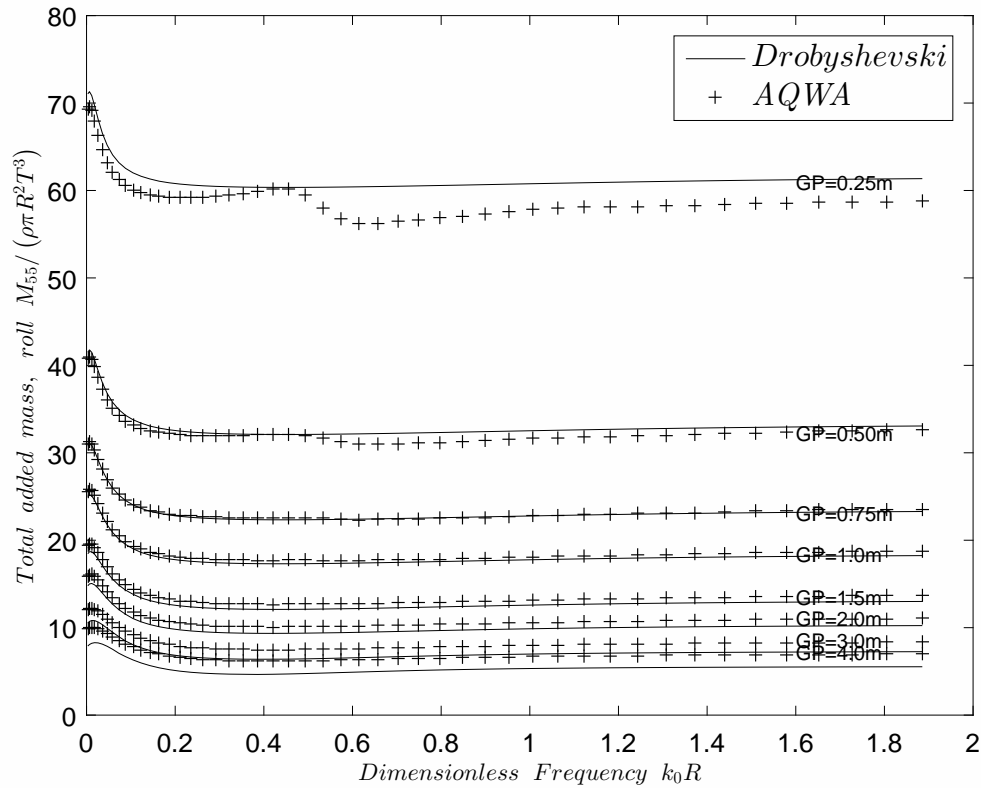
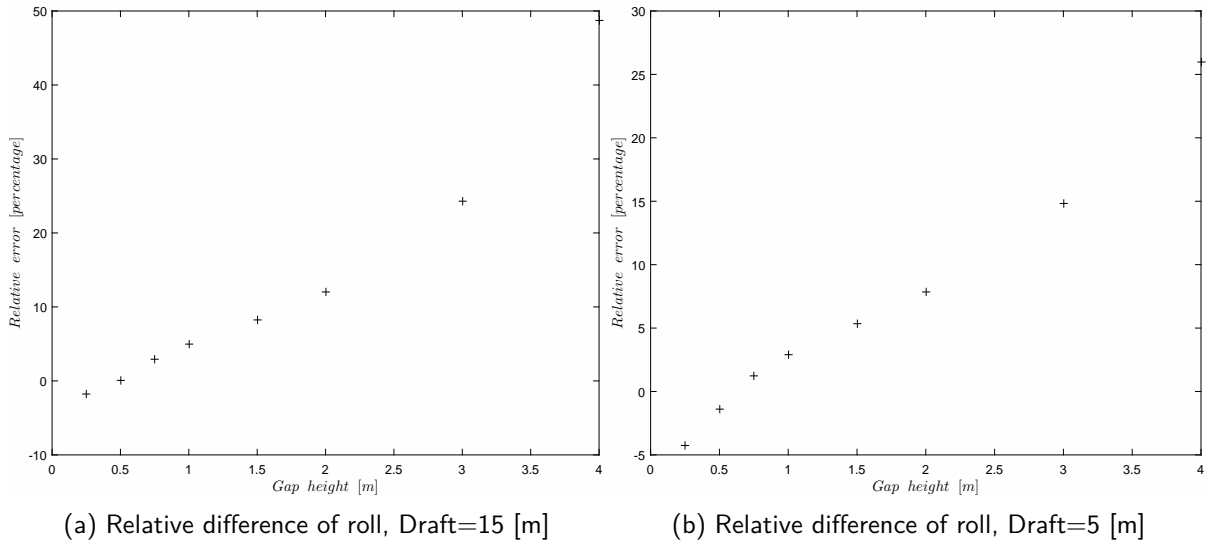


Figure B.5: Roll comparison, Draft=5 [m]



(a) Relative difference of roll, Draft=15 [m]

(b) Relative difference of roll, Draft=5 [m]

### GAP HEIGHT INFLUENCE

Analytical solutions given by Molin and Drobyshevski show that the heave added mass is somewhat inversely proportional to gap height. Remind these two analytical equations from Molin and Drobyshevski:

$$M_{33} = \rho \pi a^3 \left[ \frac{a}{8h} + \frac{1}{2\pi} \ln \left( \frac{8\pi a}{h} \right) - \frac{4}{3} + \frac{h}{2a} \right]$$

$$\mu_{33} = \rho\pi a^3 \left[ \frac{a}{8h} + \frac{1}{\pi} \left( 1 - \ln \left( \frac{4h}{H} \right) \right) \right]$$

Noting that the first term for both equations above is the inverse of gap height, the empirical formulation computed by AQWA can be constructed as the function of gap height only. This is done via power fitting technique. First we employ AQWA to compute total heave added mass for different gap heights. Then subtracting the frequency-independent terms of analytical equations above from AQWA total added mass, the frequency-independent added mass is obtained. Thus, a comparative result is shown in Fig. B.7.

Here we find that the frequency-independent added mass is inversely proportional to gap height with a power index 0.830 from AQWA.

Next, the treatment of roll added mass for heave is slightly different from heave due to difficulties to obtain the frequency-independent part for roll mode. In brief, we use total roll added mass to show the influence of the gap height. Again, we compare the analytical roll added mass from Drobyshevski with that from AQWA in Fig. B.8.

Analogous to heave mode, the roll added moment is also a inversely proportional to gap height, with a power index 0.807 in this case.

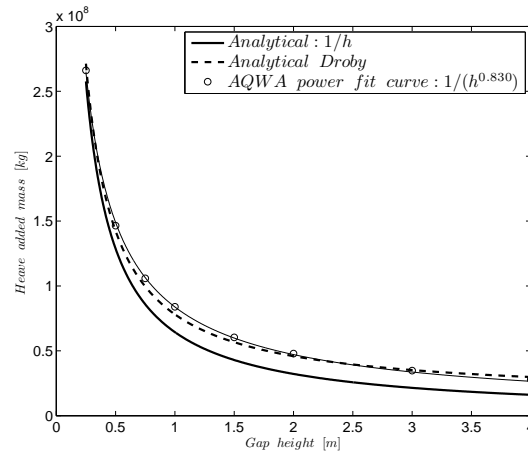


Figure B.7: Comparison between fit curve and analytical curve for heave added mass

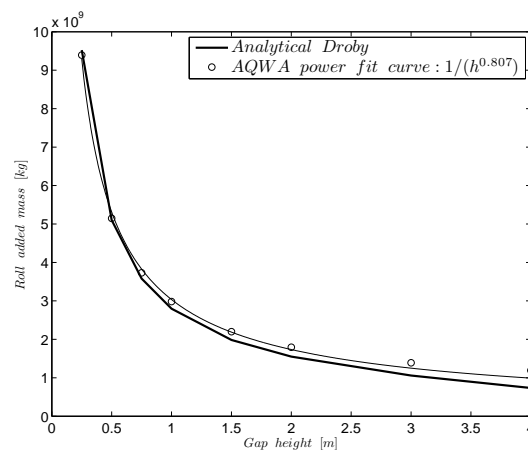


Figure B.8: Comparison between fit curve and analytical curve for roll added mass



# C

## SHAPE FACTORS

This appendix shows added mass results for different contour shapes including triangle, circle, rectangle and square. All the cases have the same bottom area( $400\pi$ ) and same draft ( $15m$ ). The CoG of all these shapes locates at the waterline. Essentially, the shape factor will not change the methodology we use to predict hydrodynamic coefficients. The main interest here is to provide more data and information on gap problem. Due to consistency between AQWA and New method, results only from AQWA will be shown. We selected four gap heights for the comparison:  $0.5m$ ,  $1.0m$ ,  $1.5m$ ,  $4.0m$ .

As shown in Fig. C.1 - C.4, for heave, the added mass of circle, square and triangle have very similar trend and approximate values while rectangle has the smallest heave added mass. For pitch mode, rectangle has a considerably larger added moment than other shapes. Understandably, this is caused by long arm of the rectangle.

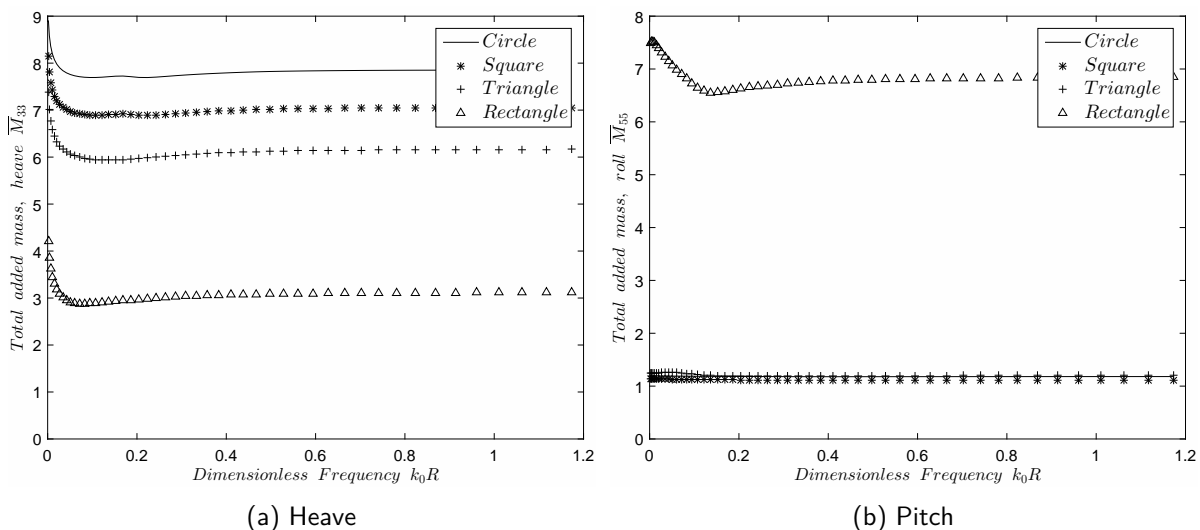
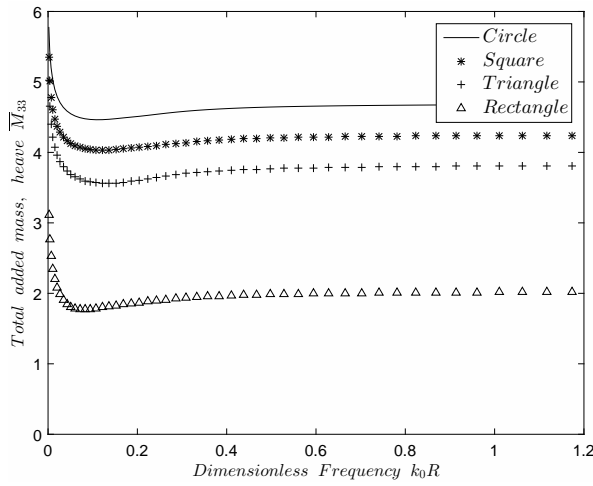
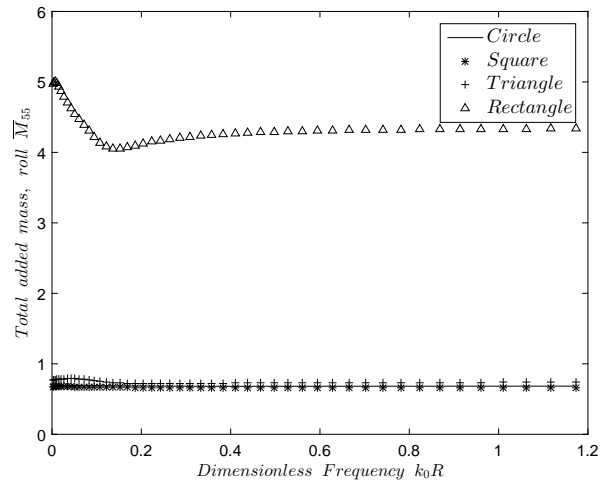


Figure C.1: Gap height =  $0.5m$

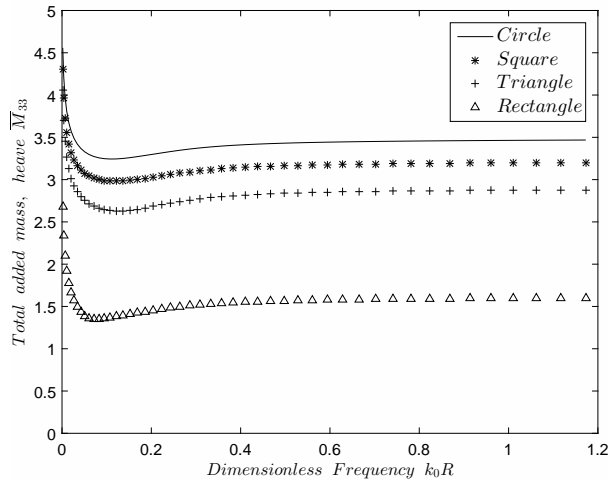


(a) Heave

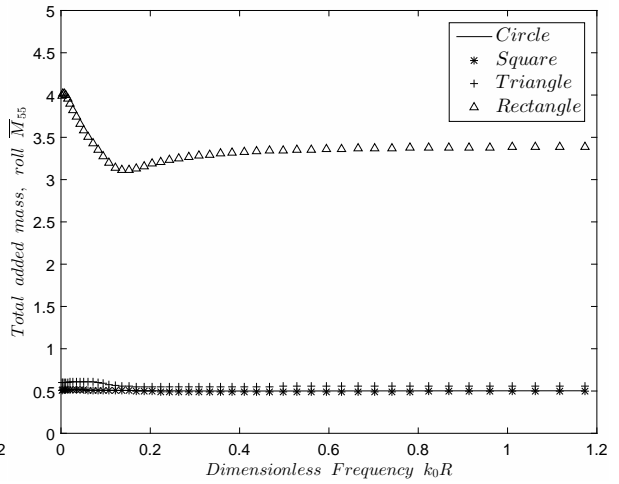


(b) Pitch

Figure C.2: Gap height = 1.0m

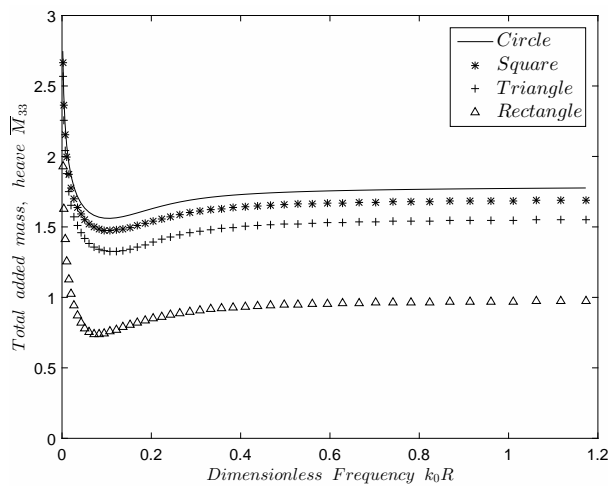


(a) Heave

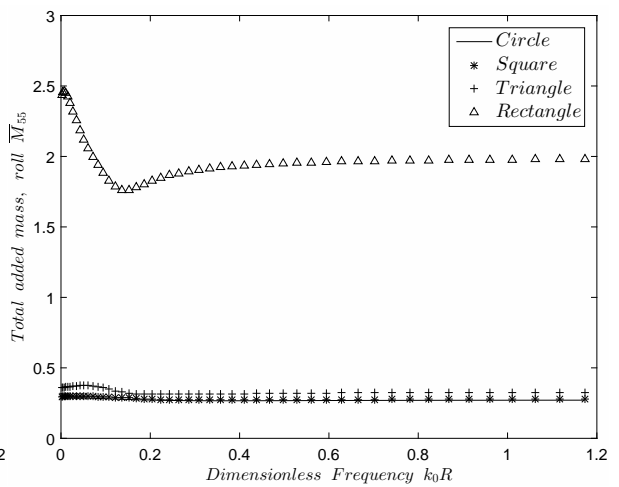


(b) Pitch

Figure C.3: Gap height = 1.5m



(a) Heave



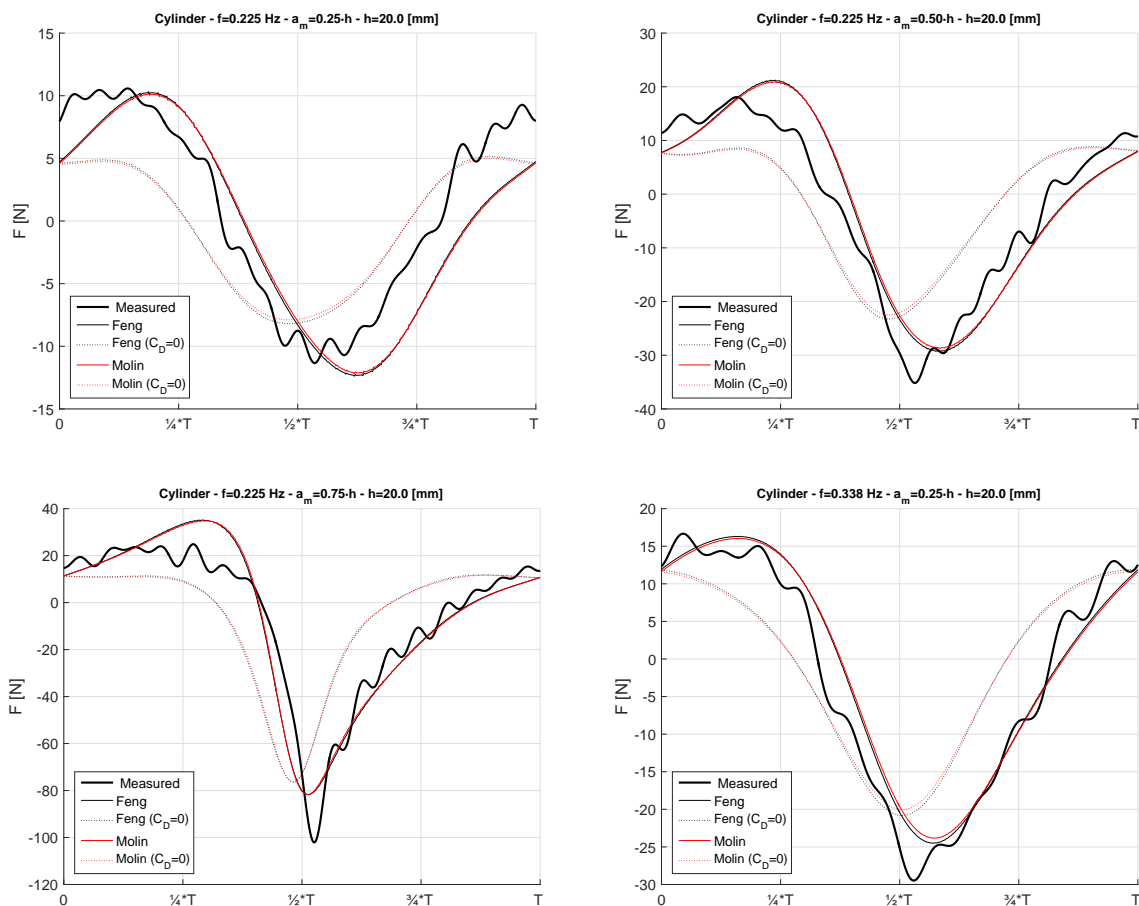
(b) Pitch

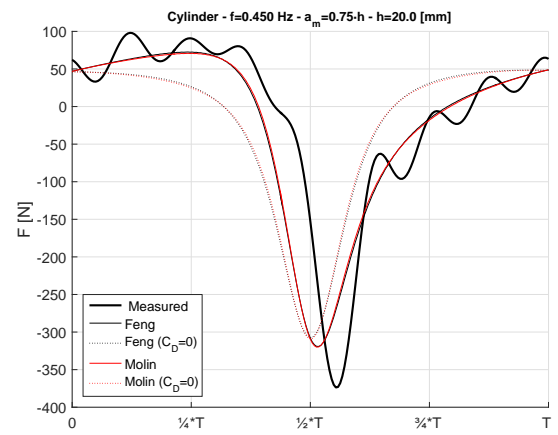
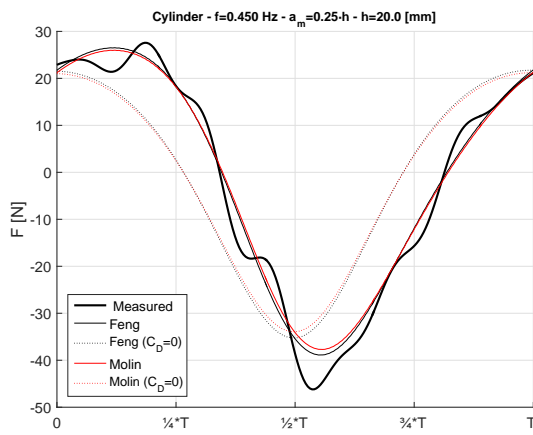
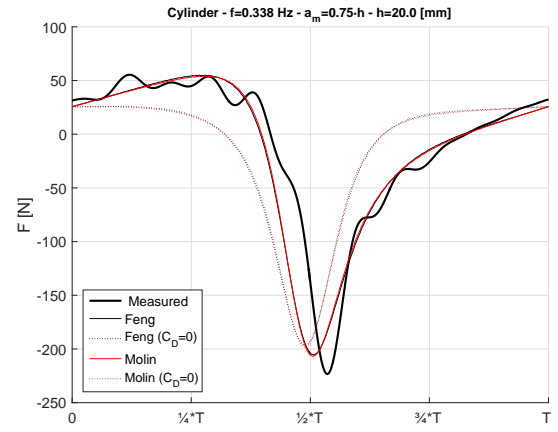
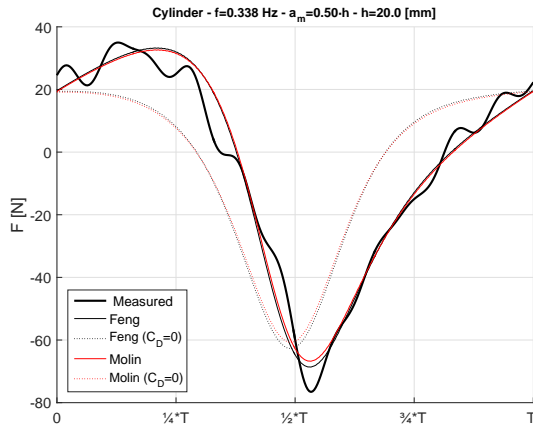
Figure C.4: Gap height = 4.0m

# D

## VERIFICATION WITH MEASUREMENT

The forced oscillation measurement (MARIN, 2008) was done for a circular cylinder case with a draft of 5[m] and a diameter of 40[m]. Here we compare Molin's analytical equations, Feng's empirical formulations with the model test measurement.





# E

## 3D POTENTIAL THEORY

The employment of both Delfrac and AQWA requires the introduction of linear potential theory. The main frame of linear potential theory [9] [22] dictates that with calculated potential everywhere in the fluid domain, the fluid pressure will be known, thus obtaining hydrodynamic force and motions for the structure. Here only first order solutions will be obtained.

The assumptions applied in linear potential theory for Delfrac and AQWA are given here:

- The fluid is inviscid and incompressible, i.e., ideal fluid; its motion is irrotational.
- wave and motion amplitudes are linearized with respect to wave length.
- The structure is considered with zero-forward speed.
- The source distribution is over mean wetted body surface

Two sets of coordinate system are defined in the theory: global axes and local axes. The global axes adopt a Cartesian coordinate system  $(X, Y, Z)$  with the origin of  $z$ -axis located on the free surface and pointing vertically upward. This global axis is mainly used to defined environment conditions and fluid domain. The local axes  $(x, y, z)$  are aligned with CoG of the structure, acting as the dynamic reference point.

### GOVERNING EQUATION

In the fluid domain, the mass conservation leads to the potential  $\Phi$  satisfying Laplace equation:

$$\nabla^2 \Phi = 0 \quad (\text{E.1})$$

where  $\Phi$  consists of three parts:  $\Phi_I$  for potential undisturbed incident waves,  $\Phi_D$  for wave potential diffracted by fixed body,  $\Phi_R$  for potential radiated by moving body.

$$\Phi = \Phi_I + \Phi_D + \Phi_R \quad (\text{E.2})$$

The technique of separation of temporal and spatial variables is used here:

$$\Phi(x, y, t) = \text{Re} \left\{ \phi(x, y, z) e^{-i\omega t} \right\} \quad (\text{E.3})$$

## BOUNDARY CONDITIONS

The fluid domain satisfying Laplace equation must be confined by boundary conditions.

The linearized free surface dictates that water particles will not leave the water surface:

$$\frac{\partial^2 \Phi}{\partial t^2} + g \frac{\partial \Phi}{\partial z} = 0 \quad (\text{E.4})$$

The fluid cannot penetrate the seabed:

$$\frac{\partial \Phi}{\partial n} = 0 \text{ on } z = -h(x, y) \quad (\text{E.5})$$

The fluid cannot penetrate the body:

$$\begin{aligned} \frac{\partial \Phi_D}{\partial n} &= -\frac{\partial \Phi_I}{\partial n} \text{ on } S_B \\ \frac{\partial \Phi_R}{\partial n} &= -V_n \text{ on } S_B \end{aligned} \quad (\text{E.6})$$

The diffracted field  $\Phi_D$  and radiated field  $\Phi_R$  must satisfy the radiation condition at the cylindrical surface of great distance  $r$  from the body:

$$\lim_{kr \rightarrow \infty} r^{1/2} \left( \frac{\partial w}{\partial r} - ik\Phi_\mu \right) = 0 \quad (\text{E.7})$$

## POTENTIAL SOLUTIONS

To solve the velocity potentials of the undisturbed, diffracted and radiated waves, the source distribution method is used in which potentials can be expressed as the distribution of sources over the body surface  $S$  with the known Green function or 'influence function' for finite water depth.

$$\phi_\mu(\vec{x}) = \frac{1}{4\pi} \iint_S \sigma_\mu(\vec{\xi}) G(\vec{x}, \vec{\xi}) dS \quad \forall \mu = 0..7 \quad (\text{E.8})$$

With Green function of a pulsating source on the potential:

$$\begin{aligned} G(\vec{x}, \vec{\xi}) &= \frac{1}{r} + \frac{1}{r_1} + \int_1^\infty \frac{2(\kappa + \nu) e^{-\kappa h} \cosh \kappa(\zeta + h) \cosh \kappa(z + h)}{\kappa \sinh \kappa h - \nu \cosh \kappa h} J_0(\kappa R) d\kappa \\ &\quad + i \frac{2\pi(\mu_0^2 - \nu^2) \cosh \mu_0(\zeta + h) \cosh(\mu_0(z + h))}{(\mu_0^2 - \nu^2)h + \nu} J_0(\nu R) \end{aligned} \quad (\text{E.9})$$

With:

$$\begin{aligned} r &= \sqrt{(\xi - x)^2 + (\eta - y)^2 + (\zeta - z)^2} \\ r_1 &= \sqrt{(\xi - x)^2 + (\eta - y)^2 + (2h + \zeta + z)^2} \\ R &= \sqrt{(\xi - x)^2 + (\eta - y)^2} \end{aligned}$$

The unknown source strength  $\sigma_j(\vec{x})$  are found by solving normal velocity boundary conditions:

$$n_\mu = -\frac{1}{2} \sigma_\mu(\vec{x}) + \frac{1}{4\pi} \iint_S \sigma_\mu(\vec{\xi}) \frac{\partial G(\vec{x}, \vec{\xi})}{\partial n} dS \quad \forall \mu = 0..7 \quad (\text{E.10})$$

For the RHS of the above

$$\begin{aligned}
n_0 &= \frac{\partial \phi_I}{\partial n} \\
n_1 &= \cos(n, x) \\
n_2 &= \cos(n, y) \\
n_3 &= \cos(n, z) \\
n_4 &= (y - y') n_3 - (z - z') n_2 \\
n_5 &= (z - z') n_1 - (x - x') n_3 \\
n_6 &= (x - x') n_2 - (y - y') n_1 \\
n_7 &= \frac{\partial \phi_D}{\partial n} = -\frac{\partial \phi_I}{\partial n}
\end{aligned} \tag{E.11}$$

The numerical procedures to solve Eq. E.10 require the discretization of body surface  $S$  into panels.

#### HYDRODYNAMIC FORCES

Now with obtained velocity potentials, the fluid pressure is derived from linearized Bernoulli equation:

$$p = -\rho g z - \rho \frac{\partial \Phi}{\partial t} \tag{E.12}$$

where the first term represents the hydrostatic pressure and the second term is the hydrodynamic pressure due to the fluid motions.

Considering only the hydrodynamic pressure part, the wave exciting force, made up of the Froude-Krylov force and the diffraction force, can be expressed as:

$$\tilde{F}_w = -\rho \omega^2 \iint_S (\phi_i + \phi_d) \zeta_a \vec{N} dS \tag{E.13}$$

For the radiation force, it can be expressed as the added mass and radiation damping, corresponding to real and imaginary part of radiation potential:

$$\begin{aligned}
A_{n,m} &= -\Re \left[ \rho \iint_S \phi_m N_n dS \right] \quad \forall n = 1..6 \wedge m = 1..6 \\
B_{n,m} &= -\Im \left[ \rho \omega \iint_S \phi_m N_n dS \right] \quad \forall n = 1..6 \wedge m = 1..6
\end{aligned} \tag{E.14}$$

With all the hydrodynamic forcing known, the response amplitude operators (RAOs) for harmonic waves will be obtained via solving a set of linear algebraic equations.

$$(M_s + M_a) \ddot{X} + C \dot{X} + K_s X = F \tag{E.15}$$

With:

$M_s$  = structural mass matrix

$M_a$  = added mass matrix

$C$  = linear damping matrix

$K$  = total stiffness matrix

$X$  = RAOs

$F$  = exciting force on the structure (per unit wave amplitude)

The solution to the above equation is:

$$X_0 = HF_0 \quad (\text{E.16})$$

where transfer function  $H = (K_s - [M_s + M_a]\omega^2 - iC\omega)^{-1}$ ,  $X = X_0 e^{-i\omega t}$  and  $F = F_0 e^{-i\omega t}$ .